



Reliability Assessment of Vehicle-to-Vehicle Communication

Von der
Carl-Friedrich-Gauß-Fakultät
der Technischen Universität Carolo-Wilhelmina zu Braunschweig
zur Erlangung des Grades einer
Doktoringenieurin (Dr.-Ing)
genehmigte Dissertation

von
M.Sc. Tetiana Zinchenko
geboren am 20.09.1985
in Donetsk

Eingereicht am: 30.09.2014

Disputation am:

1. Referentin/Referent: Prof. Dr.-Ing. Lars Wolf
2. Referentin/Referent: Prof. Dr.-Ing. Markus Fidler

2015

The results, opinions and conclusions expressed in this thesis are not necessarily those of Volkswagen AG.

Kurzfassung

Car2Car-Kommunikation ermöglicht eine Vielzahl von kooperativen Anwendungen, welche auf die Unfallverminderung, Verbesserung der Verkehrseffizienz sowie den individuellen Fahrkomfort abzielen und damit die Grenzen von aktiven Fahrerassistenzsystemen (FAS) erweitern. Diese Anwendungen werden durch den IEEE 802.11p unterstützt, ein Standard, der bei 5.9 GHz betrieben wird und für die hochdynamische Fahrzeugumgebung adaptiert ist.

Im Fokus dieser Dissertation stehen Car2Car-Sicherheitsanwendungen, denen heutzutage bereits große Aufmerksamkeit von Seiten der Industrie, Forschung und diversen Normierungsgremien geschenkt wird. Da alle diese Anwendungen auf drahtloser Kommunikation basieren, ist ihre Leistungsfähigkeit direkt von der Qualität der Kommunikationsverbindung sowie dem Paketverteilungsmuster abhängig. Daher liegt der Hauptfokus dieser Arbeit in der Entwicklung effektiver Methoden zur Bewertung der Kommunikationszuverlässigkeit und der Analyse, inwieweit Car2Car-Kommunikation im Allgemeinen die Anforderungen von Sicherheitsanwendungen erfüllt. Darüber hinaus untersucht diese Doktorarbeit die Effektivität der hier vorgeschlagenen Bewertungsmethoden in Bezug auf die Vorhersage der Kommunikationszuverlässigkeit in Echtzeit-Szenarien.

Im Speziellen verbindet diese Arbeit die Welt der klassischen Netzwerkperformance-Metriken mit Car2Car-Anwendungsspezifischen Zuverlässigkeitsanforderungen und stellt als Ergebnis eine Reihe effektiver Bewertungskennzahlen vor. Mithilfe der vorgeschlagenen Metriken wird des Weiteren untersucht, inwieweit verschiedene Umweltfaktoren die Anwendungszuverlässigkeit beeinflussen können. Diese Untersuchung basiert auf Messdaten, die in ausführlichen Feldversuchen in verschiedenen Non-Line-of-Sight-Szenarien gewonnen wurden. Im nächsten Schritt analysiert diese Doktorarbeit die erreichbare Zuverlässigkeit der Car2Car-Sicherheitsanwendungen in Netzwerküberlastungsszenarien anhand einer Simulationsstudie. Als Ergebnis werden die spezifischen Kombinationen der verschiedenen Netzwerkparameter definiert, die einen zuverlässigen Betrieb der Car2Car-Sicherheitsanwendungen gewährleisten können.

Zum Abschluss untersucht diese Dissertation, inwieweit die vorgeschlagenen Metriken für die im Echtzeit-Modus funktionierenden Anwendungen geeignet sind. Darüber hinaus werden zwei Frameworks entwickelt und implementiert, welche die Zuverlässigkeit der Kommunikationsverbindung präzisieren. Dies geschieht basierend auf Daten, die während der 4.5 Monate dauernden Feldversuche im Rahmen des sim^{TD} Projektes gewonnen wurden. Beide Frameworks werden am Ende anhand unabhängiger Messdaten auf ihre Funktionalität unter realistischen Bedingungen getestet.

Abstract

V2V communication enables a plethora of cooperative applications aimed at reducing road hazard situations as well as enhancing traffic efficiency and individual driving comfort, expanding therewith the boundaries of Advanced Driver Assistance Systems (ADAS). These applications will be supported by IEEE 802.11p, a standard operating in the 5.9 GHz frequency band and adapted for the highly dynamic vehicular environment.

The focus of this work is V2V safety applications, which have already gained a major attention from the industry, academia, as well as standardization bodies. Being a subject of wireless communication the performance of V2V applications directly depends on the communication link quality and the packet distribution pattern. Therefore, the main purpose of this thesis is to develop an effective communication link reliability assessment method and analyze to what extent V2V communication is feasible to satisfy the reliability requirements of safety applications. Furthermore, we investigate the effectiveness of the proposed assessment method when applied for real-time communication link reliability prediction.

In particular, in this work we establish the link between classical network performance metrics and specific application reliability requirements and derive a set of advanced assessment metrics. Afterwards, we investigate through these metrics how different environmental factors affect application reliability based on the measurement data, which was obtained in elaborated real-world measurement campaigns and in different non-line-of-sight scenarios. Using the suggested metrics further in this work we additionally analyze the achievable application reliability of the V2V safety applications in congested network scenarios through the simulation study. Based on these results we also define the most favorable combinations of the network parameters to support reliable operation of these applications.

Finally, in this thesis we examine to what extent the suggested metrics are suitable for applications while operating in real time. We develop and implement two frameworks for prediction of the communication link reliability, based on the data that was obtained over the 4.5 months of the sim^{TD} project field trials. Furthermore, we apply both frameworks to other measurement data, which was obtained outside the sim^{TD} project and assess the effectiveness of both frameworks under independent realistic conditions.

IN LOVING MEMORY OF MY FATHER, ALEXANDER.
DEVOTED TO MY LOVE LEVENT AND MY FAMILY

Acknowledgments

Completing this Ph.D. thesis is truly the most exciting milestone in my academic career, finishing which, however, has requested a staggering amount of energy, time and hard work. Being now in the end of my doctoral journey and looking back over the research years, I realize that it was not a "what", but most certainly a "whom", that was keeping me going. So now I would like to take the opportunity to express my heartfelt gratitude to all those people that supported me during this long but fulfilling road, without their help and guidance I would have never been able to finish this thesis.

First and foremost, I would like to express my sincere gratitude to my two supervisors, Prof. Dr.-Ing. Lars Wolf from Institute of Operating Systems and Computer Networks, Technische Universität Braunschweig and Dr.-Ing. Stefan Kubica from Volkswagen AG for their patience, constructive comments and immense knowledge which helped me to improve my work. I particularly thank Professor Wolf for being always willing to listen to my questions and encouraging me to take new challenges which would expand my horizons and help me define myself as a scientist. Furthermore, I especially would like to express my deepest gratitude to Dr. Kubica for his friendship and constant support, fresh ideas and providing me with excellent working environment and great amount of flexibility at Volkswagen AG. Second, I would like to thank Prof. Dr.-Ing. Markus Fidler for agreeing to be the assessors of this thesis. Also I would like to thank Volkswagen AG for providing me with the opportunity to write and complete my thesis. During my Ph.D. time there I have gathered colossal amount of working and life experiences.

Further, I would like to express my sincerest regards to my current and former colleagues at Volkswagen AG for their valuable comments, fruitful discussions, optimism and a healthy sense of humor. Especially, I am deeply indebted to Jan-Niklas Meier, Dr. Burak Simsek and Andreas Kwoczek, who contributed immensely to my research and whose openness and friendship supported me in the difficult times. In particular, I would like to thank Jan-Niklas Meier for his creativity, motivation and always fresh view on the problems. Furthermore, my thanks goes to Tigran Khatchatrian for proofreading of my publications and always making time for the discussions. Moreover, I would like to thank Thomas Biehle for his advising, feedback and always constructive comments, which helped me greatly throughout my work. Additionally, I would like to thank my students, who supported this work in their student and diploma theses, in particular, Yingjie Tang.

I fondly remember our joint research with doctoral students from Institute of Communication Technology, Leibniz Universität Hannover and Institut für Nachrichtentechnik, Technische Universität Braunschweig. Time that we spent during different measurement campaigns in sometimes challenging traffic and weather conditions contributed a lot to an interesting and memorable working environment. Here special thanks goes to Hugues Tchouankem for always deep going technical discussions, devotion and a hard work. He contributed greatly to my work and it has been also a great pleasure to work with him.

Finally, I owe my deepest gratitude to my family, their love and support were the key motivators throughout my Ph.D. time. In particular, I am thankful to my partner Levent for technical discussions and for always being there for me, his patience and understanding. But most importantly, for always believing in me unconditionally, without him I would not have been able to finish my doctoral journey.

Tetiana Zinchenko, January 2015

List of Acronyms

AC	-	Access Class
ADAS	-	Advanced Driver Assistance Systems
AIFS	-	Arbitration Interframe Space
AU	-	Application Unit
BER	-	Bit Error Rate
C-ACC	-	Cooperative Adaptive Cruise Control
CAM	-	Cooperative Awareness Message
CSMA/CA	-	Carrier Sense Multiple Access Method with Collision Avoidance
CA	-	Collision Avoidance
CCU	-	Communication Control Unit
CTS	-	Clear to Send
CW	-	Contention Window
C2C CC	-	Car 2 Car Communication Consortium
CCH	-	Control Channel
CCHI	-	Control Channel Interval
CCU	-	Communication Control Unit
DENM	-	Decentralized Environmental Notification Message
DIFS	-	Distributed Coordination Function Inter-Frame Spacing
DSRC	-	Dedicated Short Range Communication
EEBL	-	Emergency Electronic Brake Lights
ETSI	-	European Telecommunications Standards Institute
FCS	-	Frame Check Sequence
FCW	-	Forward Collision Warning
FCC	-	Federal Communications Commission
HMI	-	Human Machine Interface
HV	-	Host Vehicle
IC	-	Information Connector
ICW	-	Intersection Collision Warning
IO	-	Interacting Object
ITS	-	Intelligent Transport Systems
LCA	-	Lane Change Assistant
LOS	-	Line-Of-Sight
LUT	-	Lookup Table
MAC layer	-	Medium Access Layer
NLOS	-	Non-Line-Of-Sight
PCW	-	Pre-Crash-Warning
PDR	-	Packet Delivery Ratio
PER	-	Packet Error Ratio
PHY layer	-	Physical Layer
PIT	-	Packet Inter-Arrival Time
QoS	-	Quality of Service

RIF	- Required Information Freshness
RSSI	- Received Signal Strength Indication
RTS	- Request to Send
RV	- Remote Vehicle
Rx	- Receiver Vehicle
SHF	- Super High Frequency
SCH	- Service Channel
SCHI	- Service Channel Interval
SINR	- Signal to Interference plus Noise Ratio
SVW	- Stationary Vehicle Warning
TTC	- Time To Collision
TJW	- Traffic Jam Warning
Tx	- Transmitter Vehicle
VANET	- Vehicular Ad-Hoc Network
V2V	- Vehicle-to-Vehicle
V2I	- Vehicle-to-Infrastructure
V2X	- Vehicle-to-X

Contents

Kurzfassung	v
Abstract	vii
Acknowledgments	xi
List of Acronyms	xiii
1 Introduction	1
1.1 Motivation	1
1.2 Problem Statement and Objectives	3
1.3 Contributions and Scope	4
1.4 Assumptions	6
1.5 Outline	6
2 Fundamentals of V2V Communication	9
2.1 State of the Technology	9
2.1.1 VANETs as a Subclass of Wireless Mobile Ad-Hoc Networks	9
2.1.2 Survey of V2X Use Cases	12
2.1.3 Dedicated Short Range Communication	16
2.2 V2V Activities Worldwide	20
2.2.1 The USA	21
2.2.2 Japan	22
2.2.3 Europe	22
2.3 Summary	24
3 Application Reliability Assessment	27
3.1 Related Work	27
3.2 Communication Performance Requirements	28
3.2.1 Allowable Latency	28
3.2.2 Minimum Frequency	29
3.2.3 Communication Range	30
3.3 Application Reliability	30
3.3.1 Information Freshness	31
3.3.2 Communication Range	33
3.3.3 Time to Collision	34

3.4	Quantifying Application Reliability	34
3.4.1	Size of the RIF Interval	35
3.4.2	Update Time	40
3.4.3	Number of Successfully Received Packets	40
3.5	Estimation of Minimum Required Communication Range	41
3.5.1	Stopping Distance	41
3.5.2	Driver Reaction Model	42
3.5.3	Probability of Crashing	43
3.6	Assessment Method	44
3.7	Summary	49
4	Environmental Effect on the Application Reliability	51
4.1	Measurement Equipment	51
4.2	Intersections in Urban Environment	52
4.2.1	Related Work	54
4.2.2	Measurement Setup and Scenarios	55
4.2.3	Effect of Intersection Topology	58
4.2.4	Effect of Traffic Conditions	60
4.2.5	Transmitter Positions	61
4.3	Vegetation at Rural Intersections	62
4.3.1	Related Work	63
4.3.2	Measurement Scenarios	64
4.3.3	Seasonal Effect	67
4.3.4	Urban vs. Rural Intersections	69
4.4	Impact of Weather Conditions	71
4.4.1	Related Work	72
4.4.2	Rain Attenuation	73
4.4.3	Attenuation in Snow	74
4.4.4	Attenuation in Fog	76
4.4.5	Attenuation in Gases	77
4.4.6	Attenuation in Sand and Dust Storms	77
4.5	Summary	78
5	Feasibility Analysis	81
5.1	Related Work	82
5.2	Simulation Setup and Scenario Description	83
5.3	Parameter Study	87
5.3.1	Effect of Message Generation Rate	87
5.3.2	3Mbps vs. 6Mbps	89
5.3.3	Effect of the Transmitter Position	90
5.3.4	Effect of the Intersection Topology and Tx - Rx Positions	92
5.4	Feasibility Analysis	96
5.4.1	Assumptions	97
5.4.2	Use Case Requirements	97

5.4.3	Evaluation Results	98
5.5	Summary	103
6	Real-Time Prediction of the Communication Link Quality	105
6.1	Related Work	106
6.2	Experimental Data	107
6.3	Algorithm 1: LUT-Based Estimation	107
6.3.1	Implementation Details	110
6.3.2	Results	116
6.4	Algorithm 2: Model-Based Estimation	124
6.4.1	Implementation Details	124
6.4.2	Results	127
6.5	Testing	128
6.5.1	Results	129
6.6	Summary	133
7	Conclusion and Outlook	135
7.1	Contributions	135
7.2	Open Issues and Future Work	136
7.2.1	Measurement Study	136
7.2.2	Simulation Study	137
7.2.3	Communication Link Reliability Prediction	138
	Bibliography	139

1 Introduction

1.1 Motivation

The high rate of traffic-related deaths and injuries requires a reduction of the accidents. In 2009 more than 35000 people lost their lives in traffic accidents in Europe [47] and the estimated economic loss in Germany alone exceeded 30.5 billion euros [2]. Therefore, the European Union initiates a variety of projects towards reducing the number of fatalities. The European Commissioner for Transport Siim Kallas stressed that the halving of the number of traffic fatalities and injuries by 2020 is a noble goal of the EU: "Since 2001 we have made a good progress and have been able to save nearly 80000 people, but the number of fatalities and injuries on our roads is still unacceptable. That is why our goal is to halve the number of traffic deaths by 2020" [47]. Furthermore, from a customer's perspective, safety is one of the most important innovative characteristics of a modern vehicle [139], therewith, the brand image is significantly influenced by the availability of the driver assistance and safety systems. All these facts make driver assistance and safety systems a strong focus of the automobile industry.

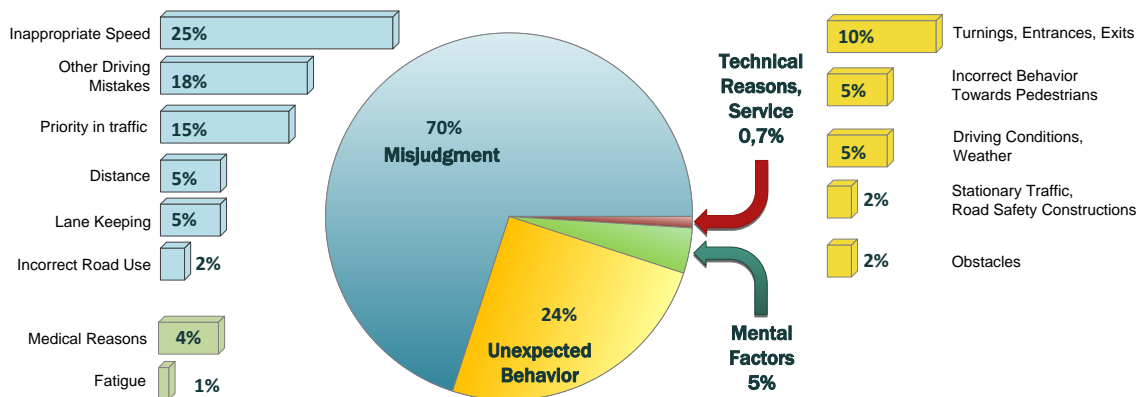


Figure 1.1: Accident causes, adapted from [93]

Safety systems can be divided into systems that aim to mitigate the severity of the accident (passive safety) and those that focus on prevention of the accidents (active safety). So far, car manufacturers have already ensured a major contribution towards reducing the accident consequences by developing a multitude of passive safety systems and, ultimately, it has come to a point where there are few further opportunities for development of this systems. The accident statistics, however, still remain depressing. Thus, further reduction of the accident number is a high-priority

aim for the OEMs. Towards this objective, the active safety is currently a strong focus of the automobile industry and research institutions. The aim of these systems is to timely notify the driver in the event of a hazardous situation and avoid a potential traffic accident.

Simultaneously with the worldwide increasing demand for the transportation, the challenges that a driver faces every day are growing considerably. Complicated traffic situations require a high level of concentration and quick reactions. According to the accident research statistics, 75% of fatal accidents are caused by such human factors as lack of attention, stress, loss of orientation, tiredness, medical condition, etc. In 24% of the cases the unexpected behavior is the cause of the accident and only 0.7% of accidents are due to technological failures (Fig. 1.1) [93]. For this reason, the potential of driver assistance and active safety systems, which support the driver in complicated traffic situations, is much higher when compared to passive safety systems (Fig. 1.2).

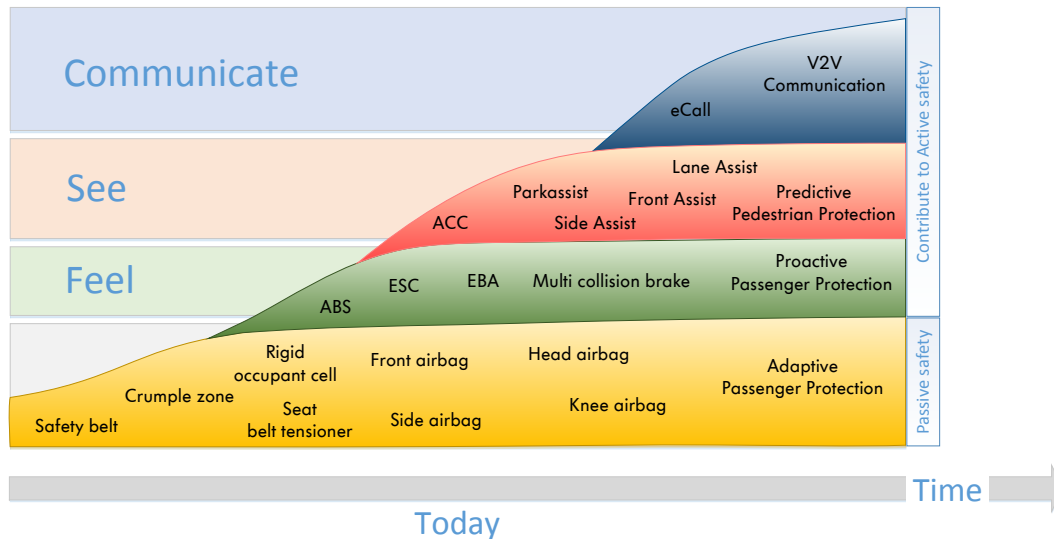


Figure 1.2: Safety potential of the driver assistance and safety systems. Passive Safety vs. Active Safety, adapted from [154]

However, despite their effectiveness, the abilities of driver assistance and active safety systems are limited by the working range of the on-board sensors, which can be additionally affected by the absence of line-of-sight (Fig. 1.3). Furthermore, these sensors cannot provide a host vehicle (HV) with such important information as acceleration, braking force, etc. of the remote vehicle (RV). In addition, the capabilities of the system with high-resolution sensors are limited by their high costs.

Vehicle-to-Vehicle (V2V) communications can significantly enhance the range of the on-board sensors and, thus, introduce a next step in the expansion of the potential of driver assistance and active safety systems. Direct communication with a possible collision object grants other traffic participants the opportunity to obtain the relevant traffic information earlier, which increases the reaction time of the driver and optimizes

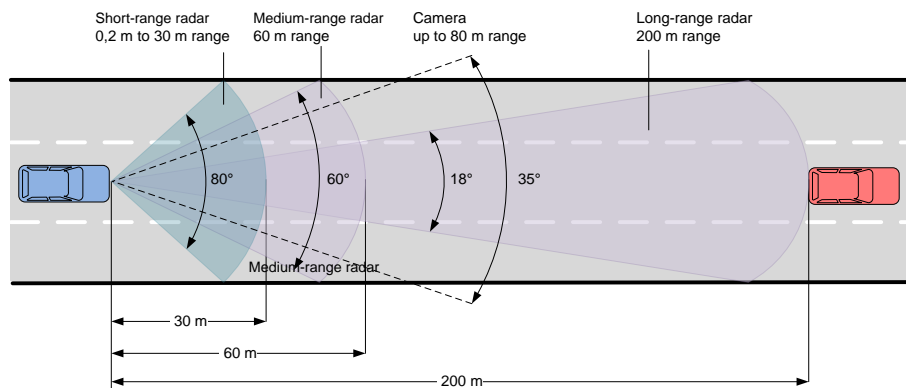


Figure 1.3: Line-of-Sight Detection, [48]

the traffic flow. From this perspective V2V communications can be considered as an additional sensor that provides usually not available environmental information. This is of particular significance in complex traffic situations, where the interpretation of the vehicle's surroundings with the on-board sensors is complicated due to a high number of mobile and static obstacles. Typical examples of V2V applications are Emergency Electronic Brake Light (EEBL), Forward Collision Warning (FCW), Intersection Collision Warning (ICW), Stationary Vehicle Warning (SVW), Traffic Jam Warning (TJW), Pre-Crash- Warning (PCW), etc. [53].

1.2 Problem Statement and Objectives

Over the past few years, safety-related V2V applications have already gained major attention from the industry, academia, as well as standardization bodies, and are envisioned to be the first V2V applications delivered to the mass market. Reliability of such systems is one of the key aspects towards achieving positive safety effect in the everyday traffic and wide customer acceptance. Thus, before the deployment phase, there are several issues concerning this topic that need to be investigated in detail.

Since V2V applications will be a subject of periodic message exchange over the wireless interface, their reliability will directly depend on the communication link quality. However, it can be negatively affected by a multitude of influencing factors, such as inhomogeneity of the ambient environment, high node mobility, frequent unavailability of the line-of-sight (LOS), sudden change of the network load, etc. Thus, the analysis of the main influencing factors on communication link quality in application-specific scenarios is vital to gain a deeper understanding of the type and severity of possible failures and their impact on the application reliability. Furthermore, it allows us to estimate how effectively V2V applications can support the driver in different traffic situations.

Due to the novelty of these applications currently there is no fully approved set of metrics, which would enable effective interpretation of the communication link quality to V2V applications. Up to date classical network metrics such as packet

delivery ratio (PDR) and received signal strength indication (RSSI) are frequently used for this purpose. However, since these metrics are not directly linked with operational requirements of V2V applications, they are also not always able to adequately address the reliability of these applications. Furthermore, different V2V applications may perform differently in the same communication conditions if they are a subject to different reliability requirements. Thus, a link must be established between communication performance metrics and application-specific reliability requirements to avoid misinterpretations in evaluation results.

Obviously, the effectiveness of new assessment metrics has to be verified in situations that would correspond to the reality as much as possible. Up to date there have been a lot of measurements done for mobile networks and applications, spanning a wide range of possible influencing factors on the communication performance. However, the knowledge about channel properties, which was obtained during these measurements, is inapplicable for assessment of communication link quality in DSRC channels. Highly dynamic vehicle terminals, low elevation of antennas, geometry of the vehicle roof, etc. make V2V systems differ greatly from conventional cellular systems. All these facts confirm the necessity of further measurements studies to investigate different environmental effects on V2V communication link quality.

Despite the importance of the measurement studies, simulations have to be used to characterize achievable application reliability in high network load scenarios. Up to today's point a plethora of simulation studies on performance of Vehicular Ad-hoc NETWORKS (VANET) have been conducted. In contrast to traditional approaches, where reception probability is obtained by taking into account each transmitter and receiver in the network, there is still a lack of simulation studies, which consider situation awareness. In such case only the nodes which are specifically relevant for the use case are evaluated while addressing application reliability. Other communication terminals will act as a source of interferences that affects the transmitters and receivers, for which reception probability is calculated. Such approach allows us to obtain more precise results, when evaluating complicated mobility scenarios.

Another important aspect towards ensuring the reliability of V2V applications when operating over the DSRC channel is to provide the application with an additional feedback about the current communication link quality in the real-time mode. Owing to the fact that the IEEE 802.11p standard does not utilize the traditional RTS/CTS (request-to-send/clear-to-send) mechanism, there is no direct possibility to realize a feedback between the transmitter and the receiver. Thus, real-time prediction mechanisms have to be used to achieve a better knowledge about application-specific traffic.

1.3 Contributions and Scope

The main contribution of this thesis is an effective approach for characterization of the attainable application reliability while operating over the DSRC channel. Further contributions cover extensive measurement and simulation studies as well as novel

method for communication link quality prediction in real-time modus. In particular, the contributions of this thesis are as follows:

- **Application reliability assessment method:** This thesis proposes an effective method for assessment of the application reliability when operating over the DSRC channel and establishes a link between underlying communication quality and specific application requirements. Specifically, we suggest a novel metric - the probability of the information freshness P_{RIF} and expand the communication range requirements through it. This metric equally allows for assessment of measurement or simulation data as well as for realization of the feedback to the application about the reliability level in the real-time modus. Furthermore, we suggest a simulation-based method towards quantifying the suggested metrics. We have presented this approach as well as evaluation results in [161].
- **Investigation of environmental effect:** Based on three measurement campaigns, this thesis provides a detailed analysis of relevant environmental factors, which can affect the reliability of V2V communications. Specifically, we focus on urban and rural intersections and investigate the effect of intersection topology, traffic conditions, transmitter positions as well as seasonal effects of the vegetation layer on the DSRC performance. To the best of our knowledge, the latter aspect has never been in the scope of previous research. We also compare attainable application reliability at urban and rural intersections and draw a conclusion about the criticality of these environments for V2V applications. Evaluation results concerning the effect of buildings and vegetation on the DSRC performance have been presented in [125], [141] and [161].
- **Analysis of traditional performance metrics:** In this thesis we also compare the assessment results obtained with the proposed P_{RIF} metric and those obtained with traditional network metrics and highlight possible risks when the latter ones are applied.
- **Weather impact:** This thesis provides a survey of weather conditions, which are relevant to V2V communications. Due to the relatively recent interest in the DSRC channels, currently the detailed knowledge about the impact of different weather conditions is not sufficient. Specifically, this research focuses on attenuation in rain, snow, hail, fog, gases, sand and dust storms.
- **Application-specific simulation approach:** In this work we propose a situation aware simulation approach, which allows for more precise evaluation of application reliability. In this case application reliability is calculated only for relevant for the use case communication nodes. Other terminals in the network, which are not relevant for the use case directly but for the overall communication picture, act as a source of interferences for the selected nodes [163].
- **Feasibility analysis of high network load communication scenarios:** This thesis conducts the feasibility analysis of communication scenarios under

high network load conditions and specifically focuses on the intersection scenarios. We analyze the effect of the buildings, positions of the communication terminals, message generation rate, data rate and penetration rate on the performance of V2V use cases, specifically ICW and FCW. The results have been presented in [163].

- **Framework for the communication quality prediction:** In this thesis we develop and prototypically implement a framework which enables real-time prediction of the communication quality. Towards this objective this work investigates two approaches, which are based on 1) learning of the context information during a certain time window in the past and 2) model-based estimation. The results have been presented in [162].

1.4 Assumptions

The focus of this research work is V2V safety applications. Therefore, owing to the current state of the art, the single-hop broadcast communication is considered. It is worth mentioning that this communication type is of major relevance for the road safety applications, as the decision of triggering the driver notification is frequently based on a highly dynamic picture of the vehicle's vicinity. Furthermore, due to the delay constraint nature of V2V applications, it is of higher importance to deliver information to the maximum number of nodes, instead of choosing the best link in order to send a message.

This research does not consider security and privacy issues [137], [25], [26], [156]. The information that is contained in successfully received packets is considered to be protected from unauthorized access or modification. Moreover, this research does not attempt to complement deliberations concerning which data is to be transmitted with application-specific messages. It considers packet size value of 500 bytes, which corresponds to those packets which are used in the key industrial and research initiatives [13], [12].

This research mainly refers to the Cooperative Awareness Messages (CAM) traffic, as it constitutes the main part of the channel load. Moreover, due to the prioritization technique implemented in the MAC layer and the event-driven nature of the Decentralized Environmental Notification Messages (DENM) triggering, it is very unlikely that timing constraints of the DENM transmissions will be exceeded. Other application-specific messages are not directly discussed in this thesis.

1.5 Outline

This thesis presents our contributions towards reliability assessment of V2V applications as well as evaluation results of our measurement and simulation studies. It further describes our approach for real-time communication link quality prediction and is organized as follows:

Chapter 2 focuses on the background of this work and discusses current state of the technology and the major research initiatives concerning V2V communications worldwide (important related work will be additionally given in the beginning of chapters 3 - 5). First this chapter highlights key characteristics and main challenges of VANETs and gives the overview of the current research activities in this field. Then we present V2V use cases, which are of particular importance to this research. Next, we introduce communication quality metrics, which are traditionally used to evaluate performance of V2V applications. Afterwards, we discuss the specifics of DSRC and give the technical details to the IEEE 802.11p standard. Finally, this chapter discusses the state of the research and highlights key V2V activities worldwide.

Chapter 3 presents our application reliability assessment approach. First, we give a survey of current research works in this area. Further, we discuss currently used communication performance metrics, specifically maximum allowable latency, minimum required frequency and communication range. Afterwards, we derive a novel application reliability metric: probability of the information freshness P_{RIF} , and expand the definition of communication range through it. After that, this chapter concentrates on quantifying application reliability by deriving numerical values of the required information freshness (RIF) interval, number of successfully received packets in this time interval. It also presents a method for estimation of the minimum required communication range based on the simulation study. Finally, we introduce our assessment method and provide several evaluation examples.

Chapter 4 presents the results of three measurement campaigns conducted to investigate the environmental effect on the application reliability. First, we give technical information about the utilized measurement equipment, measurement setup and scenarios and overview the main measurement campaigns at 5.9 GHz in urban and rural environments. It is then followed by reporting our measurement results at urban and rural intersections. Thereby, this chapter focuses on the following effects: intersection topology, traffic conditions, transmitter positions and seasonal effect of the vegetation layer. Further, this chapter compares achievable application reliability at urban and rural intersections and compares the effectiveness of P_{RIF} versus PDR towards its characterization. Additionally, we provide a survey of the weather conditions which may impact the application reliability. First, we introduce key measurement campaigns devoted to the investigation of weather impact on radio wave propagation. Finally, we focus on the attenuation of the radio waves at 5.9 GHz in rain, snow, fog, atmospheric gases, water steam, sand and dust storms.

Chapter 5 performs a feasibility analysis of different intersection scenarios specifically for ICW and FCW use cases in high network load conditions. We first provide an overview of the relevant research works. Next, we describe simulation setup and scenario topology as well as specify the use case requirements on the probability of the information freshness P_{RIF} , reliable and minimum required communication ranges. Afterwards, we identify effect of the message generation rate, data rate, penetration rate, intersection topology and distance between the transmitter to the intersection center. Finally, we report the results of feasibility analysis and define parameter combinations that are optimal for each use case.

Chapter 6 focuses on the development and implementation of the framework, which enables a real-time prediction of the application reliability. The measurement data, which was used for the development of the framework, was obtained during 4.5 months of the sim^{TD} field trials. First, this chapter surveys relevant research work in this field. Further, we investigate the approach, which is based on the learning of the context information in a certain evidence window in the past, give details to the implementation and define the optimal size of the evidence window. Further, this chapter reports achieved prediction accuracy of the framework P_a under different conditions and suggests two optimization methods towards its enhancing. Afterwards, we investigate the benefits of the model-based estimation and use a logit-model as a basis for the prediction. Next, we provide the implementation details, then report achieved prediction accuracy P_a and compare the effectiveness of both approaches. Finally, we conduct an additional measurement campaign to validate both approaches using measurement data which was obtained not through the sim^{TD} field trials and come to the conclusion on the flexibility of each approach.

Finally, *chapter 7* summarizes the results and contributions of this thesis and concludes this work by giving an outlook on open research issues and ideas, which, however, are beyond the scope of this research.

2 Fundamentals of V2V Communication

V2V communication enables a wide range of cooperative applications aimed at reducing road hazard situations as well as enhancing traffic efficiency and individual driving comfort, expanding therewith the boundaries of the modern driver assistance systems. It has attained a significant prominence after Federal Communications Commission (FCC) reserved the 5.9 GHz frequency band for the DSRC-based applications as a part of the ITS program. This chapter addresses the main technological background aspects of DSRC as well as discusses the challenges, to which the nodes will be exposed while operating over the DSRC channel. Furthermore, it provides an overview of the key research initiatives and activities in this field.

This chapter is organized as follows: section 2.1 first overviews the main characteristics and challenges of vehicular ad-hoc networks. Further, it surveys the basic Vehicle-to-X (V2X) use cases and concentrates on the co-operative safety domain (V2V safety applications). Afterwards, this section provides technical details of DSRC, specifically focusing on the protocol stack, which is utilized in Europe and on the IEEE 802.11p PHY and MAC layer modifications. Section 2.2 discusses the key V2V activities world-wide. Finally, section 2.3 summarizes the knowledge presented in this chapter.

As it has already been mentioned in chapter 1, this chapter provides a general discussion of the key technological aspects and important research projects. Additional discussion of relevant related work will be given separately at the beginning of each following chapter.

2.1 State of the Technology

This section surveys key technological aspects of V2V communications, including background information on VANETs, European C2C CC protocol stack and the IEEE 802.11p standard.

2.1.1 VANETs as a Subclass of Wireless Mobile Ad-Hoc Networks

Wireless networks have become an inseparable part of the modern industry, research and social life and can be generally divided into two groups. The first are distributed over the geographical areas and use the fixed-location wired base stations and realize one-hop connection with mobile users and base stations over a wireless interface (cellular networks and WLANs). The other type is wireless ad-hoc network, where network nodes communicate with each other over the wireless channel without a fixed

infrastructure. The nodes in such network can be mobile or static and each of them can act as a transmitter, receiver or router. In the last few years vehicular ad-hoc networks have gained a lot of attention and become an active field of research and development activities due to their high potential towards enhancing traffic safety and efficiency.

VANETs represent a highly mobile self-organized and self-managing ad-hoc network, where vehicles that share the same geographical location at the same time act as communication nodes. Such networks can be immediately deployed in any geographic area without using fixed infrastructure elements or system administration staff. Furthermore, the fact that VANETs are not going to have energy, computing performance and memory restrictions allows for realization of a wide spectrum of sophisticated V2V applications. Safety use cases will make use of broadcast transmission, since in their case the delivery of the safety messages to a maximum number of nodes in the vicinity has to be ensured. The uni- and geocasting will be mainly used to support traffic efficiency and infotainment applications.

Due to the delay sensitive nature of most services, which are supported by VANETs, the nodes in such a network are not going to aggregate and store information but rely on periodic exchange of the short status packets instead. Each packet contains up-to-date information about the current geographical position and kinematic properties of the vehicle. In this manner the vehicles create the so called distributed awareness. Due to the same reason, retransmissions and RTS/CTS strategies are typically omitted in VANETs, assuming that it can be compensated by the high updating frequency of the message exchange and constant renewal of the information transmitted with each packet. Further reason is avoiding extreme amounts of additional traffic, which can cause a broadcast storm and prevent efficient message dissemination in the network.

A wide range of services envisioned in VANETs also implies a set of specific requirements concerning reliability, delay, fairness and robustness issues. Despite their high potential, VANETs, however, exhibit a set of challenges, which need to be taken into account in order to meet these requirements. Unlike conventional mobile ad-hoc networks, VANETs are the subject of a highly dynamic and large dimension network topology with rapidly changing configurations. For instance, in the highway scenarios vehicle velocities may reach up to 250 km/h, while the node density and the penetration rate can be extremely low, which exhibits the problem of short link durations and the necessity of the forwarding strategies. This, however, can migrate rapidly to the highly dense network configuration in the event of a traffic jam, where a key issue would be to provide a fair channel access to each node in the network. Urban scenarios provide additional challenges, since vehicle routes and density change more frequently due to the traffic lights and compelled braking/turning maneuvers.

Further challenges in VANETs are exhibited by the environment itself, where the multitude of mobile and static interaction objects (IOs) can provoke signal strength degradation due to shadowing effects and when combined with high node mobility - both, time- and frequency-selective fading. For a comprehensive overview refer to [95], [96], [152], [90], where the authors provide an elaborate survey of the state-of-the-art V2V channel measurement campaigns and modeling approaches. Furthermore, the

results of extensive measurements campaigns in various vehicular environments are presented in [103], [105], [104], [43] and [140].

Another adverse medium condition is due to the channel congestion in the presence of a great number of network nodes concentrated in the small area and high penetration rates. Since in VANETs there is no "master" that would control the channel access the nodes have to regulate it themselves in a fair manner, waiting for the channel to become idle for a certain time before transmitting a packet. In congested scenarios not all nodes which compete to access the channel will be able to send scheduled packets. It will provoke a significant degradation of the reception rates due to the packet drop on the transmitter side. In the most critical cases it can paralyze a complete network, which strongly motivates the utilization of different congestion control mechanisms.

The topic of preventing network overload and maintaining connectivity under different and dynamic traffic conditions has been addressed by many researchers. The authors in [160] analyze existing concepts for network congestion control and develop a framework, which addresses stringent delay, reliability and dissemination area requirements of the safety messaging in VANETs. The analysis and design of effective low-overhead transmission power control for VANETs is presented in [94]. The protocol suggested in [147] utilizes a transmission power control strategy for minimization of packet collisions and is one of the most popular protocols for cooperative safety applications. Huang et al. in [69] propose another message generation rate and transmission power adaptation approach based on vehicular dynamics. In [70] and [71] they develop and evaluate an adaptive rate control algorithm, which utilizes a closed-loop control concept and utilize network condition and vehicle tracking error information.

An important issue of channel load minimization and simultaneous fulfillment of the application-level performance constrains is addressed in works of Sepulcre et al. In [131] the authors provide a survey of decentralized methods for channel load control in VANETs and focus on transmission power and rate control approaches. Further they discuss open research issues and challenges towards guaranteeing satisfaction of different application requirements. In their other work [128], the authors illustrate the necessity of considering the requirements of cooperative safety applications in the design of congestion control protocols. In [129] the authors propose a novel proactive congestion control policy for VANETs, where communication setting of each network node will be adapted according to individual application-level requirements. In [130] the authors develop a contextual congestion control approach, which utilizes traffic context information of each network node to reduce the channel load and simultaneously satisfy safety applications requirements.

A further challenge in VANETs is the hidden-node problem, which takes place when two nodes are out of the interference range of each other but both are able to communicate with several nodes that are located within their transmission range. In such situation both stations will sense the channel to be idle and try to transmit a packet simultaneously, which will cause a packet collision. A major work devoted to this topic is performed in a series of works of Torrent-Moreno et al. in [145], [147], [144], who have identified the hidden terminal problem as a primary reason of reception

rate degradation in VANETs and implemented a distributed fair power adjustment mechanism to address this problem. The authors in [124] investigate packet reception from the perspective of Signal to Interference plus Noise Ratio (SINR) and identify the hidden terminal problem to be one of the main factors that dominate degradation of packet reception probability. The work presented in [83] provides the analysis of the connection between selected transmission range and packet generation rate on the occurrence of packet collisions due to the hidden node problem. The authors aim to minimize the number of hidden terminals in a specific region of interest, taking into account requirements of different cooperative applications. Furthermore, the hidden node problem is addressed in [56], where the authors have shown that the hidden terminal phenomenon can considerably limit the capacity of the vehicular broadcast network and decrease performance of V2V applications. They investigate the effect of different combinations of message generation rate and broadcast range on the efficient dissemination of vehicle tracking information and suggest that channel busy ratio can be utilized as a feedback measure to develop feedback control schemes for transmission range adaptation.

The characteristics and challenges in VANETs have been reviewed in [146], [32], [86]. The authors in [158] review research works, which have been conducted in routing, broadcasting, quality of service (QoS), and security VANET areas.

2.1.2 Survey of V2X Use Cases

Future VANETs will support a wide range of applications and services, which according to [53] are generalized in three domains: co-operative road safety, traffic efficiency and infotainment.

Co-operative road safety applications aim to prevent possible cross-traffic, rear-end and frontal accidents, by earlier driver notification or active intervention of the vehicle safety systems and, therewith, decreasing the number of traffic fatalities and occupant injuries. According to [53] they are divided into five different groups: 1) vehicle status warnings, 2) vehicle type warnings, 3) traffic hazard warnings, 4) dynamic vehicle warnings and 5) collision risk warning. Since V2V safety applications contribute to the preservation of lives, such systems must constantly maintain a perfect situation awareness to prevent possible false negative and false positive cases. This implies high reliability requirements imposed on such system as well as the necessity of safeguarding strategies in case of communication failures. A great contribution to the development of these applications has been made through the VSC and VSC-A, COMeSafety, ACTIVE, sim^{TD} projects. Due to high latency requirements co-operative road safety applications are a subject of V2V communication.

As it has already been stated in chapter 1, this thesis focuses solely on V2V use cases, specifically on Intersection Collision Warning and Forward Collision Warning applications:

- *Intersection Collision Warning* informs/warns the vehicles approaching the affected intersection area about possible cross-traffic collisions. This use case

includes both traffic-light-controlled intersections and uncontrolled intersections.

- *Forward Collision Warning* assists the driver to avoid/mitigate possible longitudinal collisions between the vehicles travelling in the forward direction and in the same lane through acoustic/visual notifications.

In conjunction with the driver notification concept the future V2V safety applications are expected to notify the driver about a potentially hazardous situation with several information levels, which are defined according to the remaining time to a possible collision (TTC). The notification format alters as the collision probability increases with the decrease of TTC. According to this, three notification levels are defined: *Information*, *Awareness Warning* and *Automatic Pre-Post Crash*.

In the event of triggering the Information level, the driver will be notified via a simple graphic indication in the electronic visual display. If given information is not followed by the reaction of the driver and TTC continues to decrease, it entails the activation of the Awareness Warning level. At this stage the driver can be notified through the evolved graphic or acoustic warning, activation of several LED band segments or other technologies. In the event of expiring of the Awareness Warning level time threshold, the notification progresses into a direct intervention of the active safety systems such as automatic braking and steering (Automatic Pre - Post Crash level). According to [73] and [65] a driver assistance system should notify the driver 3s before the possible collision. The last time instant when intervention of the vehicle safety systems is still possible is often considered to be 1s before the impact.

Traffic efficiency applications address the coordination and optimization of the traffic flow as well as driver assistance by providing a comprehensive set of services, such as traffic light optimal speed advisory, announcement of contextual speed limits, enhanced route guidance and navigation, high-speed tolling [53].

Infotainment applications span comfort and entertainment spheres of everyday traffic, such as various "pay as you drive" services, point of interest notifications, media downloading, distributed passengers teleconference, instant messaging, remote diagnosis [53]. Traffic efficiency and infotainment applications are a subject of Vehicle-to-Infrastructure (V2I) communication.

Application-Specific Messages

As it has already been mentioned above in this section, V2V safety application will rely on broadcast message dissemination method to cover the maximum number of nodes in their surroundings and achieve best possible co-operative awareness. The information exchange generally follows two patterns: periodic broadcasts of short beacon messages, so called Cooperative Awareness Messages, and exchange of event-based messages that are issued only if a predefined triggering condition occurs - Decentralized Environmental Notification Messages. CAMs contain up-to-date geographical position and kinematic properties of the vehicle and are issued with a high update frequency (often 10 Hz is assumed). Additionally, specific vehicle information as, for instance, status of the turn signal can also be transmitted with a

CAM. Owing to this information exchange, vehicles are able to build a highly dynamic awareness picture of their instantaneous environment and detect complex maneuvers of other vehicles in time. For more details refer to [55].

To capture the dynamics of the vehicular environment and adjust the updating frequency to it, the CAM generation rate is envisioned to be not a constant value [55]. The CAM Management will generate and pass messages to the lower layers of the protocol stack according to certain rules, with predefined maximum generation time interval between CAMs of 1 s and minimum time interval of 0.1 s. A CAM will be generated when absolute difference between the current heading (towards North) and the heading contained in the last CAM becomes greater than 4° , when the distance between the current position and the position in the foregoing CAM exceeds 5 m or when the absolute difference between the current speed and the last speed exceeds 1 m/s. Finally, it will be evaluated every 100 ms whether a CAM is to be triggered.

On the other hand, a DENM is issued to alert traffic participants only when a specific dangerous event is detected, such as emergency braking, hazard warning lights, traffic jam, bad weather conditions, obstacles on the road, etc. Such messages will be broadcasted and forwarded to the area of interest and terminated once a certain time or spatial validity threshold is expired. For more details to the specification of DENM refer to [54]. Currently, triggering conditions are being reviewed and standardized through the Car 2 Car Communication Consortium (C2C CC) activities.

Communication Performance Requirements

V2V safety applications will impose certain communication performance requirements to build a highly precise picture of their vicinity and perform the optimal triggering of the driver notifications. Up to now, different aspects of the application requirements have been identified through several research initiatives in [45], [150], [151] and ETSI specification [53], where [53] offers the most comprehensive classification. In the present time the most up to date reference is the SAE Standard J2945 - "Dedicated Short Range Communication (DSRC) Minimum Performance Requirements" [10], which is currently under development. Communication performance requirements of the road safety and traffic efficiency applications which have been derived through the USA and EU initiatives have been summarized in the Internet Engineering Task Force (IETF) [6] internet draft in [75] and then reviewed in [76] (Table 2.1).

The numerical values of the requirements presented in Table 2.1 may vary according to the design and envisioned application purposes. For instance, according to VSC [150] and VSC-A [151] final reports as well as ETSI specification [53] most of the V2V applications require a minimum updating frequency of 10 Hz, maximum allowable latency of 100 ms and reliable communication range of 300 m. On the other hand, the Pre-Crash Sensing Warning requires due to its purposes a message generation rate of 50 Hz, maximum allowable latency of 20 ms and reliable communication range of 50 m [75]. Co-operative following applications, such as C-ACC (Co-operative Autonomous Cruise Control System) or Platoon (Co-operative Vehicle-Highway Automation System), require unicast communication, minimum beaconing frequency of 2 Hz and

Table 2.1: Communication performance requirements [75]

Type of Communication	(1) source-destination of the transmission (infrastructure-to-vehicle, vehicle-to-infrastructure, vehicle-to-vehicle); (2) direction of the transmission (one-way, two-way), and the DSRC (IEEE 802.11p) communication; (3) source-reception of communication (point-to-point, point-to-multipoint)
Transmission Mode	describes whether the transmission is triggered by an event (event-driven) or sent automatically at regular intervals (periodic)
Minimum Frequency	defines the minimum rate at which a transmission should be repeated (e.g., 1 Hz)
Allowable Latency	defines the maximum duration of time allowable between when information is available for transmission (by the sender) and when it is received by the receiver (e.g., 100 ms)
Data to be Transmitted and/or Received	describes the contents of the communication (e.g., vehicle location, speed and heading). Design considerations include whether or not vehicles make periodic broadcasts to identify their position on the roadway and how privacy is best maintained
Maximum Required Range of Communication	defines the communication distance between two units (e.g., two vehicles) that is required to effectively support an application

maximum latency of 100 ms [53]. The C&D project also derives performance communication requirements for the C-ACC [107]. According to the C&D requirements document, the C-ACC requires minimum frequency of 10-25 Hz and allowable latency less than 200 ms. The host vehicle has to receive information within a communication range less than 250 m, which approximately corresponds to maximum 15 vehicles ahead of it. It is, however, worth noting that notwithstanding differences while quantifying performance requirements, all research works predominantly refer to the performance requirements cited in Table 2.1.

2.1.3 Dedicated Short Range Communication

DSRC operates in the 5.9 GHz frequency band and is facilitated by the IEEE 802.11p standard [17], which was adopted on July 15, 2010. It is an amendment of the well-known IEEE 802.11 standard [16], which ensures robust communication in the context of highly dynamic vehicular environment by introducing several modifications to the physical (PHY) and Medium Access Control (MAC) layers.

In the following, an overview about the C2C CC protocol stack architecture will be given as well as details on the application layer, the IEEE 802.11p PHY and MAC layers.

Protocol Stack Architecture

Fig. 2.1 illustrates the protocol stack architecture of a V2V communication system (C2C CC protocol stack) as used in Europe. It can be observed, that the V2V system makes use of three basic technologies: IEEE 802.11p, IEEE 802.11a/b/g/n and other radio technologies (e.g. UMTS). Safety applications, however, specifically utilize V2V transport and network layers and IEEE 802.11p PHY and MAC layer extensions.

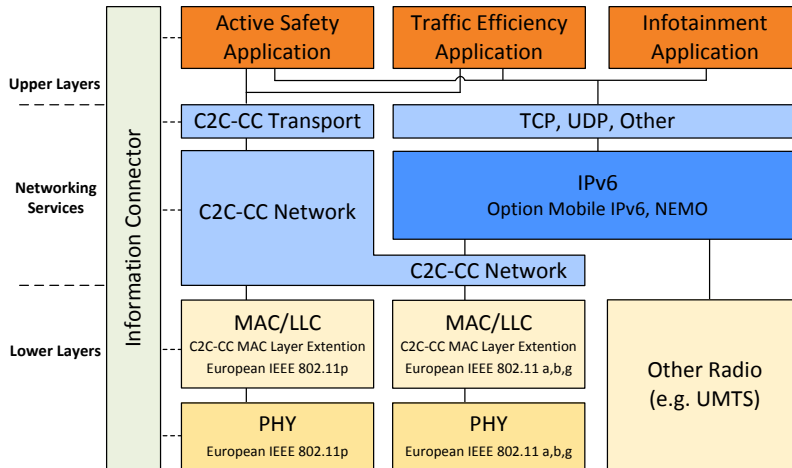


Figure 2.1: Protocol architecture of V2V Communication System in Europe [37]

The C2C CC transport layer provides a traditional set of transport layer functionalities. Among other services, data multiplexing/demultiplexing is of particular importance to the safety applications in situations when more than one application will actively communicate between two or more nodes. The V2V transport layer is currently under standardization.

The main goal of the C2C CC network layer is to enable a multi-hop communication mode, which is based on geographical addressing and routing functionalities as well as to realize V2V specific functions, such as congestion control and efficient information dissemination. The main components of the network layer protocol are: beaconing, forwarding, location-service, packet assembly/disassembly, congestion control and priority handling. The V2V network layer supports different forwarding unicast- and broadcast schemes, such as greedy forwarding with the "Maximum Progress Within

Radius" (MFR) rule or "Simple flooding with duplication detection" [121].

Fig. 2.1 demonstrates that only V2V network protocol can access the IEEE 802.11p interface, but it is also able to access regular IEEE 802.11a/b/g interface and has additional interface to Internet Protocol Version 6 (IPv6), so non-safety applications will also be able to use C2C CC network layer functionalities.

Moreover, safety applications can also transport the data over the standard IEEE 802.11a/b/g or other wireless technologies (e.g. in case of not critical safety applications) when the interaction with infrastructure elements is required.

Non-safety applications use conventional protocol stack and utilize TCP and UDP (or other) transport protocols over IPv6. As it has already been stated above, they are also able to access the functionalities which are provided by the C2C CC network layer (e. g. multi-hopping) or transport the data over IEEE 802.11a/b/g.

The aim of Information Connector (IC) module is to ensure efficient cross-layer exchange of non-interpreted raw data between layers. Each corresponding layer is responsible for the further interpretation of the raw data. The communication mechanism between layers is the publisher-subscriber mechanism, where each protocol can publish specific information or subscribe for specific information and IC manages the distribution of the published data. For more details refer to [37], [121].

V2X Application Layer Model

Special attention should be paid to the V2V application layer, which is an extension of a traditional Open Systems Interconnection (OSI) reference model. Fig. 2.2 shows, that the upper layers are divided into the application and facilities layer. In application layer each application can be assigned to one of three ITS classes: road safety, traffic efficiency and other applications. The facilities layer consists of application, information and communication support facilities.

The *application support* includes main functionalities, which facilitate the ITS applications. They are: station lifecycle management, automatic services discovery, download and initialization of the new services, Human Machine Interface (HMI) generic capabilities, etc. [53].

The *information support* facility inherits many functions of the presentation layer of the OSI model and ensures data management. The information support is responsible for the fusion of location referenced and time specific data from mobile and static sources and ensures the time validity of the data. The data fusion is achieved mainly with Local Dynamic Map (LDM) functionality, which is able to access the information from both, different data sources and ITS messages and build a local environment data model.

The *communication support* facility includes the session layer of the OSI model. The aim of this facility is to ensure the communication modes which are required by the applications through cooperation with transport and network layers.

The facility layer also manages four Service Access Points (SAPs): FA-SAP (Facilities/Applications - Service Access Point), SF-SAP (Security/Facilities - Service Access Point), MF-SAP (Management/Facilities - Service Access Point), NF-SAP (Network -

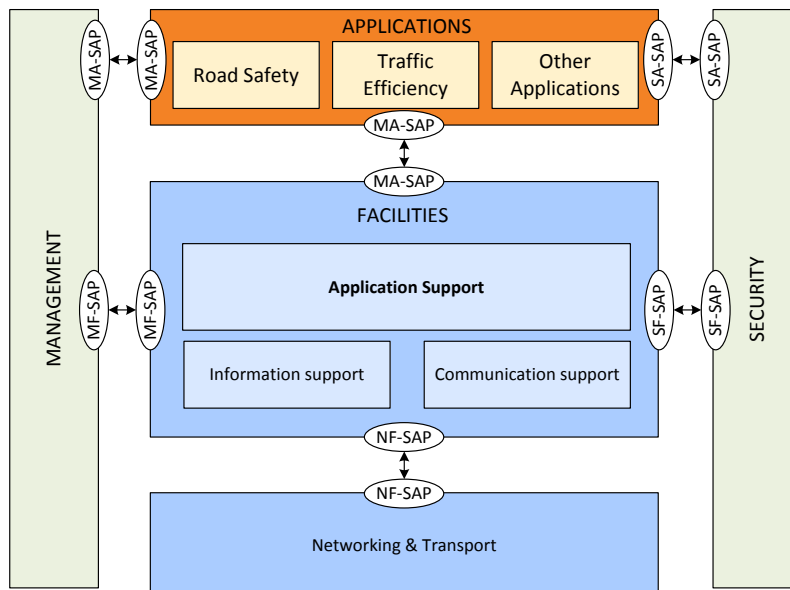


Figure 2.2: ITS Application/Facilities overview [53]

Transport/Facilities - Service Access Point). Each SAP interface enables full duplex data exchange between corresponding layers. For more details refer to [53].

Physical Layer

IEEE 802.11p PHY is inherited from IEEE 802.11a. It utilizes Orthogonal Frequency-Division Multiplexing (OFDM) modulation scheme and relies on reduced channel spacing of 10 MHz, instead of usual 20 MHz to compensate effects of time and frequency-selective fading. It also relies on a multichannel architecture, which includes one control channel (CCH) and six service channels (SCHs). CCH is assigned for the transfer of the network control and safety-related information, such as periodic information about vehicle position and kinematics or specific event-based information. The service channels can be optionally used for the transfer of non-safety related traffic, such as weather and road conditions, available parking spots as well as infotainment and internet access application traffic.

Another important feature of the IEEE 802.11p standard is an efficient channel coordination mechanism, which allows transceivers to alternately listen to CCH and SCH frequencies during a periodic time interval. The channel time is divided into 100 ms long synchronization intervals that consist of the equal-length Control Channel Interval (CCHI) and Service Channel Interval (SCHI). During the CCHI transceivers will mandatory listen to the CCH frequency and during the SCHI all devices can optionally switch to one of the six SCH frequencies. To protect transmissions from possible errors due to inaccurate time synchronization between different communication stations, PHY also defines the Guard Interval (GI) of 4 ms long, which always precedes the CCHI. In this time the channel is declared to be busy, thus, all the stations are not allowed to transmit in this time interval and are forced to choose a random back-off

time before the next transmission.

IEEE 802.11p PHY supports a dynamic Transmit Power Control (TPC) control scheme, which adjusts the transmission power for each packet if it is requested from the upper layers. The minimum threshold for the transmission power is equal to 3 dBm. Furthermore, the 802.11p PHY layer supports the following data rates: 3; 4.5; 6; 9; 12; 18; 24; 27 Mbps, where default data rate is equal to 6 Mbps. The maximum allowed equivalent isotropically radiated power (EIRP) is equal to 33 dBm. Table 2.2 gives an overview of the used physical layer implementations in IEEE 802.11a and IEEE 802.11p [97].

Table 2.2: Comparison of the used physical layer implementations in IEEE 802.11a and IEEE 802.11p [97]

Parameters	IEEE 802.11a	IEEE 802.11p half clocked mode	Changes
Bit rate (Mbps)	6, 9, 12, 18, 24, 36, 48, 54	3, 4.5, 6, 9, 12, 18, 24, 27	Half
Modulation mode	BPSK, QPSK, 16QAM, 64QAM	BPSK, QPSK, 16QAM, 64QAM	No change
Code rate	1/2, 2/3, 3/4	1/2, 2/3, 3/4	No change
Number of subcarriers	52	52	No change
Symbol duration	4 μ s	8 μ s	Double
Guard time	0.8 μ s	1.6 μ s	Double
FFT period	3.2 μ s	6.4 μ s	Double
Preamble duration	16 μ s	32 μ s	Double
Subcarrier spacing	0.3125 MHz	0.15625 MHz	Half

Medium Access Control Layer

The Medium Access Control (MAC) layer coordinates the access to a radio channel, which is shared between all the network nodes, in order to minimize packet collisions and increase the reception probability. The IEEE 802.11p MAC makes use of the enhanced distributed channel access (EDCA) mechanism which was introduced in the IEEE 802.11e amendment [15]. It added QoS to the basic distributed coordination function (DCF) found in IEEE 802.11, which is a carrier sense multiple access with collision avoidance (CSMA/CA) algorithm. Thus, the CSMA/CA in IEEE 802.11p gained the possibility to prioritize the traffic.

In CSMA/CA each node is passively listening to the channel and if it is sensed idle for a predetermined time interval, the so called arbitration interframe space (AIFS), the node is allowed to start a transmission directly. If the channel is sensed busy or becomes busy during the AIFS, the node has to perform a backoff procedure: delay its channel access according to a random time interval. In this case a node randomly chooses an integer from the uniformly distributed $[0, CW]$ interval and multiplies it by

the slot time $aSlotTime$, where CW is the current size of the contention window and value of the slot time is fixed and determined by the utilized PHY layer. The resulted value is then set as a backoff value and will be decremented per slot time only if the channel is idle. The station will be allowed to perform a transmission immediately after the backoff counter reaches zero.

EDCA, in its turn, allows each node to maintain the data in four different priority queues or access categories (ACs), where different values of AIFS and CW are assigned to each queue. ACs with higher priority have smaller AIFS and shorter CW. This allows for increase of the channel access probability for the traffic with the higher priority against the low priority traffic and thus, ensures transmission of safety messages within timely constraints even under the condition of higher channel loads.

ACs are divided into AC_VO (Voice), AC_VI (Video), AC_BE (Best effort), AC_BK (Background), where AC_VO has the highest priority and AC_BK the lowest. AIFS for each access category is found as:

$$AIFS[AC] = AIFDN[N] \times aSlotTime + aSIFSTime \quad (2.1)$$

where AIFSN is the number of slots after a short interframe space (SIFS) interval on which a node should postpone the transmission or activation of the back-off mechanism. The values of $aSlotTime = 13 \mu s$ and $aSIFSTime = 32 \mu s$ are default for 10 MHz channels of the OFDM PHY layer. The minimum and maximum values of the Content Window are equal to $aCWmin = 15$ and $aCWmax = 1023$. The default AIFSN and CW sizes for IEEE 802.11p access categories are listed in Table 2.3 [52]. For more details refer to [17] and [52].

Table 2.3: The resulting AIFS and CW sizes for 802.11p ACs [17]

AC	CW_{min}	CW_{max}	AIFSN
AC_VO	$(aCWmin+1)/4-1$	$(aCWmin+1)/2-1$	2
AC_VI	$(aCWmin+1)/2-1$	$aCWmin$	3
AC_BE	$aCWmin$	$aCWmax$	6
AC_BK	$aCWmin$	$aCWmax$	9

2.2 V2V Activities Worldwide

In the recent years V2V communications have gained a major popularity and interest in the global transportation industry. Currently, V2V research and development projects are highly prioritized and promoted by many countries. The largest contributions in this area have been made primarily through the USA, Japan and EU research and industry initiatives.

2.2.1 The USA

In the USA a great attention has already been devoted to the research and development of the V2V technology. The Department of Transportation (U.S. Department of Transportation, DOT) [14] and National Highway Traffic Safety Administration (NHTSA) [9] are among the main driving forces that initiate and promote a vast range of projects. In addition, many OEMs, suppliers, consortia like CAMP (Crash Avoidance Metrics Partnership) are actively involved in this field.

The Crash Avoidance Metrics Partnership (CAMP) was established by Ford and General Motors to accelerate the implementation of measures that can decrease the number of accidents with passenger cars and, thus, improve the road safety. Today more OEMs are the members of CAMP (BMW, Daimler Chrysler, Nissan, Toyota, Volkswagen, etc.). CAMP projects are mostly funded by the USDOT and mainly focus on the development of the industry-based research platforms as well as investigation of safety-related technologies, which can minimize the most common and most dangerous accident scenarios. Currently, CAMP concentrates on the Security and Interoperability Development project as well as the Safety Pilot project [84].

The main objective of the **CAMP Security and Interoperability Communications** project was to achieve interoperability and scalability of DSRC between vehicle manufacturers. In addition, it had to ensure the solution of such key issues as identification of weaknesses in the standards as well as definition of corresponding changes that are to be made. This activities were already performed and completed in 2012 [84].

The **Safety Pilot** project was divided into two phases: Driver Clinics and Model Deployment. The objective of the Driver Clinics was to develop per each participating OEM two to four V2V capable vehicles with an integrated driver notification system and fully operational V2V applications. The objective of the Model Deployment was to provide 60 V2V capable vehicles with integrated safety applications and 2500 "Here I Am" capable vehicles and integrate those on public roads. Further goal was to test the effectiveness, usability, system maturity, and public acceptance of V2V and V2X applications by driving demonstrations. The Safety Pilot ran from 2011 to the first Quarter of 2013 [8].

Already completed projects such as for example VSC [150], VSC-A [151] have made a significant contribution to the development of V2X technology. The following is a brief overview of the main goals and objectives of these projects.

The main objective of the **Vehicle Safety Communications (VSC)** project was to evaluate V2V safety applications. With this purpose seven car manufacturers (BMW, DaimlerChrysler, Ford, GM, Nissan, Toyota and VW) formed the VSC Consortium (VSCC) that participated in the project together with the USDOT. This project selected the initial communication requirements for specific applications and performed the DSRC tests. In addition, a strong focus of the VSC was the development of the DSRC standards that can support the requirements of the safety applications. Based on potential safety benefits, there were eight application scenarios prioritized

for the further research. Four of them are designed for V2V communication and the other four have the communication between vehicles and the infrastructure in focus [133].

The **Vehicle Safety Communications - Applications (VSC-A)** project was based on the previous achievements, which were obtained through the CAMP VSC project, as well as on previous NHTSA active safety related projects. The scope of the VSC-A project was to develop a common communication architecture for safety applications as well as required protocols and messaging frameworks for achieving the interoperability between different vehicle manufacturing. In addition, the project analyzed potential benefits of the market penetration of V2X safety applications. Furthermore, the development of the feasible and usable security solutions as well as development of the objective test procedures for V2V safety applications was within the scope of VSC-A [133].

The **Vehicle Safety Communications Consortium 3 (VSC3)** has signed a cooperation agreement with the USDOT for two projects: **V2V I (V2V - Interoperability)** and **V2V CS (V2V Communication Security)**. The V2V-I project is divided into two stages: interoperability and scalability. The V2V CS project focuses on certificate management, privacy and misbehavior detection [132]. These activities were finished in 2012.

2.2.2 Japan

In Japan V2X communication is already a well-known as well as highly prioritized by the government topic. The main contribution to the development of the V2X technology is achieved through projects, which are funded by the Ministry of Land, Infrastructure and Transportation (MLIT), the Ministry of Internal Affairs and Communications (MIC), the Ministry of Economy, Trade and Industry (METI) and the National Police Agency (NPA).

In Japan, the research and development activities are mainly concentrated in the infrastructure domain. For instance, the electronic toll collection system based on the DSRC technology (ETC, Toll Collect) has existed in Japan for many years and currently allows realization of data exchange with V2I messages in addition to the ETC messages. To enable V2V communications, the activities are focused on the development and testing of the modified WAVE standard operating at 5.8 GHz and a new standard in the 700 MHz frequency band [123].

Since the focus of this thesis is V2V communication, the research activities in Japan are beyond the scope and not going to be discussed further.

2.2.3 Europe

Due to the high implementation and maintenance costs of the V2I technology the EU concentrates a great part of its resources on the research and development of V2V communications. In the European Union, similarly with the USA, the V2V-related projects are also carried out at the national level. The Car 2 Car Communication

Consortium [38] is one of the driving forces, which focuses on the development of the standards and consolidation of the contributions obtained through the European projects and aims to enable V2V communication everywhere in Europe. However, the standardization process itself is not performed by C2C CC directly, but by the European Telecommunications Standard Institute (ETSI) [4]. Other activities of the consortium include the development of V2X market introduction strategies.

In addition to the C2C CC activities, the topic of V2X technologies has been explored in a variety of already completed projects. This has made a significant contribution to the understanding of how the future transportation systems might look like and what conditions should be met for it. Thus, it is useful to present a brief overview of the main goals and areas of application of these projects.

Great attention was attracted to a four-year project **Sichere Intelligente Mobilität: Testfeld Deutschland (sim^{TD})** [13], which was a cooperation of 18 companies and organizations from the automotive industry, academia, public and multimedia sectors in Germany. It was supported by the Federal Ministry of Economics and Technology, the Ministry of Education and Research as well the Ministry of Transport, Building and Urban Development. The project was based on the results obtained in the previous research projects such as FleetNet, GST - Global System for Telematics, Invent, Network on Wheels and PreVENT.

The goal of the sim^{TD} project was to contribute to the improvement of road safety and mobility, which can be achieved through intelligent communication systems, and to investigate the aspects of market penetration. To do that a test site was constructed in Frankfurt-Rhein-Main region, where the testing of various V2V and V2I applications in public traffic was carried out. The field trials started in July 2012 and finished in December 2012 and involved 120 V2V and V2I capable vehicles, with integrated driver notification system and fully operational applications. During this time the vehicles were driving application specific scenarios in urban, highway and rural environments several hours every day.

The project **Adaptive and Cooperative Technologies for Intelligent Traffic (ACTIVE)** was funded by the Federal Ministry of Economics and Technology in 2006-2010. The initiative consisted of three active projects: traffic management (Aktiv-VM), active safety (Aktiv-AS) and cooperative cars (CoCar). The main goal of the project was to make future traffic safer and find the solutions for the efficient traffic management as well as analyze the potential of V2V/V2I-communications for future cooperative driver assistance systems [1].

The main objective of the **Aktiv-AS** project was the development, prototype implementation and testing in the real traffic conditions of the following V2V applications: Active Hazard Braking, Integrated Lateral Assistance, Intersection Assistance, Pedestrian and Cyclist Safety, Driver Awareness and Safety [1].

The **NoW (Network on Wheels)** project started in May 2004. It was carried out by major OEMs, supplier firms and academia institutions and supported by the Federal Ministry of Education and Research. The main objective of the project was to solve the key technical issues regarding the protocol messages and data security of V2V and V2I communications. Additionally, NoW project developed an open

communication platform for V2V and V2I applications, including safety and non-safety applications. Furthermore, NoW conducted the analysis of market introduction strategies of V2V and V2I applications. The compiled results were contributed to the standardization activities of C2C CC [59].

The **Communication for eSafety (COMeSafety)** project together with its successor **COMeSafety2** were created as a collaboration between C2C CC and eSafety Forum to provide a platform for the consolidation of the results, which were obtained in European and national research projects as well as make available the collaboration with international research groups and standardization bodies. Specific objective of COMeSafety2 was to build an effective international cooperation between the EU and the USA and maximize the benefits out of the results, which were obtained through the world-wide ITS field operational tests [3].

The project **Cooperative Vehicles and Road Infrastructure for Road Safety (SAFESPOT)** had V2V and V2I communications in focus. It aimed to develop an open, flexible, modular architecture and communication platform. It additionally developed and tested scenario-based selected safety applications and conducted the assessment of their impact on the traffic safety. Furthermore, SAFESPOT aimed to define an effective strategy for the deployment of cooperative road safety applications and contribute to the standardization activities [11].

Connect & Drive (C&D) project focused on design and evaluation of automatic distance control systems such as cooperative adaptive cruise control (C-ACC) with the purpose of traffic congestion reduction and improvement of road throughput and safety. It started in January 2009 and finished in March 2011. Among other contributions, this project refined communication requirements of C-ACC and verified them through the field trials [148].

The **Cooperative ITS Corridor** is an ongoing project, which aims to transform highway Rotterdam-Frankfurt/M.-Vienna into ITS traffic corridor with first cooperative intelligent transport services by 2015. This will enable direct communication between vehicles, roadside traffic control technologies as well as traffic management centers. This project is a cooperation between the EU member states the Netherlands, Germany and Austria. Currently, there are two cooperative applications in focus: Construction Site Warning and Traffic Condition Detection. In both cases, the communication between vehicle and mobile infrastructure elements, such as construction site trailers, is realized over IEEE 802.11p or cellular network [7].

2.3 Summary

In this chapter we have presented an overview on the background of this thesis and provided the information about key technological aspects of V2V communications and related work. In particular, we have summarized basic information on VANETs and discussed benefits and challenges that they introduce. Afterwards, we have surveyed V2X use cases, specifically focusing on V2V applications. Following, we have introduced the driver notification concept with three notification levels: Information,

Awareness Warning and Automatic Pre-Post Crash. Next, we have discussed basic application-specific messages that are used in Europe: Cooperative Awareness Messages (CAMs) and Decentralized Environmental Notification Messages (DENMs). Since the aim of our research is to introduce an effective communication link quality assessment method for V2V applications we have also reviewed the current state of the art on communication performance requirements, which are: type of communication, transmission mode, minimum frequency, allowable latency, data to be transmitted and/or received, maximum required range of communication. Besides, we have discussed how different research and industrial activities defined the numerical values of these performance requirements in the past and pointed out the need for further research in this field. Furthermore, we have given the basics of DSRC communications, where we discussed European C2C CC protocol stack, V2X Application Layer Model and differences introduced to PHY and MAC layers with the IEEE 802.11p standard. Finally, we have presented a survey of related research and industrial activities worldwide that aim to investigate different aspects of V2V communications and achieve high market penetration in the future.

In the next chapter, we will introduce our concept of communication link reliability assessment and discuss definition of the suggested metrics in detail.

3 Application Reliability Assessment

Over the past few years, safety-related V2V applications have already gained a major attention from the industry, academia, as well as standardization bodies and are envisioned to be the first applications delivered to the mass market. For these applications communication is regarded as a further interface or a sensor, which grants otherwise inaccessible information about the vicinity. Channel impairments due to the interferences, environment, high node mobility and fast variation of the network load may affect communication quality to a considerable extent, making it not deterministic in nature but variable in time and according to the geographical location. Therefore, effectiveness of V2V safety applications directly depends on the immediate communication link quality and packet distribution pattern. Thus, to determine whether current level of communication link quality is enough to provide for reliable operation of V2V applications, it is vital to define an assessment approach, which would take both, underlying communication quality and operation requirements of the applications into account.

3.1 Related Work

The first work on this topic was presented in [27], where the authors define application reliability metric as *T-window reliability*: the probability of receiving at least one data packet within a specified time window T . The authors in [20] refer to it as *awareness* and define how the packet reception probability is related to T -window reliability. In their next work [21], they investigate how effectively the DSRC communication can support Forward Collision Warning (FCW) as well as address the question of balance between the network scalability and zero false rates of FCW. The study in [94] uses *awareness* in order to analyze minimum required knowledge about positions of neighbor nodes in the vehicle's vicinity, necessary to achieve the maximum beaconing network load. The authors in [51] analyze the performance of safety applications over the DSRC channel by quantifying the latency suffered at the application layer. While conducting simulation studies, they analyze the connection between packet reception probability, packet inter-reception time and separation distance between vehicles. The importance of taking into consideration application operational requirements while designing congestion control protocols is pointed out in [128]. Conducting their research, the authors make use of the application reliability metric, suggested in [27] but additionally consider required warning distance, defined by the application. In [100] analytical bounds for the maximum acceptable message delivery latency and the minimum required retransmission frequency for rear-end collision avoidance

applications are specified. The authors conduct a simulation study and demonstrate the relationship between these metrics and vehicle velocity, road conditions and wireless channel fluctuation.

Despite the great contribution of previous research works, there is still a lack of clear definition of application reliability requirements. The authors in [27] and [20] obtain T-window reliability only in the event of successful packet reception. However, it is also important to define whether the reliability condition is fulfilled at each specific time instant. Furthermore, we argue that the required level of details when defining numerical values of suggested reliability metrics is still not achieved.

Thus, the aim of this chapter is to develop communication quality assessment method oriented specifically at V2V safety applications. To achieve this objective section 3.2 provides an overview of the system performance requirements imposed by V2V applications on the communication medium and analyzes to what extent they are favorable towards characterization of the performance of safety applications. Section 3.3 defines application reliability metrics, and focuses on the (i) probability of the information freshness (ii) reliable and (iii) minimum required communication ranges as main application reliability metrics. Section 3.4 conducts the simulation study to quantify required information freshness based on MATLAB Simulink vehicle dynamics models. Section 3.5 estimates minimum required communication range based on MATLAB Simulink vehicle model for longitudinal dynamics coupled with a driver reaction model. Afterwards, section 3.6 presents our approach towards the communication link quality assessment. Finally, section 3.7 briefly summarizes knowledge accumulated in this chapter.

3.2 Communication Performance Requirements

Considering the fact, that any V2V application will be a subject of the periodic CAM broadcasts, the foremost performance requirements are maximum allowable latency, minimum updating frequency and communication range, as they ensure timing and spatial properties of driver notifications (Table 2.1). Further, this section provides a short overview of these classical network performance metrics and analyzes to what extent they can be used to characterize communication link quality in the context of V2V applications.

3.2.1 Allowable Latency

Attainable performance of V2V safety applications is mainly dependent on to what extent the information available about the current traffic situation corresponds to reality. Thus, any envisioned safety application will require low reception latency. Generally, delays experienced in wireless networks can be influenced by several main factors, such as multi-hopping, channel access, aggregation and queuing delays. Considering the fact that V2V safety applications will mostly be the subject of the single-hop message dissemination, additional channel access, processing, queuing and aggregation delays

at intermediate nodes will not dominate the delay suffered by these applications. In the event of lower node densities transmission and propagation delays are the main contributors to the overall end-to-end delay. Taking into account relatively small packet sizes and the short distances, addressed by V2V communication, transmission and propagation delays fall within a range of microseconds. On the contrary, the contention-based nature of channel access mechanism is a highly relevant contributor to a end-to-end delay. The size of the channel access delay for a given node depends on the node density within its communication range and the applied transmission power. Therefore, in the scope of increased number of nodes competing between each other to transmit a packet, the channel access delays may grow considerably due to more frequent backoffs induced by the CSMA/CA mechanism. Naturally, it contributes to the total end-to-end delay incurred by a data packet.

The end-to-end delay, in spite of its importance, is not able to illustrate the consequences of packet loss on the total latency suffered at the application layer. Hence, it is essential to select the metric, which would acquire all delays characteristic for such applications and simultaneously account for the packet loss. This can be expressed with *packet inter-arrival time (PIT)* - the time elapsed between two successfully received data packets. It accommodates channel access delay, experienced by the packet due to Distributed Coordination Function Interframe Spacing (DIFS) interval and backoffs induced by CSMA/CA in the event of a channel which is not "idle". Additionally, it accounts for packet losses as well as transmission and propagation delays.

3.2.2 Minimum Frequency

As it has already been stated above, to ensure a reliable operation of a V2V safety application, a highly precise awareness of the vehicle's vicinity must be guaranteed at any time. The latter may infer that using higher message generation rates would be an advantageous strategy decision. In [151], [75], [150], [53] according to the application purposes, message generation rate is specified in the range from 1 to 10 Hz and in separate cases, such as Pre-Crash Warning, up to 50 Hz [53]. The allowable upper limit of this value strongly depends on the quantity of communication nodes disseminating messages in the vehicle's vicinity and available channel throughput. In the context of increased node densities higher message generation rates will increase the temporal network load, which leads to additional packet losses and, therewith, degradation of the application performance. On the other hand, decreasing the updating frequency may also lead to the degradation of the application performance due to a possible outdateding of the information.

The fact that communication nodes in VANET will have to operate under highly variable channel load and high mobility conditions, makes it challenging to define a generally valid optimum for the message generation rate. Thus, CAM generation rate is envisioned to be not a constant value but dynamically adjustable according to the CAM generation rules, which depend on the kinematic properties of the vehicle.

However, we argue in our research that despite their advantages, message generation

rules are not equally effective for all V2V use cases, as they do not directly take the individual application requirements into account. For instance, two different applications operating in the same environment at two equally dynamic vehicles may still require different message generation rate. Thus, for one application a high updating frequency due to the vehicle movement may be excessive, and it will unnecessarily use the channel bandwidth, whereas for another application it still might be insufficient. Therefore, to adjust the updating frequency in the optimal way, it is necessary to take the individual application operational requirements into account.

3.2.3 Communication Range

According to [75], maximum required range of communication is defined as a separation distance between two communication nodes which is necessary for effective support of an application. Currently in the literature on vehicular networking packet delivery ratio and packet error ratio are widely used as the metrics to quantify a broadcast range of communication nodes.

- Packet Delivery Ratio (PDR) is the probability of successful reception of a data packet at the receiver after it was sent by the transmitter. PDR is computed as a ratio between delivered to the destination data packets and entire number of transmitted packets during specific time interval.
- Packet Error Ratio (PER) captures the probability of the packet loss at the receiver and is computed as the ratio between the number of data packets that failed to reach the receiver and the total number of successfully transmitted packets.

The sim^{TD} project defines a reliable communication range as the separation distance between two communication nodes, where the value of PER does not exceed the threshold of 10%. If 10% or more packets do not reach the destination, such communication range is declared to be unreliable [62]. Nevertheless, this research argues, that such definition of the reliable communication range is not effective as it does not take application operational requirements into account. Condition $PER < 10\%$ describes communication performance, but it is not clear if application can operate in a reliable way if this condition is satisfied.

3.3 Application Reliability

This research makes use of the performance requirements discussed in the previous section and refines them by taking application operational requirements into account. Thus, we formulate (i) the probability of the information freshness metric and define through it the (ii) reliable and (iii) minimum required communication ranges, the (iv) earliest and the (v) latest time to collision and the (vi) degradation distance. As application operational requirement we use the (vii) path prediction error.

3.3.1 Information Freshness

Compared to traditional network applications, V2V safety applications will not experience noticeable performance degradation in the event of losing single packets broadcasted by other communication partners. This is due to the fact that in DSRC communications the data packets are independent from each other and each newly transmitted packet always contains the most up-to-date information about the vicinity. At the moment of successful reception of a new packet, the information contained by the previous packet will already be outdated.

Additionally, V2V applications are relatively unsusceptible to sporadic packet losses because they normally make use of the path prediction. Due to it the host vehicle is able to predict future trajectories of the neighbor vehicles based on the information received with the previous packets.¹ An occasional loss of CAMs implies the availability of a still sufficient number of sampling points due to the packets, which were received between the two lost ones. Thus, the algorithm will have a possibility to timely update the information and correct computations if required.

However, this is not the case in the event of successive packet losses. It is obvious that due to highly dynamic vehicular surroundings the deviation of the predicted path from the path traveled in the reality must be minimal. The loss of several consecutive CAMs will result in longer delays between two successfully received packets and therewith, constantly growing inaccuracy between predicted and real trajectories. In the end this will lead to an unacceptable information age at the application layer and thus, insufficient knowledge about the vicinity. For an end-user it increases the probability of experiencing false positive/negative notifications, which could provoke additional hazardous traffic situations.

To ensure accurate path prediction the information available to the host vehicle about the remote vehicle must be up-to-date at any given moment. In the first approximation it might seem that to realize this it is necessary to define a maximum allowable *PIT* between two successfully received packets (section 3.2.1). However, *PIT* can be obtained only in the event of a successful packet reception, while the information about a current reliability level must be available to the application at each time instant. Furthermore, *PIT* cannot always reflect the freshness of the information contained in the current packet adequately: at the time instant t_i when a new packet has not been received yet, the information in the current packet might still not be outdated.

To overcome this problem application reliability has to be obtained periodically with a certain update time. To do this, we define a certain maximum allowed size of *PIT* as a fixed time interval. The application is claimed to be reliable at the time instant t_i if a current packet received from the remote vehicle belongs to the interval $[t_i - PIT, t_i]$ and unreliable otherwise. It suggests that to ensure reliable operation of an application, the host vehicle has to successfully receive at least n packets from the

¹ Here the path prediction algorithm will be given as an abstraction only and without further specification of the key operational principles or implementations details.

remote vehicle within this time interval, where $n \in N$. Further in this research we refer to this interval as to *required information freshness (RIF) interval*.

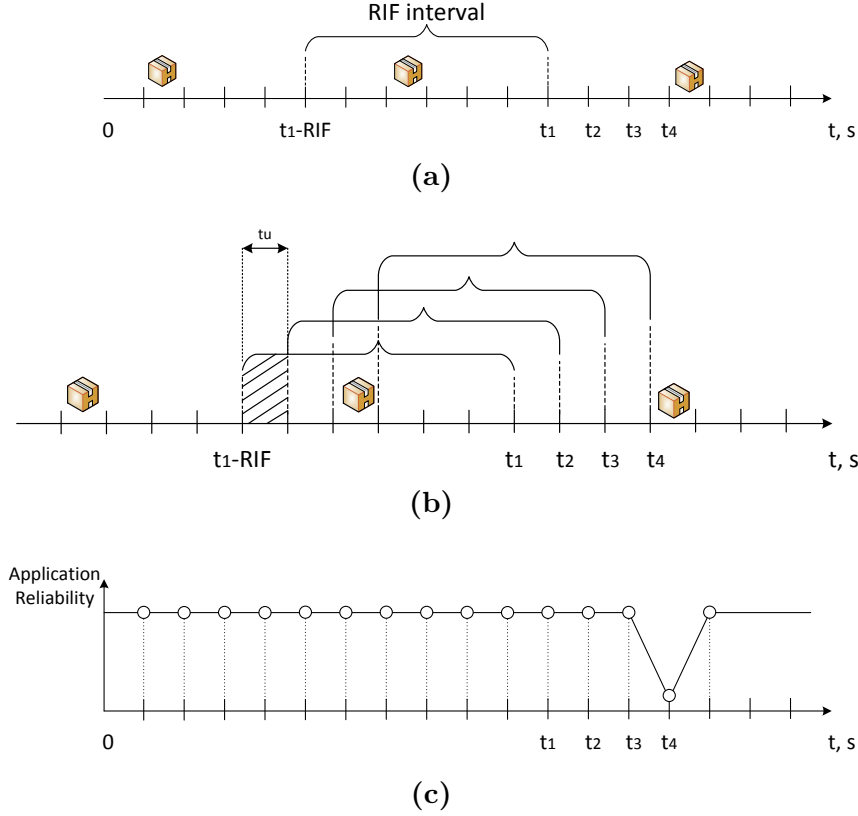


Figure 3.1: Application reliability

The above confirms the conclusion made by Bai et al. in [27] where the authors define application reliability with the *T-window reliability* metric. However, the authors in [27] obtain T-window reliability only in the event of successful packet reception and do not evaluate whether the information which is contained in the current packet is *still* valid, which exhibits the major difference between these two metrics. Furthermore, the authors in [27] are interested in the density of the *T-window reliability* and suggest calculating it as a ratio between reliable time instances and the total number of the time instances. We do not use such representation method, as while assessing application reliability it is of more interest for us to define whether the reliability condition is fulfilled at each specific time instant.

To characterize the application reliability we propose a new metric *probability of the information freshness* P_{RIF} . This is a probability of receiving at least n packet during the *RIF* interval. If the number of actually received packets during the *RIF* interval n is equal or greater than what is required by the application, the condition is considered to be "true" and "false" if otherwise. We control whether this condition is fulfilled at the time instant t_i with a certain update time t_u (e.g. 100 ms). It is

illustrated in Fig. 3.1. A packet is received in the *RIF* interval in the $[t_1 - RIF, t_1]$ interval (Fig. 3.1a), so in moment t_1 the application reliability is equal to 1 (Fig. 3.1c). Further, the *RIF* interval will be shifted with a certain update time t_u and condition will be controlled again. In the time intervals $[t_2 - RIF, t_2]$ and $[t_3 - RIF, t_3]$ there is still a packet which belongs to those intervals (Fig. 3.1b), so the application is reliable in t_2 and t_3 (Fig. 3.1c). In $[t_4 - RIF, t_4]$ there is no packet that belongs to this interval, thus in moment t_4 the application reliability is equal to 0 (Fig. 3.1c).

The benefit of this metric is that it allows us to obtain precise information about the freshness of currently available information in each moment of time and independently of the packet reception status. Furthermore, due to the possibility of a flexible parameterization of t_u this feedback can be realized with any required frequency.

3.3.2 Communication Range

The communication range metric stems from the driver notification concept, in conjunction with which future V2V safety applications will notify the driver about a potentially hazardous situation within several information levels, which are defined according to the remaining time to a possible collision. In the optimal case the triggering time of the last notification level should correspond to the minimum stopping distance necessary for the driver to perform a safe braking maneuver. Furthermore, the distance where communication becomes reliable should satisfy the requirements of the first notification level.

Therefore, we define *reliable range of communication* $d_{0.99}$ between two nodes as the maximum separation distance, at which a node is able to receive at least n packets from the neighbor node within *RIF* interval with a certain probability. The target probability value is set individually, according to the application type. In our work we assume that $P_{RIF} = 99\%$. The definition of $d_{0.99}$ correlates with the *awareness range*, which was proposed in [20].

Minimum required communication range d_{min} lies within reliable range of communication and defines a minimum stopping distance, necessary to perform a safe braking maneuver and reach a complete stop. It is obtained from Fig. 3.7 in the next section as the distance at which the probability of crashing equals to 0.

In case of the use cases that do not impose high requirements on the information freshness probability the communication range is to be defined with a different metric - the *maximum communication range*. It is the maximum separation distance at which communication between nodes becomes possible for the first time (the first packet is received). This metric is relevant for such use cases as Stationary Vehicle Warning or Roadwork Warning, as the remote vehicle in these cases is a static object. Therefore, in the event of receiving at least one packet from this vehicle, the host vehicle will be able to obtain all necessary information to notify the driver.

In low network load scenarios the packet loss is mainly caused by the path loss and other physical effects. Thus, with shortening the distance between two communication partners the information freshness probability grows and after achieving 0.99 at some point P_{RIF} stays constant. In the high channel load scenarios, on the other hand, the

information freshness can get worse also in the direct proximity of the transmitter due to the strong hidden nodes interferences and packet drop at the transmitter. To address this problem we propose the *degradation distance* d_{deg} metric, which defines maximum separation distance between two communication partners, where P_{RIF} is allowed to be lower than required by the application threshold.

3.3.3 Time to Collision

In addition to communication range metrics, it is also important to define the earliest time, when it is possible to issue the driver notification as well as the latest time, when the notification can be still optimally triggered. Therefore, $t_{TTC(F)}$, defines the earliest time, which is possible for the triggering of the driver notification level under the condition that the application reliability has already reached 99%. It is calculated as:

$$t_{TTC(F)} = \frac{d_{0.99}}{v_0} \quad (3.1)$$

where $d_{0.99}$ is the reliable communication range in m and v_0 is the speed of the vehicle in m/s.

The latest time, possible for the optimal triggering of the notification level is expressed with $t_{TTC(L)}$ metric. After this time, the actual distance travelled by a vehicle will be less than what is required by the stopping distance d_{stop} . Therefore,

$$t_{TTC(L)} = \frac{d_{0.99} - d_{stop}}{v_0} \quad (3.2)$$

Case when $t_{TTC(L)} = 0$ implies that to notify the driver in the optimal way, the notification has to be triggered immediately. The negative value means that the notification cannot be optimally triggered. It should be emphasized that $t_{TTC(F)}$ and $t_{TTC(L)}$ are not the recommended time thresholds for the first or the last driver notification levels, but the maximum achievable forewarn time in a specific scenario. While defining $t_{TTC(F)}$ and $t_{TTC(L)}$, we assume that vehicle velocity stays constant.

3.4 Quantifying Application Reliability

In this section we quantify the metrics, which were proposed in previous section based on simulations. To build a strong basis for our study and obtain the numerical results with high accuracy, the data for the simulation is obtained through real-world experiments. The results, which are included in this section were published in [161].

3.4.1 Size of the RIF Interval

The authors in [27] advocate that diverse V2V safety applications will require a different maximum length of the T-window. They also state, that the value of this window belongs to the interval of $T \in [0.3, 1.0] s$. To refine these values we present a novel simulation approach for calculation of the *RIF* interval based on MATLAB braking model for longitudinal dynamics coupled with a driver reaction model and a non-linear single-track model of the 5th order.

To define the size of the *RIF* interval we make use of the *path prediction error* E_{pred} . It is defined as the maximum allowable longitudinal and lateral deviation x and y of a predicted path from that travelled by the vehicle in reality. Therefore, *RIF* is obtained as the time interval, where the current value of the path prediction error does not exceed the threshold value specified by the application. For that we identify possible worst case scenarios for FCW and ICW applications and conduct a simulation analysis. We make use of the assumption, that both vehicles are driving in the ideal conditions, where GPS signal is always available. The prediction is focused solely on losing DSRC messages due to communication outage and not necessarily GPS issues. It is also worth noting, that the prediction can be done for the RV and HV. However, for our study it is sufficient to do it only for the RV, as the purpose is to obtain the size of the *RIF* interval. The main steps to be carried out towards defining the size of *RIF* interval are listed below:

- specify maximum allowable threshold value for the path prediction error
- define application specific scenarios, where a possible communication outage will provoke exceeding of the specified E_{pred} threshold and simultaneously cause a hazardous traffic situation
- calculate E_{pred} between predicted and real trajectories provoked by the loss of consecutive data packets
- define the value of the *RIF* interval as the time when a current prediction error will become equal to maximum allowed by the application

Forward Collision Warning For experimental purposes the following selects the prediction error thresholds of $E_{pred} = [0.25, 0.5, 1, 2]m$. $E_{pred} = 0.25 m$ corresponds to near to perfect operation conditions and $E_{pred} = 2 m$ is assumed to be a threshold after which safety applications will not be able to assist the driver in a reliable way. We further investigate two traffic scenarios, both critical and frequent in a vehicular environment: sudden braking and avoiding an obstacle ahead (Figs. 3.2 - 3.3).

Scenario 1 (Sudden braking): At the time instant t_0 the host vehicle follows the remote vehicle with the constant velocity v_{HV} . Distance d between HV and RV is slightly bigger than minimal stopping distance. RV travels ahead of HV with acceleration a_{RV_1} (Fig. 3.2a). We assume that at the time instant t_1 , owing to a link distortion between HV and RV, there is no communication available during a certain

period of time (Fig. 3.2b). At the same moment due to a possible hazardous traffic situation, overlooked red light, etc., RV has to perform a sudden braking maneuver. Thus, at the time instant t_2 HV predicts the trajectory of RV according to the latest received data: RV travels ahead of HV with a certain acceleration a_{RV_1} (Fig. 3.2c), whereas in reality RV is decelerating with $-a_{RV_2}$ (Fig. 3.2d).

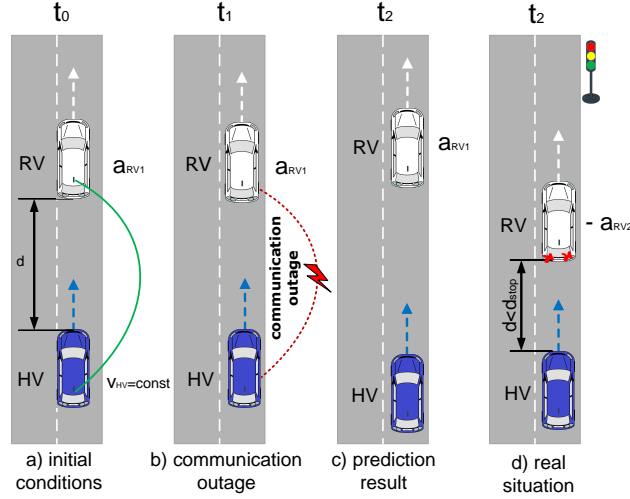


Figure 3.2: Sudden braking maneuver

Each CAM that is lost due to communication outage brings a certain inaccuracy to the prediction result with it. The longer the communication outage is, the more consecutive CAMs are lost. Therefore, in this event the difference between predicted and real trajectories is constantly growing with each new lost CAM and, as a result, exceeds the threshold value defined by the application. Simultaneously, despite the decreasing distance between HV and RV, the driver of HV would not receive a corresponding notification until fresh information is received even when the distance between two vehicles becomes less than minimal braking distance $d < d_{stop}$.

To capture *RIF* interval this research examines various emergency and soft braking situations. Deceleration values of $|a_{RV_1}|$ and $|a_{RV_2}|$ for the case of emergency braking range from 10.98 m/s^2 to 8.61 m/s^2 . They were obtained through the test runs at the test site (dry road, braking system activated by a professional test driver, maneuvers with summer/winter tires). It is worth noting that the values obtained through these test runs are on average higher than those which are typically reached in the normal traffic conditions. Further, the deceleration values for soft braking maneuvers are chosen with respect to the average value of 3.82 m/s^2 [79] and span the range of values in $[1.00, \dots, 3.82] \text{ m/s}^2$ interval (Table 3.1).

To obtain prediction errors in scenario 1, we utilize MATLAB Simulink braking model for longitudinal dynamics. This model describes a 2-piston braking system and takes desired values of initial vehicle velocity v and longitudinal acceleration a_x as inputs. Outputs of the model are actual values of velocity v , longitudinal acceleration a_x and longitudinal deviation x . The values of response time and rise time of the system correspond to the non-autonomous braking. The simulation setup for scenario

1 consists of two identical models described above and represents predicted and real states of RV. The Predicted State model calculates the path that RV travelled along the x-axis according to the latest information available at HV (S_{predX}). The inputs are v_{RV} and a_{RV_1} (Fig. 3.2c). The Real State model calculates the path that RV travels along the x-axis in reality (S_{realX}) and takes v_{RV} and a_{RV_2} as inputs (Fig. 3.2d). The computation steps of scenario 1 are carried out as follows:

- First, predicted distance S_{predX} traveled by RV within time interval $[t_1, t_2]$ with positive acceleration a_{RV_1} is calculated (Fig. 3.2c)
- Next, real distance S_{realX} traveled by RV within time interval $[t_1, t_2]$ with negative acceleration $-a_{RV_2}$ is obtained (Fig. 3.2d)
- Finally, the difference between the predicted and real travelled distances is determined as prediction error $E_{predX} = S_{predX} - S_{realX}$. The value of the maximum allowed *RIF* interval is found as the time when the prediction error exceeds the allowable threshold value (0.25 m; 0.5 m; 1 m; 2 m)

Table 3.1: Sudden braking maneuver ($|a_{RV_1} = a_{RV_2}|$)

v_{RV}	a_{RV_1}	a_{RV_2}	<i>RIF</i> by different E_{pred}			
			$E_{pred} = 0.25$	$E_{pred} = 0.5$	$E_{pred} = 1$	$E_{pred} = 2$
50	10.98	- 10.98	0.23	0.3	0.39	0.53
50	10,52	- 10.52	0.23	0.3	0.39	0.53
50	9.53	- 9.53	0.24	0.31	0.41	0.55
50	9,22	- 9.22	0.24	0.31	0,41	0.55
50	8.61	- 8.61	0.25	0.33	0,43	0.58
50	3.89	- 3.89	0.37	0.49	0.66	0.9
50	3,00	- 3.00	0.37	0.49	0.66	0.9
50	2.00	- 2.00	0.43	0.58	0.79	1.08
50	1.00	- 1.00	0.58	0.79	1.08	1.5

The following combinations of positive and negative acceleration of RV are used: $|a_{RV_1}| = |a_{RV_2}|$ and $|a_{RV_1}| \neq |a_{RV_2}|$. In the second case the value of a_{RV_1} equals to the maximum deceleration, registered during emergency braking maneuvers (10.98 m/s^2). The value of $|a_{RV_2}|$ varies from 10 m/s^2 to 0 m/s^2 with a step of 1 m/s^2 . It is worth noting, that a growing difference between acceleration and deceleration magnitudes lead to a smaller change of the *RIF* interval when compared to the $|a_{RV_1}| = |a_{RV_2}|$ case (Tables 3.1 and 3.2). Therefore, the $|a_{RV_1}| \neq |a_{RV_2}|$ case is of minor importance for this research. Table 3.1 summarizes the computation results for the $|a_{RV_1}| = |a_{RV_2}|$ case and illustrates that in the worst case (emergency braking) the length of *RIF* interval varies from 0.23 s to 0.53 s.

Scenario 2 (Avoiding an obstacle ahead): This scenario illustrates the avoidance of an obstacle ahead of RV and HV. At the time instant t_0 the host vehicle follows the

Table 3.2: Sudden braking maneuver ($|a_{RV_1}| \neq |a_{RV_2}|$)

v_{RV}	a_{RV_1}	a_{RV_2}	<i>RIF</i> by different E_{pred}			
			$E_{pred} = 0.25$	$E_{pred} = 0.5$	$E_{pred} = 1$	$E_{pred} = 2$
50	10.98	- 10.00	0.23	0.3	0.39	0.53
50	10.98	- 9.00	0.23	0.3	0.4	0.54
50	10,98	- 8.00	0.23	0.3	0.4	0.54
50	10.98	- 7.00	0.24	0.32	0.42	0.56
50	10.98	- 6.00	0.25	0.33	0.43	0.58
50	10,98	- 5.00	0.25	0.33	0.44	0.6
50	10.98	- 4.00	0.26	0.34	0.46	0.61
50	10.98	- 3.00	0.27	0.35	0.47	0.63
50	10,98	- 2.00	0.28	0.37	0.49	0.66
50	10.98	- 1.00	0.29	0.38	0.51	0.68

remote vehicle at a certain distance with the constant velocity v_{HV} (Fig. 3.3a). RV travels in front of HV with the speed $v_{RV} = v_{HV}$. At the time instant t_1 RV starts a lane change maneuver with a certain steering angle δ_{L_1} . Communication breaks down when RV has already started the maneuver (Fig. 3.3b). Thus, at the time instant t_2 the prediction algorithm at HV calculates the future trajectory of RV according to the latest received data: RV performing a turning maneuver with δ_{L_1} (Fig. 3.3c). In reality, RV changes to the left lane in order to escape the obstacle ahead, then changes back to the same lane with δ_{L_2} and again travels in front of HV (Fig. 3.3d). Thus, the application running at HV will assume that at the time instant t_2 RV is not a relevant object any further, although in reality RV is driving in front of HV in the same lane. In the same way as with scenario 1, in case of communication outage the difference between predicted and real trajectories is constantly growing with each new lost CAM and, as a result, exceeds the threshold value defined by the application.

The computation steps of scenario 2 are carried out by following the same logic as in scenario 1, taking additionally the travelled distance along the y-axis into account. To obtain E_{predX} and E_{predY} , we make use of a MATLAB Simulink implementation of a non-linear 5th order single-track model. This model takes steering angle δ_L , wind lateral force F_{LY} and curvature of the desired path κ_p as inputs. The outputs are: sideslip angle β , yaw rate $\dot{\psi}$, velocity v , lateral deviation y , lateral acceleration a_y and longitudinal force F_x . Similar to scenario 1, simulation setup of scenario 2 consists of two models which represent real and predicted states of RV. The Real State model calculates the avoidance maneuver with v_{RV} and δ_{L_1} as inputs and obtains the values of S_{realX} , S_{realY} . The distance traveled along the x-axis is obtained from the actual value of velocity. In the same way, Predicted State model takes initial velocity of the remote vehicle v_{RV} and the steering angle δ_{L_2} as inputs and calculates the turning maneuver. It delivers the values of S_{predX} , S_{predY} as outputs. Prediction errors with respect to x- and y-axes E_{predX} and E_{predY} are defined as the difference between

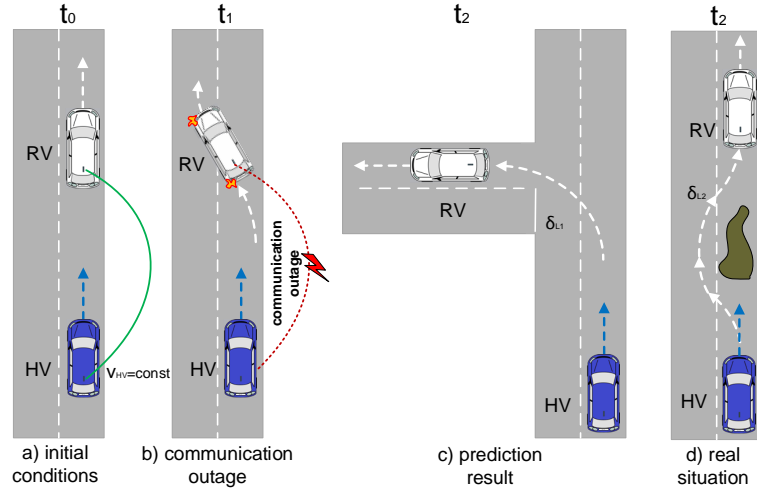


Figure 3.3: Avoiding the obstacle ahead

predicted and real traveled distances with respect to each axis:

$$E_{predX} = S_{predX} - S_{realX} \quad (3.3)$$

$$E_{predY} = S_{predY} - S_{realY} \quad (3.4)$$

RIF is determined when E_{predX} or E_{predY} exceeds the allowable thresholds of 0.25m, 0.5m, 1m or 2m. To define the size of the RIF interval the computations in scenario 2 use the data, derived from Lane Change Assistant (LCA) test runs, conducted at the test site on the dry road. The vehicle initial velocity is chosen to be one of 80 km/h, 70 km/h and 50 km/h. Time t_m represents the time required to perform a collision free lane change maneuver. While performing the avoidance maneuver, RV changes the lane with t_m of 3s and 2s for each speed. The turning maneuver is performed with a steering angle δ_{L1} and created with the following values: $[0^\circ, 100^\circ, 100^\circ, 100^\circ]$. While performing avoidance maneuver δ_{L2} is created as $[0^\circ, 100^\circ, -100^\circ, 0^\circ]$. The communication link breaks down when $\delta_{L2} = 100^\circ$.

Table 3.3: Avoiding the obstacle ahead

v_{RV}	t_m	RIF by different E_{pred}			
		$E_{predY} = 0.25$	$E_{predY} = 0.5$	$E_{predY} = 1$	$E_{predY} = 2$
80	3	0.53	0.67	0.83	1.01
70	3	0.5	0.64	0.8	1.00
50	3	0.52	0.67	0.85	1.06
80	2	0.04	0.15	0.29	0.45
70	2	0.04	0.15	0.29	0.45
50	2	0.06	0.18	0.8	0.51

Table 3.3 presents the results solely for the RIF interval with respect to y-axis, as

E_{predY} grows faster than E_{predX} . We can see that in the worst case ($t_m = 2$ s) the size of RIF interval ranges from 0.04 s to 0.45 s. However, in the city traffic conditions it is highly unlikely to perform a lane change maneuver within 2 s, therefore we can see that by $E_{predY} = 0.25$ m the size of RIF does not exceed 0.53 s.

Intersection Collision Warning Since ICW addresses longer forewarn distances than FCW, the requirement of the information freshness probability is different in the far- and the near-field intersection areas.

Due to the fact that in the intersection far-field area it is more important to detect whether RV will leave a relevant for HV zone (e.g. turn in a neighboring street) than to know precisely in which lane RV is currently driving, requirement of the P_{RIF} is relaxed. We assume that $RIF = 1$ s is a reasonable value, which allows for timely detection of turning maneuvers as well as entering of the near-field intersection area (e.g. 50 - 70 m before the intersection center). This is based on the fact that a vehicle, when travelling at the speed of 50 km/h, performs a turning maneuver in approximately 3 s. This value is obtained by simulating the turning maneuver with a 5th order single-track MATLAB Simulink model, which has been described above. On the other hand, by $RIF = 1$ s the maximum E_{predX} is equal to 13.89 m (no CAMs were received during 1 s), which is assumed to be an acceptable error when RV is still 50 - 70 m away from the intersection center.

In the near-field intersection area the ICW inherits the requirements of the FCW due to the possible automatic braking or steering maneuvers.

3.4.2 Update Time

As it has already been mentioned in this chapter, the update time t_u is a flexible parameter and can be adjusted according to the purposes of the application developer, provided the fact that related to it computational effort is not too high. One possibility is to set t_u equal to the cycle time of the on-board sensors, which are available in the vehicle. For instance, cycle time of the long range radar ARS 30X /-2 /-2C/-2T/-21 is equal to 66 ms [44]. Another possibility is to set t_u equal to the sensor fusion frequency (e.g. 20 ms).

3.4.3 Number of Successfully Received Packets

We advocate that the required number of successfully received packets of $n = 1$ within the RIF interval is sufficient to provide the application with all necessary information based on the following facts.

- if a packet is successfully received, the information is 100% reliable due to the frame check sequence (FCS) mechanism at the MAC level
- each message received from a given node contains complete information about this node

- the content of a currently received packet is independent of the content of a previous packet
- interchangeability of messages due to cyclic broadcasts

These facts were also partially presented in [27]. It is also worth noting, that due to a random packet distribution within the *RIF* interval, the reception of several not successive packets does not bring additional benefits to already gained knowledge about the underlying vicinity. However, if the envisioned V2V application will, for instance, require a certain plausibility to guarantee the exclusion of misuse cases, the requirement of reception $n = 2, 3, \dots, k$ successive packets within the *RIF* interval is possible. Hence, the required number of successfully received packets n is a subject of a design philosophy. Further in this research we use the assumption that the required number of successfully received packets n is equal to 1.

3.5 Estimation of Minimum Required Communication Range

As it has been defined in section 3.3.2 minimum required communication range between two nodes refers to a minimum stopping distance necessary to perform a safe braking maneuver and reach a complete stop. To obtain it, a credible simulation-based approach that summarizes a modeling of the road traffic environment including vehicle dynamics, road conditions and driver behavior is required. This section presents the implementation of the driver reaction model and provides information about the estimation of a stopping distance. Based on the obtained knowledge, we conduct a simulation study and derive the crash probability for the velocity range of 50 to 100 *km/h* utilizing a vehicle braking model for longitudinal dynamics coupled with the driver reaction model.

3.5.1 Stopping Distance

The stopping distance d_{stop} is the distance, which a vehicle travels from the moment of activation of its braking system until reaching a complete stop. It depends on the vehicle velocity at the moment when brakes are activated, the reaction time of the driver, the coefficient of friction between tires and the road surface, the slope of the road and the type of the braking system. The reaction time of the driver t_{react} is the time interval between the instant of hazard recognition and the instant of actually applying the brakes. Therefore, a complete stopping distance is given as:

$$d_{stop} = d_{brake} + d_{react} \quad (3.5)$$

where d_{brake} is the distance travelled after the moment when brakes are activated in m; d_{react} is the distance travelled due to driver reaction time in m.

In kinematics the distance traveled while performing a braking maneuver according to equations of uniformly accelerated motion is given by the equation (3.6):

$$d_{brake} = \frac{v_0^2}{2 \times \mu \times g} \quad (3.6)$$

where v_0 is the vehicle velocity in m/s; μ is the coefficient of friction between the tires of a vehicle and the surface; g is the acceleration due to gravity of the Earth in m/s^2 .

Table 3.4 summarizes the values of μ for rubber on different surfaces based on reference data in [5], [28], [142].

Table 3.4: Approximate coefficients of friction between rubber and different surfaces

Rubber on different surfaces	Coefficient of friction μ
Rubber on dry asphalt	0.5-0.8
Rubber on wet asphalt	0.25-0.75
Rubber on concrete (dry)	0.6-0.85
Rubber on concrete (wet)	0.45-0.75
Rubber on wet snow	0.30-0.60
Rubber on ice	0.15

The additional distance d_{react} traveled by the vehicle due to the reaction time of the driver is given by:

$$d_{react} = v_0 \times t_{react} \quad (3.7)$$

Finally, d_{stop} can be rewritten as:

$$d_{stop} = \frac{v_0^2}{2 \times \mu \times g} + v_0 \times t_{react} \quad (3.8)$$

3.5.2 Driver Reaction Model

The driver reaction model used in this work is represented as a time-shifted Gamma distribution mentioned in publications of Zöllner et al. [164] and Derichs [49]. It is based on empirical data reported in [36]. The authors conducted series of field tests in order to investigate the driver reaction times while performing emergency braking maneuvers. The experimental set-up consisted of two passenger vehicles, where the driver of the first vehicle was initiating the activation of the braking rear lights and the driver in the following vehicle was instructed to press a braking pedal as fast as possible. The time was protocoled from the moment of activation of the braking rear lights of the leading vehicle until the braking pedal in the following vehicle is activated. In total, 41 test persons participated in the experiment. In this process, approx. 100 measurements were taken per test person.

The Probability Density Function (PDF) of the driver reaction time within this experiment is depicted in Fig. 3.4. The authors in [36] report that the driver reaction

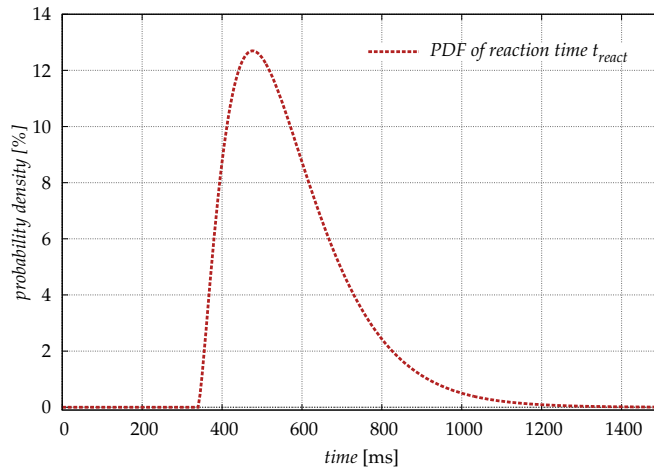


Figure 3.4: PDF of the driver reaction time based on work of Zöllner et al. [164]

time is well approximated by the Weibull distribution, whereas Zöllner et al. argue in [164] that the Weibull distribution is not completely adequate to characterize the distribution of the driver reaction time and show that a time-shifted Gamma distribution provides accurate results. The distribution function of the driver reaction time t_{react} is given as:

$$f(t) = \frac{1}{T^B \times \Gamma(B)} \times (t - t_0)^{B-1} \times \exp\left(-\frac{t-t_0}{T}\right) \quad (3.9)$$

where shape parameter $B = 3.43$ ms; characteristic time $T = 95.4$ ms and scale parameter $t_0 = 243$ ms. The coefficients were calculated with method of moments [49].

3.5.3 Probability of Crashing

To obtain the values of the stopping distance d_{stop} and corresponding probability of crashing at this distance we use the MATLAB Simulink braking model for longitudinal dynamics described in section 3.4.1 coupled with the driver reaction model presented in section 3.5.2. The simulation setup is shown in Fig. 3.5.

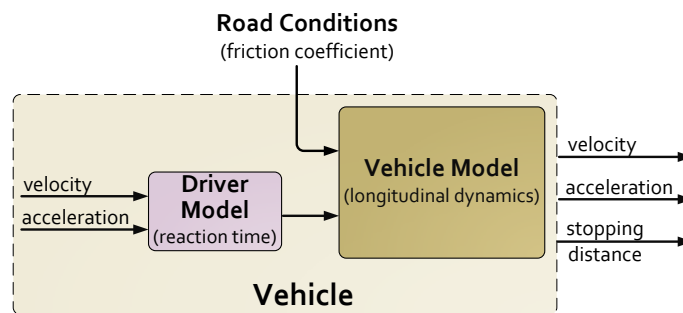


Figure 3.5: Driver and vehicle model

All simulation runs were conducted under the assumption that the vehicle performs the maneuver on a dry asphalt surface ($\mu = 0.5 - 0.8$). The vehicle speed ranges from 50 to 100 km/h. In all scenarios the driver brakes without additional assistance systems. Each time the vehicle travels along a straight road towards a pre-defined crash point (oil patch) with a certain speed, then performs a braking maneuver and reaches a complete stop (Fig. 3.6). Herewith, we investigate whether the vehicle was able to perform a safe braking before reaching the hazard point.

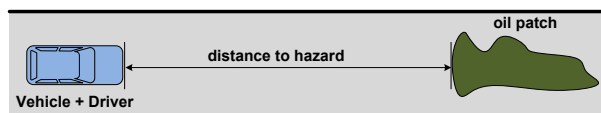


Figure 3.6: Simulation setup

The Cumulative Distribution Functions (CDF) of the stopping distance for various velocities are presented in Fig. 3.7. As expected, the probability of crashing increases with the increased speed, which is reflected by an augmentation of the stopping distance. Fig. 3.7 shows that to perform a safe braking, a vehicle driving at the speed of 100 km/h has to start the maneuver approx. 85 m before the obstacle. Thus, minimum required communication range in this case is equal to $d_{min} = 85$ m.

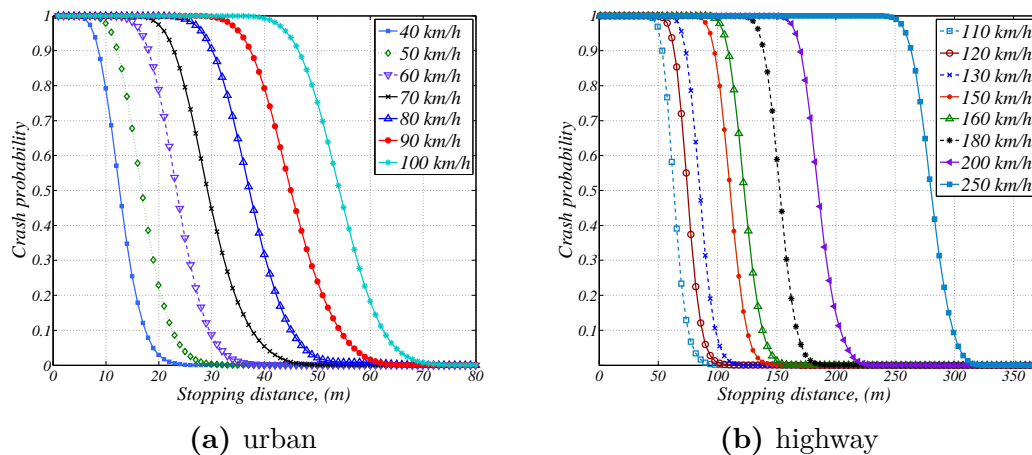


Figure 3.7: CDF of the stopping distance for various vehicle's velocity

3.6 Assessment Method

This section summarizes the knowledge obtained in sections 3.2 - 3.5 and presents the assessment method, which ensures an adequate characterization of the reliability of V2V safety applications while operating over the DSRC channel. Towards this objective Table 3.5 first highlights the key application reliability metrics. Further, we list the main steps that are to be carried out while evaluating application reliability.

The presented method is oriented on evaluation of the measurement or simulation data. The main steps towards defining the application reliability are listed below:

1. Determine key operational requirements of an application and choose corresponding metrics from Table 3.5
2. Analyze application reliability with respect to the chosen metrics:
 - Information freshness probability P_{RIF} :
 - a) define the target P_{RIF} value ($P_{RIF} = 0.99$ by default).
 - b) obtain the size of the RIF interval using the method presented in section 3.4.1.
 - c) specify the value of t_u according to the application requirements (section 3.4.2)
 - d) define the required number of data packets n which have to be successfully received in RIF interval. The default value is set to $n = 1$ (section 3.4.3).
 - e) obtain the value of P_{RIF} with a certain update time t_u .
 - Communication range:
 - a) obtain reliable communication range $d_{0.99}$ using P_{RIF} metric.
 - b) obtain minimum required communication range d_{min} from Fig. 3.7 as the distance when the probability of crashing equals to zero.
 - c) obtain maximum communication range d_{max} as the distance, where the first packet from the communication partner is received.
 - d) obtain degradation distance d_{deg} as the maximum separation distance, where P_{RIF} is lower than the required by the application threshold (in saturated network conditions).
 - Driver notification time:
 - a) obtain the earliest driver notification time using Eq. 3.1.
 - b) obtain the latest driver notification time using Eq. 3.2.
 where:
 - i. $t_{TTC(L)} < 0$ indicates poor communication conditions, as in this case the reliable communication range is less than the stopping distance.
 - ii. $t_{TTC(L)} = 0$ suggests marginal communication conditions.
 - iii. $t_{TTC(L)} > 0$ indicates a sufficient time for more than one notification levels.

Additionally, the optimal triggering of the driver notification can be also analyzed based on the distance ratio $D = \frac{d_{0.99}}{d_{min}}$.

- i. $D = 1$ is equivalent to $t_{TTC(L)} = 0$ and illustrates marginal communication conditions.
- ii. $D > 1$ is equivalent to $t_{TTC(F)}$ and describes favorable communication conditions.
- iii. $D < 1$ is equivalent to $t_{TTC(L)} < 0$ and indicates that under the current communication conditions the driver cannot be timely notified of potentially hazardous situation.

The following illustrates the application reliability assessment method by analyzing the requirements of two use cases: Stationary Vehicle Warning and Intersection Collision Warning. Furthermore, we analyze which of V2V safety applications specified in [53] may impose the same requirements.

Stationary Vehicle Warning alerts other traffic participants about a vehicle, which is hazardously immobilized due to a collision or a breakdown. In this case to prevent/mitigate possible collision the stationary vehicle broadcasts short messages containing its status and current position to other vehicles within its communication range. Since the collided vehicle is static, SVW imposes the requirement on the maximum communication range. In the moment of receiving the first packet from such vehicle the oncoming vehicle will obtain its position and will be able to adequately notify the driver. Therefore, this use case does not require a certain information freshness level to be achieved, or, in other words, one packet is enough to achieve the required information freshness level. Earliest time to collision $t_{TTC(F)}$ in such case will be calculated based on the maximum communication range instead of reliable communication range. Considering the fact that every safety use case assumes that the driver performs a braking maneuver if required, SVW also imposes the requirements on the minimum required communication range and $t_{TTC(L)}$. Degradation distance requirement d_{deg} is not relevant to the SVW use case for the same reasons as reliable communication range. To summarize, SVW imposes the following reliability requirements:

- maximum communication range d_{max}
- minimum required communication range d_{min}
- earliest and latest driver notification times $t_{TTC(F)}$ and $t_{TTC(L)}$

According to the basic set of applications (BSA) specified in [53] such V2V safety applications as Slow Vehicle Warning, Roadwork Warning and Hazardous Location Notification impose the same application reliability criteria. While issuing the Hazardous Location Notification or Roadwork Warning the host vehicle communicates the position of a static dangerous location on the roadway. The Slow Vehicle Warning implies that the velocity of the host vehicle relatively to the approaching remote vehicle is very low, therefore this application also requires low information freshness probability.

Intersection Collision Warning will have to operate in the highly dynamic environment where nodes change their routes very frequently. Therefore, this application will require a much higher information freshness level than the Stationary Vehicle Warning. It also implies, that the reliable communication range, which defines the distance where a node is able to receive sufficient number of packets to capture the dynamics of vehicle's surroundings will be of great importance. Earliest time to collision $t_{TTC(F)}$ will be calculated according to reliable communication range. Obviously, this use case also imposes the requirements on the minimum required communication range and $t_{TTC(L)}$. In congested network conditions degradation distance d_{deg} is an important requirement for the ICW, as communication link quality can suffer in the intersection center due to the increased number of interferences. To summarize, the relevant requirements are:

- probability of the information freshness P_{RIF}
- reliable communication range $d_{0,99}$
- minimum required communication range d_{min}
- degradation distance d_{deg}
- earliest and latest driver notification times $t_{TTC(F)}$ and $t_{TTC(L)}$

Applications that impose the same requirements are: Emergency Electronic Brake Lights, Emergency Vehicle Warning, Co-operative Forward Collision Warning and Motorcycle Warning.

Table 3.5: Application reliability assessment metrics

Metric	Description	Benefit
Probability of the information freshness P_{RIF}	probability that a given node at the time instant t_i is able to receive at least $n = 1$ packet from its communication partner within a specified RIF interval	knowledge about the information freshness at each time instant
Reliable communication range $d_{0.99}$	maximum separation distance between two nodes at which one node is able to receive at least $n = 1$ packet from the neighbor node within a certain RIF interval with $P_{RIF} = 0.99$	guarantee of the reliable communication within a certain distance
Minimum required communication range d_{min}	minimum separation distance between two nodes, which is necessary for the driver to perform a safe braking maneuver and reach a complete stop (d_{stop})	guarantee of a sufficient stopping distance in the moment when the last driver notification is triggered
Maximum communication range d_{max}	maximum separation distance, when communication between two nodes becomes possible for the first time (first packet is received)	knowledge about the maximum possible communication distance
Degradation distance d_{deg}	maximum separation distance, when P_{RIF} is allowed to be lower than it is allowed by the application	guarantee of a sufficient information freshness under high network load conditions
Earliest driver notification time $t_{TTC(F)}$	the earliest possible time to trigger the driver notification under condition that $P_{RIF} = 0.99$	guarantee of a sufficient time for the earliest driver notification
Latest driver notification time $t_{TTC(L)}$	the latest time, possible for the timely triggering of the last driver notification level under condition that $P_{RIF} = 0.99$. After this time, the actual distance travelled by a vehicle will be less than what is required by the stopping distance d_{stop}	guarantee of a sufficient time for the latest driver notification level

3.7 Summary

In this chapter we have introduced our concept of communication link quality assessment for V2V safety applications. First, we have reported important related work on the topic of reliability assessment and analyzed three commonly used communication performance metrics, which are of the most relevance for us: allowable latency, minimum frequency and communication range. We have discussed challenges for characterization of the application reliability if only these metrics alone are used and pointed out the importance of establishing a link between communication performance requirements and operational requirements defined by applications. Specifically, we have shown that end-to-end delay is not able to illustrate the consequences of packet loss on the total latency suffered at the application layer. We have also pointed out that due to the broad range of V2V safety use cases general message generation rules may not necessarily be applied for all of the applications in the most effective way. Furthermore, we have discussed that a commonly used way to define the reliable communication range as the separation distance between two communication nodes, where the value of PDR exceeds a certain threshold (e.g. $\text{PDR} > 90\%$) is not always beneficial. For instance, PDR higher than 90% might describe communication quality but does not necessarily mean that the application will operate in a reliable way if $\text{PDR} = 90\%$ condition is met. Thus, neglecting the aspect of individual operational requirements of V2V applications could bring unnecessary confusion in the evaluation process and compromise comparability of the results.

Motivated by these conclusions we have suggested a novel metric - probability of the information freshness P_{RIF} . It depicts the probability that a given node at the time instant t_i is able to receive at least n packets from its communication partner within a specified time interval RIF , where size of the RIF depends on the individual operational requirements of the application. This condition is controlled with a certain update time t_u , which can be flexibly parameterized according to how frequently the application requires this information. The benefit of the P_{RIF} metric is that it allows us to obtain the precise information about the freshness of the currently available information in each moment of time and independently of the packet reception status. Having this metric in scope we have additionally extended the definition of communication range requirements. Additionally, we have suggested a metric that is of particular importance for congested scenarios - degradation distance d_{deg} .

Since our aim was to achieve a high level of granularity when defining numerical values of suggested metrics, we conducted a separate simulation study based on MATLAB Simulink vehicle dynamics models where we calculated the size of the RIF in relevant application-specific scenarios. To increase the quality of our results we used real-world measurement data for our study. As a result we have obtained reasonable RIF values for Forward Collision Warning and Intersection Collision Warning. Additionally we have suggested some ideas on what is the best way to define update time t_u as well as the number of successfully received packets n .

In the literature while calculating minimum required communication range, such

effects as vehicle dynamics and driver reaction time are frequently simplified. Since it is an important metric for our research we have conducted a separate simulation study to calculate the minimum required communication range with a high precision level. For that we again used MATLAB Simulink vehicle dynamics models and additionally implemented the driver reaction model introduced in [164]. It is based on an elaborate measurement study and therefore provides trustable driver reaction times. As a result we have obtained reliable communication ranges in urban and highway environments for [40 - 250]km/h velocity range.

Finally, we have introduced our concept of application reliability assessment and gave an example of how it can be applied for V2V safety use cases with different requirements. In the next chapter we are going to apply our concept for evaluation of environmental effects on the application reliability.

4 Environmental Effect on the Application Reliability

High node mobility and low elevated antennas make the DSRC channel exhibit higher temporal fluctuations than, for instance, in cellular networks. Furthermore, it increases the probability of link distortions due to the interaction with mobile and static obstacles. This results in challenging communication conditions and together with a new operational frequency makes the knowledge about channel properties, which were obtained for the cellular systems, not effective for assessment of V2V communications.

Thus, the aim of this chapter is to dwell upon the aspects of environmental effects on the reliability of V2V safety applications while operating over the DSRC channel. It includes the analysis of the urban and country road environments, specifically focusing on the intersection scenarios. Towards this objective, we provide research results from several real-world measurement campaigns and characterize the communication performance with the packet delivery ratio and application reliability using the probability of the information freshness. Moreover, since V2V use cases are the subject of the outdoor communication, we additionally discuss the impact of the weather conditions, which are relevant for vehicular communications.

This chapter is structured as follows: first, section 4.1 briefly describes the utilized measurement equipment. The analysis of the application reliability at urban intersections is introduced in section 4.2. First this section describes measurement setup and scenarios. Afterwards, it specifically discusses the intersection topology, traffic conditions and the effects different transmitter positions can have on the application reliability. Section 4.3 discusses the measurement results at rural intersections and compares them with those which were obtained in urban scenarios. Further, it analyzes application reliability specifically focusing on the seasonal effect of the vegetation layer. Finally, the impact of the weather conditions is discussed in section 4.4.

The results, which are presented in this chapter were partially published in [125], [141] and [161].

4.1 Measurement Equipment

During all measurement campaigns the test setup consisted of two passenger vehicles of a comparable height. However, the models of the test vehicles were different in different campaigns, which induced small changes. For more details refer to [125] and [141]. While conducting the measurement one vehicle was configured as the

transmitter (Tx) and the other one as the receiver (Rx). Each vehicle was equipped with a communication module and a magnetic mount antenna.

The communication module includes an ALIX3D3 board running an Ubuntu Linux distribution with kernel version 2.6.32 and commercial off-the-shelf Compex Mini PCI 802.11abg wireless interface cards based on the Atheros AR5006X (AR5c414) chipset. To meet the IEEE 802.11p or ITS-G5 specifications, a modified driver based on ath5k and the Linux wireless subsystem is used. Additionally, the communication module includes a Navilock NL-402U Global Positioning System (GPS) receiver and uses the u-blox5 chipset in order to log the vehicle positions and the distance between the vehicles.

The antenna is a vertically polarized magnetic mount antenna (Mobile Mark ECOM6-5500) with an omni-directional radiation pattern and a nominal antenna gain (including antenna cable attenuation) of 3.2 dBi at zero degrees elevation on a metal ground plane. During all measurements the antenna was placed in the center of the vehicle roof at the height of approx. 1.5 m.

The transmission power was configured to be 23 dBm. The antenna gain and a cable attenuation of approx. 3 dB resulted in an equivalent isotropically radiated power (EIRP) of 23.2 dBm. A packet generator at the transmitter was configured to send periodic messages with a generation rate of 100 Hz and a payload size of 500 bytes. Including UDP, IP, LLC and MAC header (8/20/8/28 bytes), this resulted in a MAC frame size of 564 bytes. Table 4.1 lists the measurement system parameters.

Transmission power (EIRP)	23.2 dBm
Center carrier frequency	5.9 GHz
Channel bandwidth	10 MHz
Data rate	6 Mbps
Antenna height	1.5 m
Packet generation rate	100 Hz
MAC frame / message payload size	564 / 500 Bytes

Table 4.1: Measurement system parameters [125]

The receiver was configured to passively listen to frames on the configured channel and log the measurement data. To log the measured RSSI as well as the transmitter and receiver position values for each received frame the software tool that utilizes the libpcap library and radiotap header generation mechanism was used. Each packet contained a 32-bit sequence number in the payload. For more details refer to [125].

4.2 Intersections in Urban Environment

The urban environment is characterized by heavily built-up areas and complex patterns of man-made structures, therefore, the corners of urban intersections are obstructed with buildings most of the time. This results in a frequent unavailability of a dominant line-of-sight (LOS) propagation path between vehicles approaching the intersection

from perpendicular directions for a long period of time. In such cases, the availability of V2V communication depends on NLOS reception, which is enabled by the multipath propagation. However, NLOS reception in urban environments can be complicated due to difficult radio fading character, frequent spatial variations of building profiles, arbitrary motion of vehicles and high operation frequency (5.9 GHz).

Multipath propagation implies that the transmitted signal will reach the receiver over the multiple propagation paths, while being reflected, scattered or diffracted from the various interacting objects (IOs) located in the proximity of Tx and Rx. The number of propagation paths can be large and due to interaction with obstacles each multipath component (MPC) has a different amplitude, delay and phase. When multiple MPCs of the transmitted signal arrive at the receiver it sums them up coherently, in amplitude and phase, being not able to distinguish between the different replicas of the signal. Consequently, this results in interferences, which can be constructive or destructive, according to the phases of the arriving MPCs. Constructive interference takes place when the MPC reaches the receiver in-phase (the amplitudes of arrived waves are equal in sign) and causes the amplification of the signal. If several MPCs reach the receiver out-of-phase (the amplitudes of arrived waves are different in sign) it causes destructive interferences and, hence, weakening of the received signal and increase of the bit error rate (BER). Two MPCs can also completely cancel each other if they arrive at the receiver with difference of π ("null zones"). The effect of multipath makes the channel vary in frequency (frequency-selectivity). Furthermore, the phase of MPCs depends on the length of propagation paths between Tx, Rx and IOs. Therefore, if mobile terminals or IOs are moving, it results in the Doppler shift and leads to the channel change in phase over time due to the phase shift of the received signal replicas (time-selectivity). Both these phenomena define the *small-scale fading* or *fast fading* and cause a rapid variation of the phase and amplitude of the total received signal over the time. The more rapidly the receiving and transmitting stations are moving, the more rapidly the channel fades. Due to high node mobility and availability of a multitude of propagation paths in urban environment the channel fluctuations can be great and result in severe attenuation of the received signal.

Another major challenge, which characterizes urban environments, is the shadowing effect, which occurs when a large interaction object obstructs LOS or MPCs between Tx and Rx, resulting in a big amount of attenuation of the radio waves as they propagate through this obstacle. In this case the received signal strength varies gradually, partially due to diffraction of radio waves and partially due to spatially extended shape of the buildings. This effect is called *large-scale fading* or *slow fading*. In urban environment it is mainly determined by the geometry of the propagation path and presence of other vehicles. Due to low elevation of the vehicle antennas the probability of shadowing of V2V radio is extremely high.

It is also worth noting that the capabilities of electromagnetic waves to diffract around the interacting objects depend on the operating frequency. At higher frequencies, when the wavelength is small relatively to the size of the obstacle, the diffraction will occur seldom. Considering the wavelength of 5 cm, the diffraction effect in case of the DSRC communication will be minor. It means that in intersection scenarios, if

there are no significant scatters in the proximity of Tx and Rx, the receiver will be able to receive a signal from the transmitter only shortly before LOS occurrence in the intersection center. The measurement reported in [77] confirms that at 5.9 GHz the diffraction effect does not dominate radio wave propagation.

4.2.1 Related Work

So far a lot of measurement campaigns have been conducted in various vehicular environments when operating over the DSRC channel (see section 2.1.1). However, only several research works address channel properties at urban intersections and additionally consider requirements of V2V safety applications. The following briefly describes the most significant research works over the past years.

The authors in [120] investigate the radio wave propagation characteristics at urban crossroads under various NLOS conditions at 5.9 GHz operating frequency. Based on the measurement campaign, they compare the obtained results with 3D ray-optical path loss prediction model. Furthermore, the authors derive a stochastic propagation model, which allows for estimation of the maximum communication ranges under the condition of different data rates. The results of empirical study of V2V propagation channels in four different types of urban crossroads are presented in [77]. The measurement campaign was performed at 5.6 GHz, at that the authors characterize power delay profiles, path loss and delay spreads. They showed that the availability of roadside buildings can create strong propagation paths, which account for a considerable part of the received power in NLOS scenarios. The authors in [89] conducted the analysis of building positions at urban intersections. They characterized the degree of LOS obstruction due to buildings and used resulting data to derive a set of representative intersection scenarios. This provided a great contribution towards selecting meaningful simulation and measurement scenarios for more effective characterization of V2V communication channels. In their next work [88] they performed an elaborate measurement campaign at urban crossroads and specifically addressed achievable NLOS reception quality. For this study the intersections were methodically selected to address most typical urban intersections. The collected data has shown, that NLOS reception is possible and that the reception rates at selected crossroads mostly exceed 50 % at distances of 50 m before the intersection center. Further, the authors in [87] present a 5.9 GHz NLOS path-loss and fading model based on measurements in [88]. They show that the collected measurement data can be well fitted into the presented analytical model. The main advantage of this model is its low complexity and therefore usability in large-scale packet-level simulations. The authors in [63] provide a realistic urban propagation model for VANET. Despite the low computational cost, the model provides accurate prediction for ad-hoc networks in urban scenarios. The authors prove the effectiveness of their method by comparison of their results with real-world measurement data. Furthermore, measurements of the LOS and NLOS propagation characteristics at urban intersection are presented in [98]. Thereby, the authors specifically focus on the influence of surrounding vehicles on the communication link quality. They showed that in the LOS environment, the

received signal was significantly attenuated due to the influence of the surrounding vehicles. In the NLOS conditions, however, no significant signal strength degradation due to vehicles was observed. Furthermore, [19] reports the result of an extensive measurement campaign conducted in several countries, totaling over 1100 km. The authors specifically address various V2V safety applications including intersection collision warning and perform channel measurements followed by the application performance assessment. With this the authors aim at establishing a link between channel characteristics and performance of V2V safety applications.

The lack of extensive measurement campaigns at 5.9 GHz, which would cover aspects of urban intersection environment on the reliability of V2V safety applications, motivates research conducted in this section.

4.2.2 Measurement Setup and Scenarios

The following presents the results of a measurement campaign conducted in the city of Braunschweig at five intersections with different street topology, geometry, building density and traffic conditions. In all following scenarios, the transmitter is parked at a certain distance to the intersection center in the street canyon, while the receiving vehicle Rx is moving along the adjacent street and approaching the intersection center with a speed of approximately 15-20 km/h. During all measurements the vehicles always have no LOS connection until they reach the intersection center. It illustrates the situation where the drivers of both vehicles would not see each other until a line-of-sight contact at the intersection center is established. To ensure statistical validity of the results, the measurement in each scenario was conducted 10 times.

The following investigates the effect of the intersection topology, traffic conditions and variable transmitter positions on the achievable application reliability and obtains the packet delivery ratio and information freshness probability P_{RIF} at each intersection. To analyze the application reliability, we obtain reliable communication range $d_{0.99}$ and calculate it as a sum of two distances d_{RX} and d_{TX} . The distance between the receiver and the intersection center when P_{RIF} reaches 0.99 is depicted with d_{RX} . It means that the condition of receiving at least one message within a specified RIF interval always fulfilled at this distance. On the other hand d_{TX} is the distance between the transmitter and the intersection center when P_{RIF} reaches 0.99. The sufficient level of PDR is selected to be 95%, as according to [20] it is a minimum necessary value to guarantee a reliable communication for the safety applications. Therefore, when defining reliable communication range with respect to PDR metric, the following obtains d_{RX} when PDR reaches 95% and does not fall lower than this threshold and calculates $d_{0.99}$ also as $d_{0.99} = d_{RX} + d_{TX}$. Further, this chapter compares evaluation results when utilizing P_{RIF} and PDR metrics.

It is important to note, that all measurements were conducted in the real traffic environment and at different locations, making it impossible to guarantee the same driving conditions and the same distance between Rx and the intersection center in all scenarios. Therefore, the time when Rx reaches the intersection center may vary considerably in different scenarios, which would compromise the results, while

comparing the performance of different intersections. To overcome this problem, the P_{RIF} and PDR in Figs. 4.2 - 4.12 are depicted with respect to the distance between the receiver and the intersection center d_{RX} . The intersection center is represented with $d_{RX} = 0$ m. The following selects the value of the RIF interval equal to 0.5 m, 1 m and 2 m, which approximately correspond to 0.15 s, 0.3 s and 0.6 s considering that the average speed during all measurements was approximately the same.

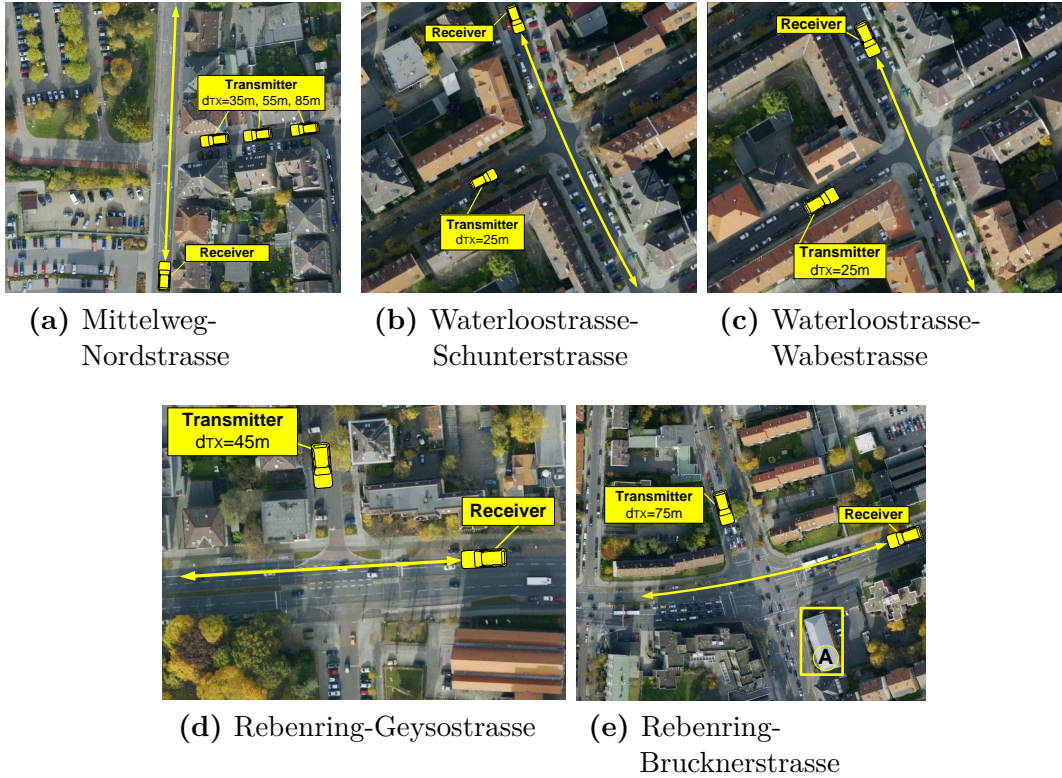


Figure 4.1: Urban intersections

Mittelweg - Nordstrasse is a four-way intersection of a medium width with the buildings located only in two quadrants of it (half-open intersection). The width of the street, where Tx is located, is approx. 16 m. The transmitter was positioned at d_{TX} equal to 35 m, 55 m and 85 m before the intersection center. The streets where Rx and Tx are positioned have three to two lanes and no traffic lights in their direct proximity. The density of the buildings in the street where Tx is located is high.

This intersection topology was selected to investigate the shadowing effect of the buildings when no significant reflectors are available in two quadrants of the intersection opposite to Tx (Fig. 4.1a). From the communication perspective, this scenario is expected to be challenging, as such geometry will cause less number of MPCs in the absence of LOS. However, it is worth noting that the opposite to Tx side of the intersection offered a certain number of vehicles parked along the road and a few distant buildings, which could provide additional propagation paths for the

transmitted signal.

Furthermore, the measurements at this intersection were conducted in variable traffic density conditions: first during the rush hour, when the traffic density is high and at night, with minor to no traffic density. This allows us to analyze the effect of the traffic conditions on the achievable application reliability. Moreover, several measurements were conducted with respect to the different transmitter positions.

Waterloostrasse - Schunterstrasse is a four-way intersection of a medium width, closed with buildings from all sides and with no traffic lights. The streets where Tx and Rx are located are two-lane and intersect each other at an angle which is greater than 90° . It allows us to assume that LOS in this scenario will occur before Rx reaches the intersection center. The distance between the transmitter and intersection center is $d_{TX} = 25$ m. The width of the street where the transmitter is located is approx. 20 m, which is typical for the majority of intersections in the urban environment [88]. This intersection offers a minor to no traffic density. Since there are many objects, this scenario is expected to offer a considerable number of MPCs when LOS is not available (Fig. 4.1b).

Waterloostrasse - Wabestrasse is an example of a very narrow intersection with the width of the street where Tx is located of approximately 10 m (single-lane). It is a four-way intersection, with buildings in each quadrant of it. The distance between the transmitter and intersection center $d_{TX} = 25$ m. The street where Rx is located is two-lane with no traffic lights. This intersection offers a minor to no traffic density. Similarly to the previous scenario, this intersection has reflecting objects of a comparable structure and size that are also located close to the roadside. The main difference is due to considerably narrower streets and less than 90° opening angle of the streets where Rx and Tx are located. This scenario is expected to offer a later occurrence of LOS component than at *Waterloostrasse - Schunterstrasse* (Fig. 4.1c).

Rebenring - Geysostrasse is a wide, 90° intersection on the main road, which offers a dense grid of the roadside scatters in its two quadrants, relatively sparse building density in the third quadrant and a park area in the fourth one. The distance between the intersection center and the transmitter d_{TX} is equal to 45 m. The street where Tx is located offers one lane in each direction with no traffic lights. The main street (Rebenring) offers two lanes in each direction and a high traffic density during the measurements, with vehicles often stopping at the red lights. The passenger vehicles constitute the main part of the traffic but buses and small trucks are also sometimes present. This scenario is expected to provide earlier occurrence of LOS due to the wider streets, although vegetation area and sparse building density at the opposite to Tx part of the intersection can be challenging (Fig. 4.1d).

Rebenring - Brucknerstrasse also represents a wide, 90° intersection on the main road (Rebenring) with buildings in four quadrants of it and the traffic lights on each side. The number of lanes at this intersection varies from five to seven. The transmitter is positioned at $d_{TX} = 75$ m in the intersection canyon. It can be observed that the placement of the buildings is less dense than in the first three scenarios. The buildings at the opposite to Tx side of the intersection are located very close to the main road (Fig. 4.1e area "A"). Similarly to *Rebenring - Geysostrasse*, the

traffic density during the measurements was very high with a small percentage of buses and small trucks. This scenario is expected to provide a lot of propagation paths long before the occurrence of LOS between Tx and Rx due to the wide streets, favorable building placement and availability of significant reflecting objects close to the roadside.

Due to the space limitations the streets names are abbreviated in the legends of Figs. 4.2 - 4.12, Fig. 4.13 and 4.14.

4.2.3 Effect of Intersection Topology

The following investigates to what extent intersection topology can affect the application reliability and additionally compares the evaluation results when PDR and P_{RIF} metrics are applied. Figs. 4.2-4.3 illustrate achieved PDR and P_{RIF} at the intersections, which are described in section 4.2.2. We can observe that in several cases the intersection topology can affect the packet distribution pattern differently when compared to the application reliability.

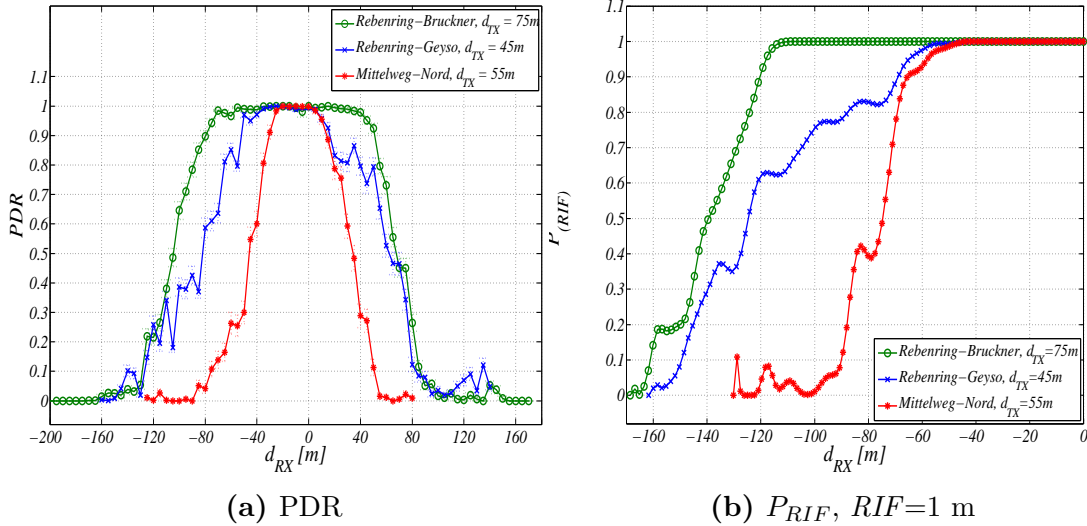


Figure 4.2: PDR (a) and P_{RIF} (b) as a function of the distance d_{RX} between the receiver and the intersection center at different urban intersections

Fig. 4.2a compares PDR that was achieved at *Rebenring-Brucknerstrasse*, *Mittelweg-Nordstrasse* and *Rebenring-Geyssostrasse* with the transmitter positioned 75 m, 55 m and 45 m away from the intersection center respectively. We can see that the fluctuations of PDR at *Rebenring-Geyssostrasse* are much stronger than in the *Mittelweg* and *Brucknerstrasse* scenarios. We can also see that due to the absence of significant reflecting object at one side of the *Mittelweg-Nordstrasse* intersection the transition from a low PDR to high and vice versa is more rapid when compared to other intersections. When the reliable communication range is obtained with PDR = 95 % criterion the *Brucknerstrasse* scenario offers the best communication conditions and the *Mittelweg*

scenario the worst ones. This clearly shows that the half-open intersection topology exhibits the most negative effect on the packet reception probability when compared to other investigated topologies. Furthermore, despite $d_{TX} = 75$ m, the *Brucknerstrasse* scenario offers the best performance due to its wide streets and static interaction objects located close to the intersection center, which results in strong MPCs (Fig. 4.1e, area "A"). On the other hand, low building density and the park area in the third and fourth quadrants of the *Geysostrasse* scenario offer fewer stable MPCs, which creates more challenging communication conditions despite the fact that both of these intersections have similar topology.

While comparing the same intersections according to P_{RIF} metric we can observe that the *Brucknerstrasse* scenario also offers the best application reliability. However, the communication link between Tx and Rx becomes reliable 40 m earlier than when PDR reaches the target value of 95%. Furthermore, Fig. 4.2b demonstrates that the P_{RIF} obtained in the *Brucknerstrasse* scenario reaches 0.99 approximately 60 m earlier than the P_{RIF} achieved in other two scenarios, which makes the *Brucknerstrasse* scenario considerably better. This is not the case when PDR metric was applied: PDR at *Brucknerstrasse* reaches 95% approximately 20 m earlier than in *Geysostrasse* scenario and 30 m earlier than in the *Mittelweg* scenario. It should also be noted, that the improvement of P_{RIF} in the *Geysostrasse* scenario is slower when compared to the other scenarios. Thus, P_{RIFs} in *Geysostrasse* and *Mittelweg* scenarios reach the target value of 0.99 almost at the same time, despite more distant Tx position in the *Mittelweg* scenario. This effect is also not captured when PDR metric was used. It allows us to conclude, that distribution of the IOs in the *Geysostrasse* scenario together with the unfavorable traffic conditions (frequent stops due to traffic lights and traffic jams) made the communication channel much more variant when compared to the *Brucknerstrasse* and *Mittelweg* scenarios. All these facts made the *Geysostrasse* scenario comparable to *Mittelweg - Nordstrasse* by $d_{TX} = 55$ m and minor traffic density, which has the poorest performance among these three intersections.

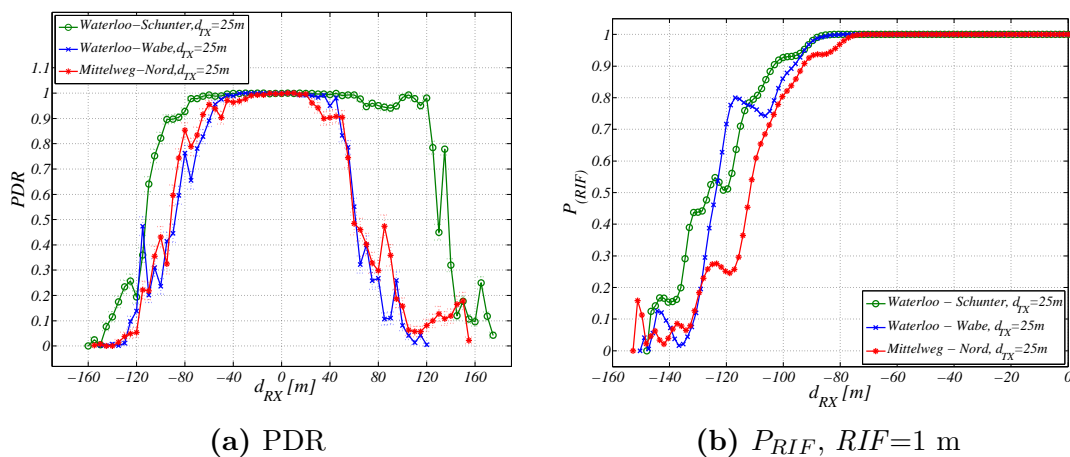


Figure 4.3: PDR (a) and P_{RIF} (b) as a function of the distance d_{RX} between the receiver and the intersection center at different urban intersections

Fig. 4.3a compares the PDRs at *Waterloo-Schunterstrasse*, *Waterloo-Wabestrasse* and *Mittelweg-Nordstrasse* with the transmitter positioned $d_{TX} = 25$ m away from the intersection center in each case. It demonstrates that the communication link quality in the *Schunterstrasse* scenario is better when compared to the *Wabestrasse* scenario. It allows us to conclude that despite a multitude of static IOs in the *Wabestrasse* scenarios, a small width of the street where Tx is located and unfavorable opening angle of the intersecting streets can significantly impact communication link quality. It is also to be noted, that the communication link quality in the *Wabestrasse* scenario is very similar to the *Mittelweg* scenario, which additionally proves the severity of these effects on the packet distribution pattern.

However, Fig. 4.3b demonstrates, that *Schunterstrasse* and *Wabestrasse* scenarios exhibit very similar P_{RIF} performance despite the fact that the *Schunterstrasse* scenario offers more favorable intersection geometry. It brings us to the conclusion that the street width and opening angle do not have a pronounced positive effect on the application reliability, as it could be concluded from Fig. 4.3a. It is also worth noting that the *Mittelweg* scenario still demonstrates the worst P_{RIF} performance and confirms the assumption that the half-open intersection topology is one of the most challenging for the DSRC communications.

The comparison above has shown that the intersection topology as well as the type of interaction objects, which are located in the relevant quadrants of the intersection, can affect application reliability to a considerable extent. Furthermore, we can conclude that the street width and opening angle do not always play the most significant role with regard to the application reliability. On the other hand, the static IOs of a significant size and their location close to the roadside have pronounced positive effect. The comparison has also shown that P_{RIF} metric is highly susceptible to the channel fluctuations.

Additionally, the evaluation results for PDR and P_{RIF} metrics allow us to conclude that the definition of the application reliability in urban environment only through PDR metric does not always provide accurate results.

4.2.4 Effect of Traffic Conditions

Several measurement studies have been performed to investigate how the traffic conditions can affect the quality of the communication link when operating over the DSRC channel [91], [98]. Due to the high susceptibility of the communication link to the shadowing effects, a lot of research has been done for the highway environment, where the interruptions of the communication link are highly frequent due to the trucks and vans driving between Tx and Rx [33], [105]. It is, however, also of a major importance to investigate to what extent the application reliability can be affected by the traffic conditions in urban environment with mostly sedan-type vehicles. This is due to the fact that a high number of mobile scatters can contribute greatly to the channel variance. The following presents PDR and P_{RIF} obtained through two series of measurements, which were conducted at the *Mittelweg - Nordstrasse* intersection under different traffic conditions: rush hour and low to no traffic at night.

Both series of measurements were performed at the same day and under the same weather conditions. During the day measurements Tx was located 25 m inside of the intersection approach and during the night at $d_{TX} = 35$ m.

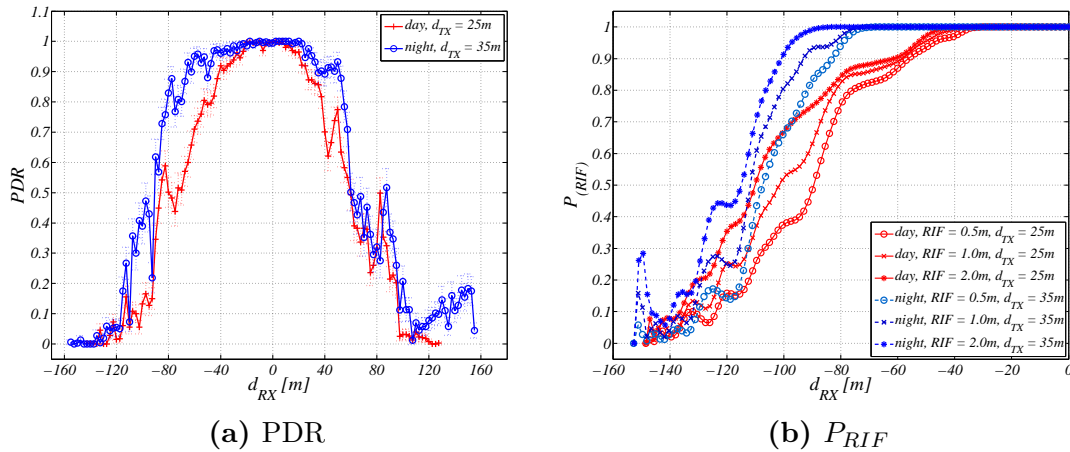


Figure 4.4: PDR (a) and P_{RIF} (b) as a function of the distance d_{RX} between the receiver and the intersection center under different traffic conditions

Fig. 4.4a demonstrates that the PDR which was obtained during the night measurements is slightly better than the one in the day, regardless the fact that at the night Tx is positioned 10 m further from the intersection center. This allows us to make a conclusion that in this scenario such difference in Tx positions is neglectable and both measurements are comparable. Generally, we can see that the PDR values, which were achieved during the day and the night measurements have minor differences between each other. Moreover, the reliable communication range, when obtained with $PDR = 95\%$ criterion is approximately the same in both measurements and equals 40 m (night) and 35 m (day).

Fig. 4.4b, however, establishes that the P_{RIF} in the rush hour scenario reaches 0.99 approximately 40 m later than during the night measurements. This strongly advocates that the effect of the traffic conditions at the application reliability cannot be neglected. The latter also allows us to conclude that the effect of the traffic conditions on the application reliability cannot always be adequately captured with the PDR metric.

4.2.5 Transmitter Positions

Here we investigate how various transmitter positions affect PDR and P_{RIF} performance. Figs. 4.5b-4.5a illustrate the results of three measurement series, which were obtained at *Mittelweg - Nordstrasse* intersection at night and with no traffic. The transmitter was located at 35 m, 55 m and 85 m away from the intersection center.

Fig. 4.5a demonstrates that with the increasing distance between the transmitter and the intersection center the required time for PDR improvement is also increasing.

P_{RIF} shows the same behaviour (Fig. 4.5b). However, for each d_{TX} the reliable communication range is approximately 15 - 30 m greater when defined with $P_{RIF} = 0.99$ criterion than when PDR = 95 % condition is used. This fact again demonstrates that the PDR metric cannot always accurately depict the application reliability.

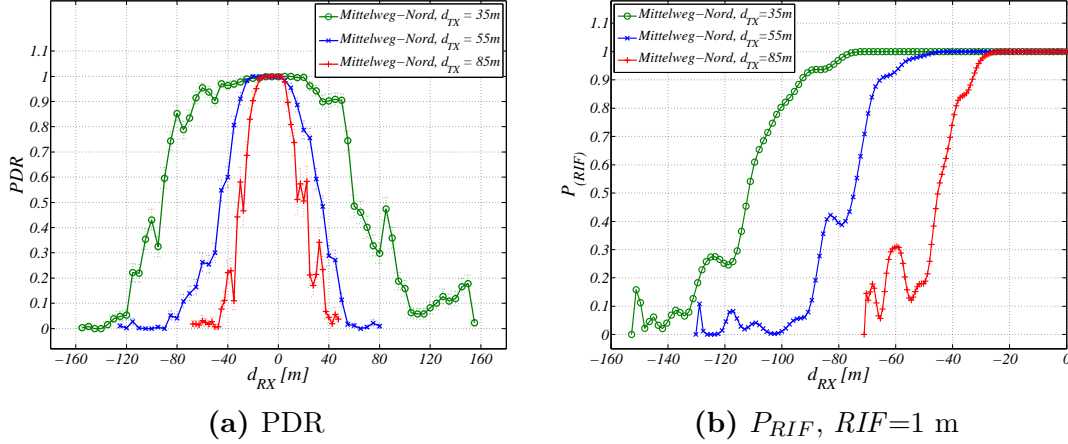


Figure 4.5: PDR (a) and P_{RIF} (b) as a function of the distance d_{RX} between the receiver and the intersection center under the condition of different transmitter positions

4.3 Vegetation at Rural Intersections

Vegetative areas, which obstruct the line-of-sight propagation path between Tx and Rx, are frequent in rural environment and are the most characteristic phenomena at rural intersections. For the radio waves propagating through the foliage channel vegetation is a random medium, where radio waves interact with a multitude of the randomly distributed scatters (leaves, branches, twigs, tree trunks) and hence, experiencing absorption, depolarization, multiple scattering as well as edge- and top-diffraction. Consequently, a transmitted signal reaches the receiver over multiple propagation paths resulting in frequency-selective fading. The total received signal power additionally manifests spatial and temporal fluctuations due to variable vegetation density and movement of vegetation elements [119].

The main propagation mechanisms show dependence on the wavelength. For instance, the measurement conducted in [92] with 700 MHz ($\lambda = 0.43$ m) and 240 MHz ($\lambda = 1.25$ m) signals shows that the effect of the vegetation channel is stronger at the higher frequency. It is due to the fact, that the average diameter of the tree trunks at antenna height is approximately $d = 0.43$ m, making them much better attenuators for 700 MHz signal than for 240 MHz one, where the trunk diameter constitutes only one third of the complete wavelength. The above also implies, that longer radio waves are mostly absorbed in the tree trunks and branches, whereas the absorption of radio

waves at SHF band occurs primarily in the foliage, needles and twigs.

In addition to absorption, a big amount of transmitted signal is attenuated due to scattering. It takes place when a radio wave enters a medium, which is dense with objects of smaller or comparable to the wavelength size. If the scattering objects are much smaller than the wavelength, a strong impact due to the vegetation can be observed [119]. Therefore, it is expected that radio waves at 5.9 GHz ($\lambda = 5$ cm) will be significantly scattered by small branches and twigs and attenuated by the foliage. Additionally, when a radio wave enters a scattering medium, such as vegetation, depolarization of the incident signal takes place [109].

Radio waves mainly diffract from the side and top of the foliage, thus due to the used antenna heights the diffraction is not expected to be the key propagation mechanism for V2V links [109].

Despite the importance of understanding each of these propagation mechanisms separately, this research does not aim at investigating exactly which of the propagation mechanisms results in the main part of the signal attenuation in V2V links. Instead we characterize a total attenuation produced by the vegetation layer. According to [109] the most significant factors leading to signal attenuation are: the state of the foliage, geometry of the measurement and vegetation density. The authors also state that the tree species or leaf shape has minor impact on the signal attenuation. Considering the fact that in real driving conditions the measurement geometry is unpredictable, the vegetation depth and the state of the foliage are more important factors for our research. In case of the short vegetation depth, the radio signal is dominated by coherent wave and almost not affected by scattering, however at greater vegetation depth the radio wave becomes incoherent and has random amplitude and phase [18], [109]. Moreover, excess signal attenuation when compared to the free space attenuation can be caused by the accumulation of water in the foliage, which depends on the current weather conditions and additionally varies due to seasonal effects. Thus, deciduous forest in winter causes less attenuation on the centimeter radio waves, whereas in spring or summer vegetative regions can cause significant signal strength impairment. However, during the out-of-leaf measurement the difference between experienced attenuation of these signals is minor. The above can be confirmed by the measurements conducted in [119].

Taking into account low elevated antenna used by V2V communication, even small trees or groups of high bushes can provoke radio signal attenuation. This makes investigation of the vegetation layer effect on the communication link quality highly relevant for our research.

4.3.1 Related Work

Up to today's point comprehensive measurement campaigns that characterize channel impairment due to vegetation have already been carried out. A substantial summary of models for prediction of attenuation due to vegetation layer in the frequency range of 200 MHz up to 9000 MHz as well as the measurement data reported in the literature, were resumed in Weissberger's final report in [155] in 1982. Furthermore, the authors

in [18] conducted series of measurements at 11.2 GHz at a uniformly planted apple orchard to determine the experienced attenuation of the radio signal due to increasing foliage depth. The work presented in [109] is a final report of a 15-month research project aimed at investigating the effects of the vegetation layer on millimeter radio waves and develop a generic model of signal attenuation due to vegetation for 1-60 GHz narrowband systems. The model is based on the elaborate empirical data gathered at twelve locations in England and combines edge diffraction, ground reflection and a direct (through vegetation) signal, which was modeled using Radiative Energy Transfer (RET) theory. The main goal was to characterize the effect of the different three types, state of the leaf, geometry of the measurement and vegetation density. The authors in [92] presented a new method for modeling the near-ground short-range propagation loss in forested areas at the VHF and the UHF bands. They show that reflections due to the dense tree canopy are of particular importance for short-range propagation at the VHF band and cannot be neglected. Moreover, the authors in [74] evaluate near-ground radio-wave propagation with the scope on emerging military applications (battlefield sensor networks, wireless communication between dismounted soldiers) and conduct narrowband and wideband channel measurement at 300 and 1900 MHz. They investigate the effect of antenna heights, radiation patterns, foliage environments and leaf humidity. The authors in [119] report the result of an extensive wideband channel sounding measurement campaign, which investigated radio wave propagation through the vegetation layer. The measurements were performed at 1.3, 2 and 11.6 GHz at sites with different measurement geometries and tree species. The authors evaluate the existing narrowband empirical vegetation attenuation models and investigate which characteristics of the vegetation layer (leaf state, measurement geometry, vegetation density, trunk diameters, etc.) have a more pronounced effect on the signal attenuation at 1.3, 2 and 11.6 GHz frequency bands.

Nevertheless, these research works were conducted under conditions that are not directly applicable to V2V communication (different operating frequencies, antenna height of 10 m and more, no mobility aspects were considered). Therefore, this section contributes to the existing research by investigating the LOS obstruction caused by clusters of trees and high bushes in terms of PDR and P_{RIF} . Specifically, our focus is intersection layout, vegetation types, densities, average trunk diameter and presence of branches at the antenna heights as well as seasonal effect. Furthermore, this chapter compares achievable P_{RIF} at urban and rural intersections and draws conclusions about the criticality of each environment in the scope of the DSRC communications.

4.3.2 Measurement Scenarios

We select following scenarios for our research: a sub-urban intersection in the park area with high and thick trees, an intersection with densely growing trees and bushes in rural environment and a rural intersection with a cornfield as line-of-sight obstruction between the vehicles. To capture the seasonal effect of the vegetation on the application reliability the measurements in all three scenarios were conducted in the in-leaf (summer) and out-of-leaf (winter) states. All measurements were performed under

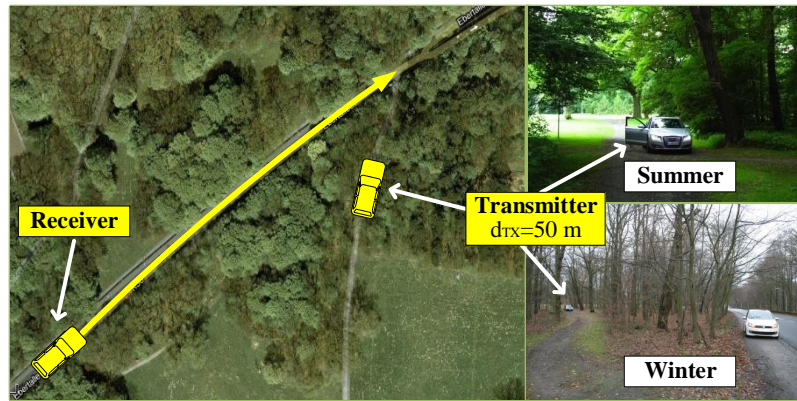


Figure 4.6: City park area with vegetation of a mixed type. $52^{\circ}15'59.4''\text{N}$, $10^{\circ}33'28.2''\text{E}$.

sunny and no-wind conditions with limited to almost no other traffic conditions.

City park scenario is characterized by the vegetation of a mixed type: trees and bushes of unequal height and irregularly spaced, with different foliage density, type of wood, leaf size, etc. Due to a great number of high trees in this scenario general branch and leaf density at antenna height is significantly lower than in the other two scenarios. Tx vehicle was placed 50 m inside in the intersection approach (Fig. 4.6). Due to the measurement geometry and location of Tx, the vegetation completely obstructs LOS between the vehicles. This scenario exemplifies a typical intersection scenario in the city park area. However, it can also be regarded as a highway exit scenario, when a breakdown occurs in the end of the curve with one vehicle (Tx) and another vehicle approaching it at the high speed (Rx).

Forest scenario addresses a typical intersection in rural environment. In this scenario the forest is densely planted with trees, which are on average lower than the trees in the previous scenario. Moreover, their branches start to grow only several centimeters higher the ground level, resulting in significantly higher leaf and branch density at the antenna height than in the city park. The vegetation density is additionally increased due to the intense underbrush of scrubs and high grass (at some places up to approx. 1 m) (Fig. 4.7). In this scenario the trees are also irregularly spaced, however we can observe that the vegetation density pattern approximately follows the "L"- shape: extremely dense at the roadside (high trees, grass and bushes) and less dense in the middle area (small saplings, a lot of high grass and less bushes). Moreover, at $d_{RX} = 70$ m and further at $d_{RX} = 25$ m before the intersection center the shrubbery is considerably expanded in the direction orthogonal to the driving direction of Rx (Fig. 4.7, "A" and "B" areas, and 4.8). The transmitting vehicle Tx was located 50 m away from the intersection center (Fig. 4.7).

Cornfield scenario illustrates another rural intersection with a cornfield as a NLOS condition between Tx and Rx. A cornfield does not belong to a mixed vegetation type, unlike in the previous scenarios. Corn plants have approximately identical height, width, leaf size, chemical composition, etc. Typically, they grow very densely

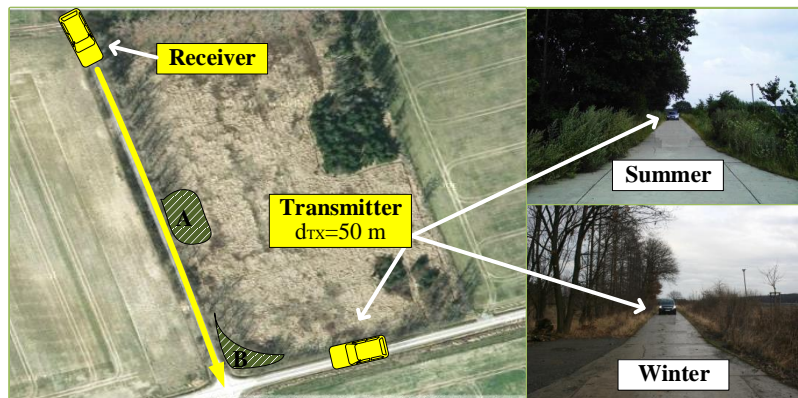


Figure 4.7: Rural area with thickly growing trees and bushes. $52^{\circ}15'22.2''\text{N}$, $10^{\circ}38'54.6''\text{E}$.



Figure 4.8: drop area "A", $d_{RX} = 70m$

and with approximately same distances from each other. Therefore, the cornfield vegetation layer can be considered homogeneous to a certain extent. The height of the plants exceeds 1.5 m, which ensures high vegetation density at the antenna height and complete obstruction of LOS between vehicles. The transmitter was positioned 30 m away from the intersection center (Fig. 4.9).

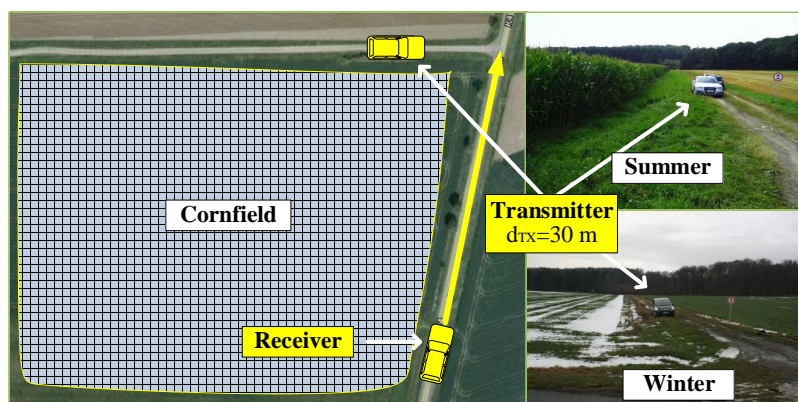


Figure 4.9: Rural area with a cornfield. $52^{\circ}17'10.8''\text{N}$, $10^{\circ}47'00.0''\text{E}$

4.3.3 Seasonal Effect

This section compares PDR and P_{RIF} in the *Forest*, *Cornfield* and *City park* scenarios to capture communication quality and application reliability in summer and winter.

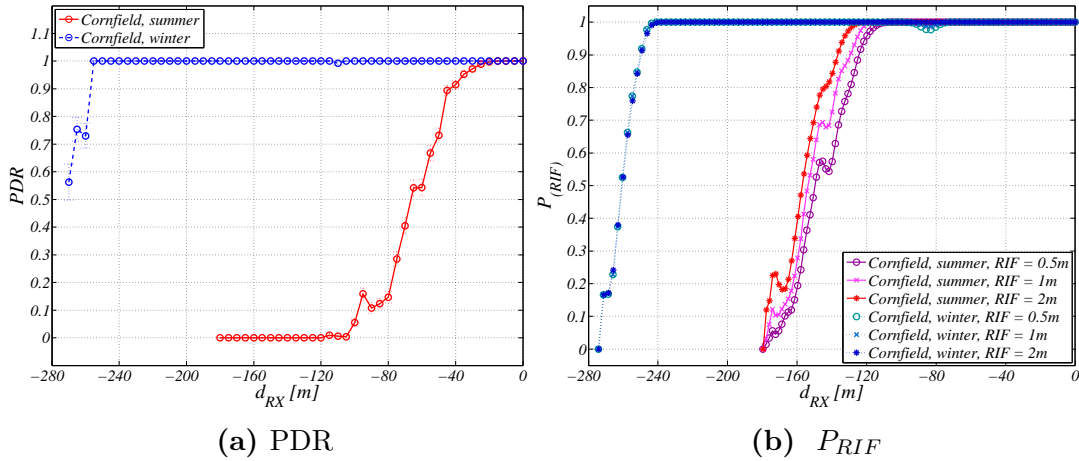


Figure 4.10: PDR (a) and P_{RIF} (b) as a function of the distance d_{RX} between the receiver and the center of the intersection for the cornfield scenario

Fig. 4.10a shows that the PDR obtained in the *Cornfield scenario* during the summer measurement starts to grow rapidly after a certain distance (approx. $d_{RX} = 100$ m), being completely attenuated by the vegetation layer before this point due to its high density. Due to the homogeneous distribution of the corn plants in this scenario and their strong similarity to each other, such vegetation type offers nearly constant foliage density over the whole measurement geometry. It results in a certain d_{RX} before which the received power is not enough to successfully decode the radio signal and after which it becomes sufficient over a short period of time. During the winter measurement the corn plants are not present in this scenario, thus it offers a close to free-space propagation conditions, which is demonstrated in Fig. 4.10a.

Fig. 4.10b depicts the P_{RIF} obtained during the summer and winter measurements in the *Cornfield scenario* for various RIF sizes. It can be observed, that in summer, similarly to PDR, P_{RIF} rises from 0 to 0.99 rapidly and all curves start to grow almost simultaneously. However, all P_{RIF} curves rise after passing approx. 180 m and then reach 0.99 with a minor difference, which significantly outperforms the results obtained with PDR. Further, the probabilities show much less fluctuation, when compared to the other two scenarios (Figs. 4.11b - 4.12b). Fig. 4.10b also shows that the P_{RIF_s} obtained during the winter measurements in the *Cornfield scenario* are almost identical regardless of the different RIF interval sizes. It leads to the conclusion, that in the event of near to free-space propagation conditions and small penetration rates P_{RIF} does not depend on RIF interval size, as any requirement of the information freshness will always be fulfilled. The reason is that due to LOS in winter the multipath components do not dominate the propagation of the radio signal,

thus leading to a minor variance of the communication channel.

Furthermore, the comparison of the P_{RIF} and PDR obtained in the *Cornfield scenario* during the summer measurements show an immense difference in d_{RX} ($\Delta d_{RX} \approx 85$ m) when the target $P_{RIF} = 0.99$ and $PDR = 95\%$ are achieved. It again confirms the fact that PDR cannot capture the application reliability adequately. The disagreement between PDR and P_{RIF} metrics in case of the *Cornfield scenario* is considerably larger than what can be observed at urban intersections (section 4.2).

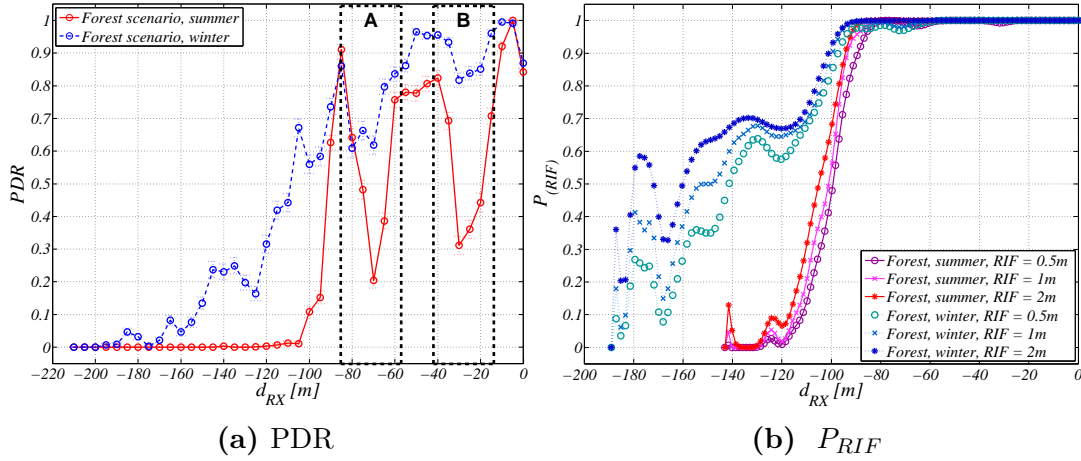


Figure 4.11: PDR (a) and P_{RIF} (b) as a function of the distance d_{RX} between the receiver and the center of the intersection for the forest scenario

The *Forest scenario* is of special interest due to "A" and "B" drop areas, where vegetation is denser due to the clusters of high bushes (Fig. 4.7). During the summer measurements PDR reaches 95% already at approx. $d_{RX} = 85$ m and then drops down at $d_{RX} = 70$ m and $d_{RX} = 25$ m to 20-30% (Fig. 4.11a). Therefore, in summer PDR reaches 95% only after a second drop area "B" when LOS between vehicles is available (approx. 7-10 m before the intersection center). This phenomenon is explained by the extremely high leaf and twig density at the antenna height, which forms a thick "green wall" (Fig. 4.8). The strong attenuating effect of branches and twigs is also confirmed by winter measurements, where the drop areas "A" and "B" are still noticeable even without the leaf attenuation. PDR in this case reaches 95% only at $d_{RX} = 20$ m. This shows that the attenuation of the radio waves due to dense branches at 5.9 GHz cannot be neglected. Thus, the vegetation effect in winter cannot be omitted while evaluating the DSRC performance.

The "A" and "B" drop areas do not have pronounced effect on the P_{RIF} s, which ensures much higher reliable communication range: P_{RIF} in summer reaches 0.99 at approximately 90 m before the intersection center (Fig. 4.11b). Furthermore, the P_{RIF} obtained in winter outperforms the summer one only with a minor difference due to a strong scattering effect of twigs. Moreover, the P_{RIF} obtained during the winter measurements in the *Forest scenario* reaches 0.99 later than the P_{RIF} obtained in the *Cornfield scenario* in summer despite thick growing corn plants (Fig. 4.10b,

Fig. 4.11b). The reason is extremely high twig density and simultaneously variable thickness of the vegetation layer, which characterizes the forest environment even in winter.

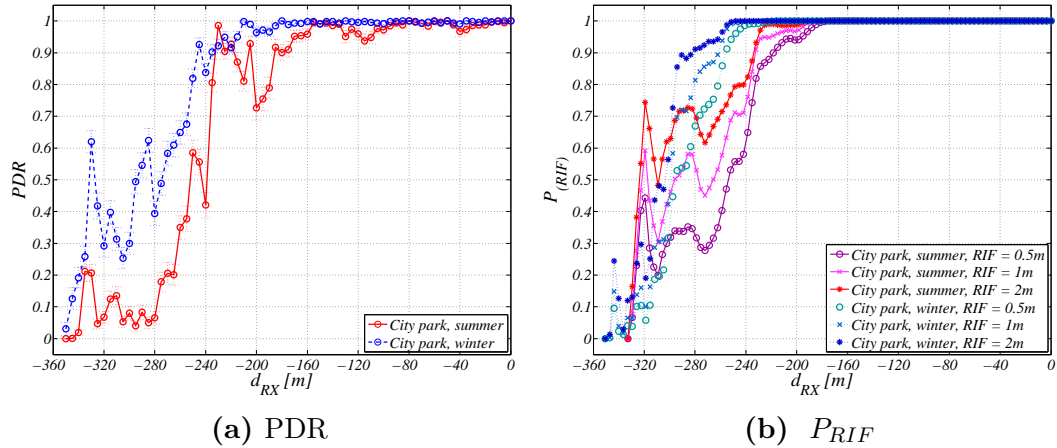


Figure 4.12: PDR (a) and P_{RIF} (b) as a function of the distance d_{RX} between the receiver and the center of the intersection for the city park scenario

The *City park scenario* demonstrates best performance, where PDR exceeds 95 % as early as 220 m during the winter measurements and at 160 m in summer (Fig. 4.12a). It proves that the radio waves in DSRC channels will be mostly attenuated due to foliage and small branches and not the tree trunks.

Fig. 4.12b demonstrates the P_{RIF} obtained in the *City park scenario* in winter and summer. The probability functions reach 0.99 at $d_{RX} \in [260...240]$ m in winter and at $d_{RX} \in [220...180]$ m in summer. In contradiction to other scenarios, the P_{RIFs} obtained in summer and in winter in the *City park scenario* start to grow at approximately the same distance to the intersection center. It proves that the foliage attenuation does not dominate the propagation character in this scenario. Unlike the *Forest scenario*, the P_{RIF} obtained during the summer measurement in the *City park scenario* demonstrates higher fluctuation of values. It allows us to conclude that the vegetation density in this scenario is much more varied.

Comparing PDR and P_{RIF} in Figs. 4.12a and 4.12b during the summer and winter measurements we can see that similarly to other scenarios, P_{RIF} reaches 0.99 earlier than PDR becomes equal to 95 %. Furthermore, comparing Figs. 4.10b, 4.11b 4.12b we can conclude that the density of the leaf and twig layer at the antenna height has the most significant effect on the application reliability. The second most significant factor is the homogeneity of the vegetation layer.

4.3.4 Urban vs. Rural Intersections

Here we analyze PDR and P_{RIF} metrics based on the measurements conducted at rural intersections in winter and in summer, compare them with already discussed

urban intersections and determine which environment has a more pronounced effect on the application reliability (Fig. 4.13 - 4.14).

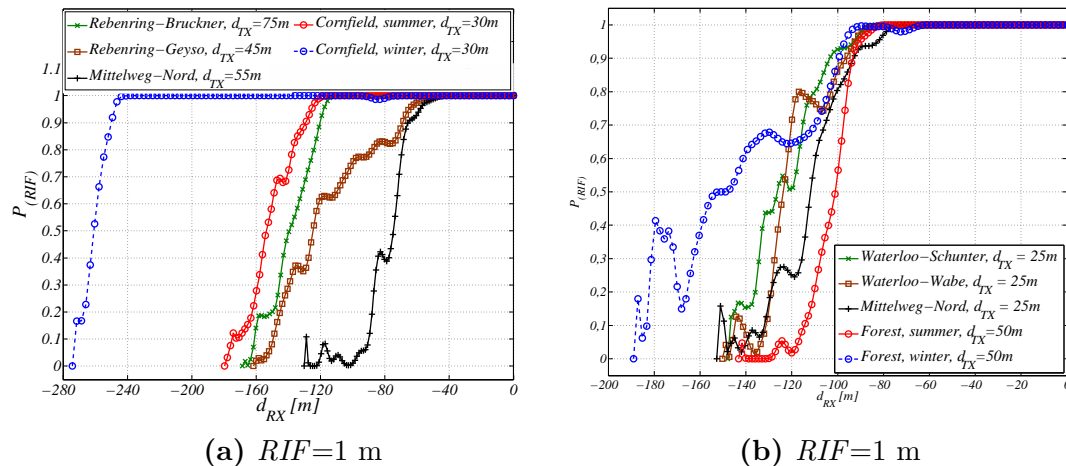


Figure 4.13: P_{RIF} as a function of the distance d_{RX} between the receiver and the center of the intersection for different intersections in urban and rural environment

Fig. 4.13a demonstrates, that the *Cornfield scenario* in winter represents an ideal case, as nothing obstructs LOS between the vehicles from the beginning of the measurement. Interestingly, the *Cornfield scenario* still outperforms the majority of urban intersections even during the summer measurements. An exception is *Rebenring-Brucknerstrasse*, where the measurements were conducted at 75 m. Therefore, it can be expected that this intersection will have a better performance than the *Cornfield scenario* in summer by a comparable d_{TX} .

Fig. 4.13b demonstrates that the probability functions obtained in the *Forest scenario* reach 0.99 approximately at the same distance as those obtained at the majority of the urban intersections. Interestingly, according to the measurement results presented in 4.3.3 this intersection represents the worst-case rural scenario due to a strong vegetation impact (Fig. 4.11a, drop area "A" and "B").

Fig. 4.14 demonstrates the P_{RIF} obtained in the city park area. We can see that the P_{RIF} achieved during the winter and summer measurements considerably outperforms those at all urban intersections, making this scenario more favorable than all urban intersections.

Results in Figs. 4.13 and 4.14 demonstrate that even the worst-case vegetation scenario (forest), when evaluated with P_{RIF} metric, offers equivalent application reliability in summer and winter, when compared with the results obtained at urban intersections. Furthermore, by minor leaf density at the antenna height (park area) vegetation scenarios tend to outperform urban intersections. Interestingly, due to the homogeneity of the vegetation layer such critical vegetation scenarios as cornfield can exhibit comparable results or even outperform urban intersections in terms of the application reliability.

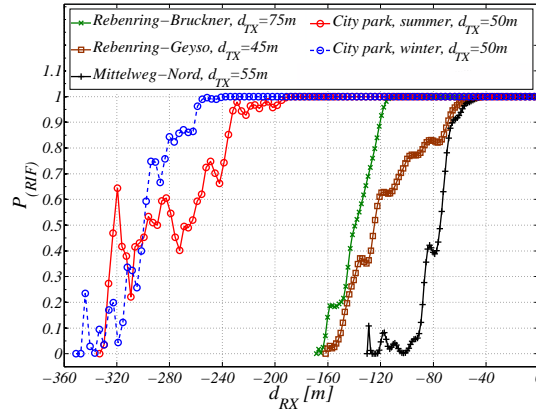


Figure 4.14: P_{RIF} as a function of the distance d_{RX} between the receiver and the center of the intersection for different intersections in urban and rural environment

4.4 Impact of Weather Conditions

The interaction of radio waves with different combinations of hydrometeors is another factor that may affect radio wave propagation and cause additional field strength degradation. The attenuation due to hydrometeors is provoked by several additional factors: absorption of radio waves in water or dust particles, scattering in clusters of water drops and depolarization phenomenon.

Absorption takes place due to the transformation of the radio wave energy into the heat energy. It happens because of the polarization currents, which are induced in each attenuating particle (raindrop, hail, gas molecules, etc.) as the radio wave transverses through the medium filled with precipitation. Scattering of radio waves occurs due to the redirection of the incident wave into back (back scatter) and side (side scatter) directions, preventing the total amount of energy to propagate in the initial direction. Moreover, it is also conditioned by the redistribution of energy in space: owing to the induced polarization currents, every water drop emits the energy uniformly in all directions [118]. Absorption and scattering depend on physical state of the hydrometeors, size, intensity, temperature as well as the wavelength and polarization of the incident waves. In case of the low frequencies the particle size is considerably smaller when compared to the wavelength, therefore, the attenuation is mainly due to the absorption process. However, the amount of attenuation due to scattering grows with the increase of drop sizes and shortening of wavelength [118]. Therefore, at the higher frequencies signal degradation due to scattering constitutes a significant part of the total attenuation experienced by the incident wave.

Depolarization is caused by the non-spherical form of the raindrops. It is noteworthy, that it decreases the performance of a communication system only in the event of using dual-polarization and can be neglected otherwise [149].

4.4.1 Related Work

Up to the present, the attenuation due to rain and snow has already been investigated in many research works. The authors in [22] report measurements results for millimeter wave wireless network and characterize rain rate, Bit Error Rate and corresponding received power levels. They have measured rain attenuation constant, cumulative rain rate distribution, relation between availability and path distance and compared rain attenuation at 25 GHz and 38 GHz. The authors in [67] performed the measurements in 120 GHz frequency band during several heavy rain seasons and investigated the reliability of the wireless link. They have found that the measurement results show a good agreement with the ITU, Laws and Parsons models. A rain fading simulation model for broadband wireless channels in millimeter wavebands based on elaborate measurement data is derived in [68]. The model includes the signal attenuation due to multipath and path loss effects under different rain rates. The authors have found out that the amplitude of the waveforms due to rain effect follows Rician distribution with the K factor as a function of rain intensity. The authors in [64] investigate rain attenuation in terrestrial communication links at high microwave and millimeter wave frequencies. They discuss challenges while applying traditional ITU-R statistical prediction model and propose alternative approach to estimate attenuation statistics due to rain by using the radar data. Furthermore, the authors in [82] investigate attenuation of the signal strength due to rain at 20-40 GHz frequency bands and also suggest the use of weather radar images for building rain attenuation prediction models. The authors in [106] conduct an elaborate analysis of intercell interference for a spectrally efficient broadband wireless access cellular network. They focus on the investigation of the spatial inhomogeneity of the signal attenuation due to precipitation over multiple paths and provide simulation results. In their series of works [116], [114], [112], [110], [113], [115], [111] Sakarellos et al. present an extensive research of link reliability at millimeter radio wave frequency band, considering the rain effect as one the biggest concerns. In their works the authors present a method for the rain channel fading estimation and provide extensive numerical results. Furthermore, the authors investigate optimum placement of radio relays in dual and triple-hop networks. They also present the results of the outage performance analysis due to rain attenuation at operating above 10 GHz and at extremely high frequencies above 50 GHz.

The authors in [126] investigate attenuation due to snow in the frequencies of GSM communication (900 MHz, 1800 MHz and 2270 MHz) by using Discrete Propagation Model. They have found out that due to the inhomogeneity of the snow particle sizes the snow attenuation can be higher than rain attenuation. The authors in [72] investigate attenuation due to melting snow layer at the higher microwave frequencies and evaluate the effect of the melting profile, velocity profile and average-density of the melting-snow particles. Another work, which investigates the effect of the melting snow layer on the radio wave attenuation, is presented in [159]. The authors investigate specific attenuation of the melting snow in the frequency range 1-1000 GHz and the precipitation rate below 12.5 mm/h. The results of comparative quasi-synchronous measurement study of millimeter radio wave attenuation by snow at 138 GHz and

247 GHz are presented in [61]. The authors in [143] specifically focus on the attenuation prediction due to rain and wet-snow combined. The work in [46] derives the coefficient of absorption in moist snow layer at low microwave frequencies, specifically concentrating on the effect of the water particles shapes within wet snowflakes and presents simulation results. In [57] the authors investigate the attenuation and the phase shift of radio waves at microwave frequencies between 6-100 GHz and snow rate between 0.5-3 mm/hr.

Despite the vast amount of research devoted to the radio wave attenuation due to hydrometeors, the existent works do not consider these effects in scope of V2V communication due to the relatively recent research activities in this field. Thus, the following analyzes to what extent individual forms of precipitation can affect radio wave propagation when operating at 5.9 GHz frequency band.

4.4.2 Rain Attenuation

The attenuation of the radio waves as they propagate through the rain infested medium depends on the raindrop size and density as well as the length of the propagation path. The amount of the experienced attenuation due to rain is greater compared to other precipitation forms. Nonetheless, the following demonstrates that the rain impact at the 5.9 GHz frequency band can be neglected.

Total rain attenuation loss A_r in dB is given by [149] as follows:

$$A_r = \alpha_r \times L_{eq}(R) \quad (4.1)$$

where α_r is the attenuation per unit length (specific attenuation) in dB/km and the $L_{eq}(R)$ is the equivalent path length in km. The specific attenuation is given by:

$$\alpha_r = a(f) \times R^{b(f)} \quad (4.2)$$

where R is the rain intensity in mm/h and $a(f)$ and $b(f)$ are the frequency dependent coefficients.

According to [149], specific attenuation is proportional to the rain rate and grows rapidly with the operational frequency (Fig. 4.15). The rain intensity R is classified according to [34] into: drizzle, light rain, moderate rain, heavy rain and heavy rain shower (Table 4.2).

Rain type	drizzle	light rain	moderate rain	heavy rain	heavy rain shower
$R, mm/h$	0.5	1 - 5	5 - 20	20 - 40	≥ 40

Table 4.2: Rain rate [34]

$L_{eq}(R)$ is determined by the height of the freezing level, thus it is not relevant in the event of V2V communication. Therefore, further only specific attenuation is considered. If it is required to define the amount of attenuation in rain with respect

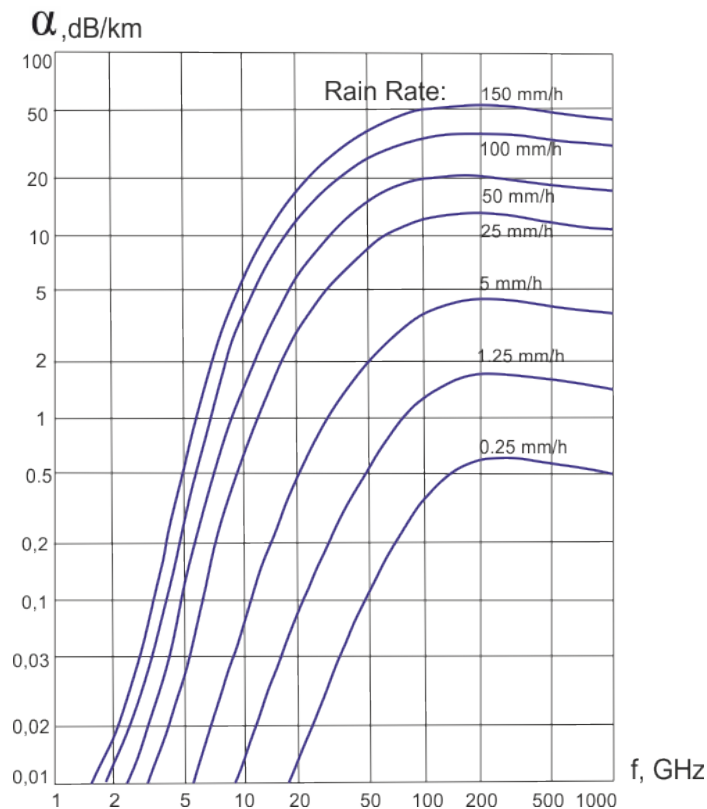


Figure 4.15: Attenuation per unit length vs. frequency and rain rate [149]

to a specific air temperature, the obtained value of α_r is to be adjusted in conjunction with correction coefficients reported in Table 4.3 [34]. By air temperature of 18 °C adjustment coefficient for listed frequencies equals to 1.

In the event of higher rain rates, due to the non-spherical form of the raindrops, specific attenuation α_r demonstrates dependence on the polarization type. Greater attenuation values are registered in the case of horizontal polarization. According to empirical data, the values of α_r , for horizontal polarization are greater than those for the vertical one at approx. 10-25% [42], [34]. The values obtained from Figure 4.15 are closer to the ones for vertical polarization.

In view of the foregoing, we can conclude that even by rain rates close to 50 mm/h, vertical polarization and air temperature 0 °C, the attenuation of radio waves at 5.9 GHz in rain does not exceed 1 dB/km.

4.4.3 Attenuation in Snow

Calculation of the attenuation due to snow is a challenging task, owing to irregular size and shapes of snowflakes. Considering that the attenuation of the radio waves due to dry and wet snow may vary significantly, the following examines these two phenomena individually.

$R, \text{mm/h}$	f, GHz	0°C	10°C	30°C
2,5	60	0.87	0.95	1.03
	24	0.85	0.99	0.92
	9.4	0.82	1.01	0.82
	3	2.02	1.4	0.7
12,5	60	0.9	0.96	1.02
	24	0.83	0.96	0.93
	9.4	0.64	0.88	0.9
	3	2.02	1.4	0.7
50	60	0.94	0.98	1
	24	0.84	0.95	0.95
	9.4	0.62	0.87	1.99
	3	2.01	1.4	0.7

Table 4.3: Values of correction coefficients for computation of specific attenuation in rain [34]

Dry Snow and Hail

Attenuation of the radio signal in the medium filled with dry snow or hail α_s is considerably lower compared to the effect caused by the rain of the same rate due to smaller permittivity of solid particles (for water $\varepsilon \approx 80$, for ice $\varepsilon \approx 2 - 3$). Table 4.4 presents the values of the specific attenuation in dry snow in case of the snowfall rate of 10 mm/h as well as the corresponding values of α_r in case of the rain of the same intensity [34].

f, GHz		8	11	15	18	25	35
$\alpha_s, \text{dB/km}$	dry snow	0.0067	0.0107	0.02	0.0312	0.0362	0.281
	rain	0.085	0.24	0.5	0.78	1.5	2.6

Table 4.4: Comparison of specific attenuation due to dry snow and rain [34]

The gathered empirical data infer that for $f < 50$ GHz the impact of dry snow and hail is to be neglected [34].

Wet snow

Specific attenuation in wet snow is on average comparable with the one due to rain of the same rate. However, in separate cases, owing to the formation of large wet snowflake clusters the value of α_s can grow in 5 - 10 times [34].

4.4.4 Attenuation in Fog

While calculating the amount of attenuation in fog, it is considered as another form of rain. Since it remains suspended in the atmosphere, the attenuation is determined by the quantity of water per unit of volume and by the size of the droplets [42], [34]. The attenuation due to fog is given as follows:

$$\alpha_f = k_e \times M \quad (4.3)$$

where α_f is the specific attenuation due to fog in dB/km, M is the quantity of the liquid water per volume unit (the water content) in g/m^3 and k_e is the attenuation coefficient per volume unit $\frac{\text{dB} \times \text{m}^3}{\text{km} \times \text{g}}$.

Figure 4.16 [34] demonstrates the dependence of k_e on the operational frequency for air temperatures ranged from -8 to $+20^\circ\text{C}$. The most common values of M are listed in Table 4.5 [34]. According to [34], water content of $0.3 \text{ g}/\text{m}^3$ corresponds to optical view of 137.5 m; $M = 1 \text{ g}/\text{m}^3$ to 55 m and $M = 1.7 \text{ g}/\text{m}^3$ to 37 m.

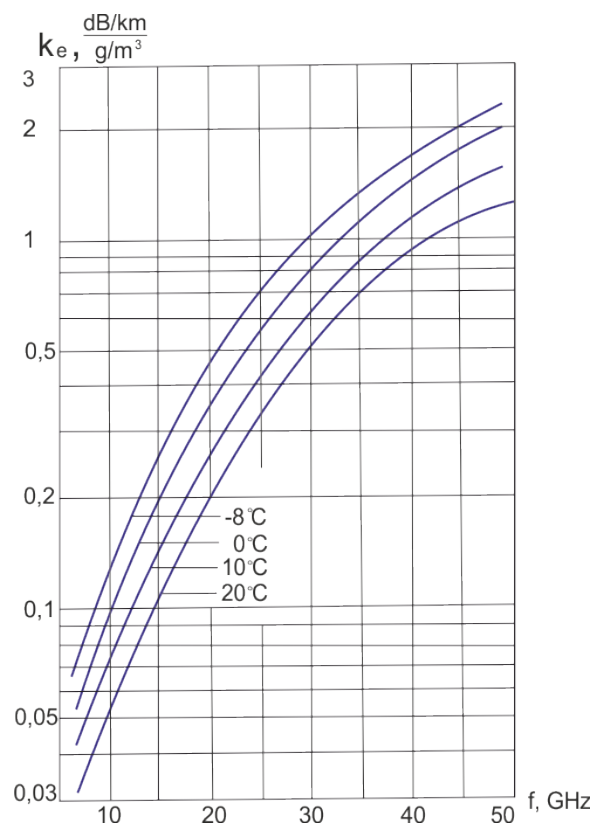


Figure 4.16: Specific attenuation in fog α_f vs. operating frequency [34]

Aggregate state of particles	$M, g/m^3$
liquid drops, ($t > 0^\circ C$)	0.3-1, rare until 1.7

Table 4.5: Water content in fog [34]

4.4.5 Attenuation in Gases

In addition to previously discussed types of attenuation, radio waves also experience the field strength degradation due to absorption in the molecules of oxygen (O_2) and water vapor (H_2O)². According to [118], the absorption effect is more significant in the case of the molecules of H_2O due to the molecular polarity. The opposite charges in such a molecule force it to align with the applied field of the incident wave. Due to a continuous change of the electromagnetic field direction as a radio wave propagates through the communication medium the realignment of these molecules also happens continuously and thereby induces the field strength degradation. Obviously, with the increase of the operation frequency the absorption loss also increases, as the realignment takes place more rapidly. The absorption in non-polar molecules, such as oxygen (O_2) takes place due to the interaction of the incident field of a wave and the gas molecules, which possess electric and magnetic moments. The molecules of H_2O and O_2 both contribute to the total absorption amount, which is frequency-dependent. Several resonance peaks are reached when the frequency of the influencing field concurs with the own frequencies of molecular vibrations.

The attenuation in gases is given by equation 4.1. Specific attenuation in gases $\alpha_g, dB/km$ for oxygen (air pressure of 1013 mb, temperature of $15^\circ C$) and water vapor (specific humidity $7.5 g/m^3$) is illustrated in Fig. 4.17 [41]. We can see that attenuation due to oxygen and water vapor at the frequencies below 15 GHz is less or equal to 1 dB/km and, thus, can be neglected [34].

4.4.6 Attenuation in Sand and Dust Storms

In the worst case sand and dust storms may reduce the vision to less than 10 m. The average size of particles equals to 0.015 cm for sand and 0.008 cm for clay dust [40]. At the frequency of 10 GHz and particle density of $10^{-5} g/cm^3$ (approximately equals to the 10 m optical view) attenuation in sand storms corresponds to 0.1 dB/km and into the clay dust 0.4 dB/km [42], [34]. Due to insufficient experimental data this type of attenuation requires further research work. Nevertheless, currently available information allows us to conclude that, similarly to attenuation due to other weather conditions, attenuation in sand or clay dust storms is negligible.

² Other atmospheric gases may also have a significant impact on the field strength in very dry air at the frequencies above 70 GHz [34]

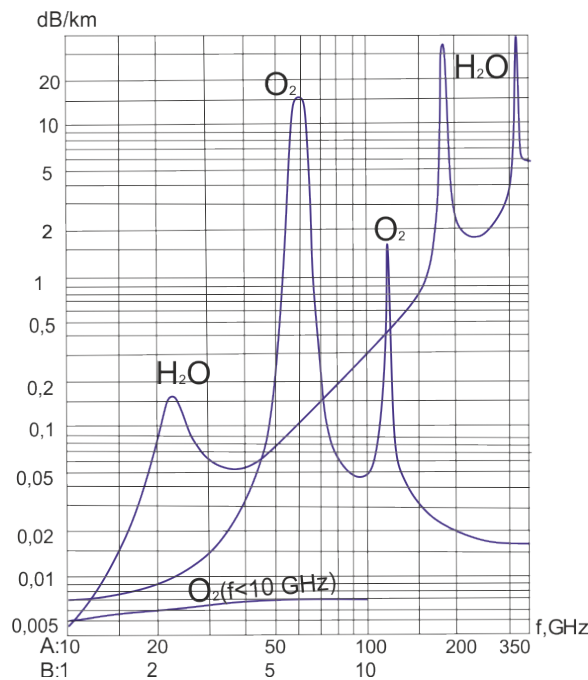


Figure 4.17: Dependence of α_g for oxygen O_2 and water vapor H_2O on operating frequency: A - scale for O_2 and H_2O at the $f > 10$ GHz; B - scale for O_2 at the $f < 10$ GHz [34]

4.5 Summary

The goal of this chapter was to evaluate environmental effects on the application reliability based on real-world experiments. In each measurement scenario this research obtained communication ranges using two metrics: packet delivery ratio and probability of the information freshness P_{RIF} . Based on the analysis of the measurement data this research has demonstrated a significant difference in reliable communication range values when obtained with these metrics. It has been observed, that in all urban and rural intersection scenarios the PDR metric delivered more pessimistic results than P_{RIF} metric. The evaluation has also shown that defining communication ranges only with a single PDR metric cannot always adequately translate communication link quality to V2V safety applications.

The measurements results in urban environment demonstrated that the presence of the significant roadside scatters in the relevant quadrants of the intersection plays the most important role towards reliable V2V link provision. Thus, the half-open intersection topology has shown itself to be the most unfavorable among the selected topologies. On the other hand, closed intersection topology exhibited in many cases high communication ranges. It is, however, worth noting, that diffuse scatters, such as park areas, or distant placement of significant scatters from the intersection center can result in considerable performance degradation and make closed intersection topology comparable to the half-open in terms of achievable communication ranges.

This chapter has also confirmed that traffic conditions have a considerable impact on

the application reliability and cannot be neglected. The measurements were performed with sedan-type vehicles, whose effect is frequently neglected as these vehicles do not directly obstruct the line-of-sight between a transmitter and a receiver. However, the measurements have shown that the resulted channel variance due to the presence of a multitude of highly mobile scatters result in a significant reduction of the achievable communication ranges.

During the measurements in urban environment reliable communication ranges at the selected intersections fell in the range of [100...185]m when defined with the P_{RIF} metric, which is enough to provide all future driver notification levels. Assuming that the vehicle speed in urban environment is equal to 50 km/h the earliest driver notification level can be issued at 13.3s in the best case and at 7.2s in case of the half opened intersection topology when braking on the dry asphalt surface. In case of wet and snow-covered surfaces, minimum stopping distance is equal to 30m and 62m respectively. This means that in case of all selected intersection topologies in urban environment a V2V collision avoidance application can effectively support the driver when driving on dry, wet and snow-covered surfaces.

When assessing rural intersection scenarios this research also evaluated packet delivery ratio and achieved application reliability with respect to varying vehicle positions, intersection layout, vegetation type and densities. The results have shown that in all selected rural scenarios the vegetation density at the antenna height is the most significant impact factor for the V2V communications. Furthermore, we have observed that different vegetation type structures influence the communication link reliability in a different way and that the homogeneity of the vegetation layer has a pronounced effect. For instance, a cornfield as a LOS-obstruction between a transmitter and a receiver has shown to be not the most critical intersection scenario despite high vegetation density. On the other hand, mixed vegetation type and a variable density in the forest scenario have resulted in shorter communication ranges. Moreover, this research has confirmed that the vegetation effect has to be taken into account not only in summer but also in winter, as dense twigs attenuate the signal at 5.9 GHz even in out-of-leaf state. The comparison of urban and rural intersection scenarios has shown that the resulted communication ranges due to vegetation obstruction are comparable to those in urban environment or outperform them when the vegetation density at the antenna height is minor.

Finally, the theoretical analysis of the weather impact at 5.9 GHz has shown that out of selected precipitation types the attenuation due to rain or wet snow is the most prominent. However, even this does not exceed 1 dB/km and therefore can be neglected.

In the next chapter we are going to analyze application reliability in different intersection scenarios and under the high network load conditions. Furthermore, based on suggested metrics we are going to perform a feasibility analysis of different intersection scenarios specifically for ICW and FCW.

5 Feasibility Analysis

Due to the nature of VANETs the cooperative vehicular systems will have to operate under constantly changing network load conditions. Thus, to achieve the future large-scale deployment of V2V safety use cases several important issues concerning network scalability still need to be answered. Specifically, it is important to gain a deep understanding of how reliably V2V applications can operate in saturated networks as well as define the most favorable and the most challenging communication scenarios.

By higher penetration rates such network parameters as message generation rate f_g and data rate R_b can considerably affect the communication picture. Therefore, this chapter establishes how these network parameters will affect application reliability as well as defines their optimal values towards enabling effective work of V2V safety applications in various application-specific scenarios. Furthermore, we also investigate the effect of the buildings and positions of Tx and Rx vehicles relatively to the intersection center in the high network load scenarios. Moreover, we perform a feasibility analysis and evaluate whether timing and spatial requirements of V2V applications can be fulfilled in these scenarios. Thus, the aims of this chapter are:

- apply the metrics, which have been proposed in chapter 3 for Intersection Collision Warning and Forward Collision Warning when operating in the high network load conditions;
- study the effect of message generation rate f_g , data rate R_b , intersection topology as well as combination of Tx-Rx positions on the application reliability under the condition of different penetration rates;
- perform a feasibility analysis of the selected scenarios and show their potential for future V2V safety applications, specifically for ICW and FCW.

This chapter is organized as follows: section 5.1 gives a brief overview of related work. Section 5.2 describes the simulation setup and provides a detailed description of the simulation scenarios. Section 5.3 discusses the results of the simulation study and draws conclusions about the investigated parameters. Finally, section 5.4 overviews the ICW and FCW reliability requirements and presents the results of the feasibility analysis.

5.1 Related Work

To date a lot of research concerning efficient message dissemination in congested scenarios has been done: [122], [23], [153], [157]. The most elaborate measurement study on V2V safety communications scalability was conducted by V2V Interoperability Project [85].

Several research works investigate the performance of V2V safety applications in different congestion scenarios and take their operational requirements into account. The authors in [128] evaluate *traffic safety effective range* at which communication partners are able to receive 1-hop broadcast messages with a success probability of 90% or higher while designing congestion control protocols. They evaluate overtaking and lane change assistance applications and show how individual operational requirements imposed by different safety applications impact communication settings on each node. The authors in [78] also investigate the problem of congestion control in large wireless networks, but do so from the perspective of the *information age*. They propose a fully distributed application layer broadcast rate adaptation framework, which is able to estimate the information age at each node and adapt to the rapid changes of the network size. The study in [83] addresses the performance of safety applications by defining another key operational metric: *amount of invisible neighbors* within a certain region of interest (ROI). The authors conduct a simulation study in highway and urban scenarios aiming to find the best combination of transmission range and message generation rate which would result in the minimum number of invisible neighbors in the ROI. The performance of Cooperative Adaptive Cruise Control and the Lane Change Assistant is evaluated in [81] considering the *update delay* metric. Resting upon this metric, the authors define the probability of exceeding maximum update delay threshold for these applications in a highway scenario.

The authors in [31] investigate performance of V2V safety use cases and V2I commercial use cases in saturated channel conditions in urban environment. They focus on Emergency Vehicle Routing (EVR) use case, where the aim is to dynamically route vehicles upon receiving a broadcast from approaching emergency vehicle. This allows for shorter travelling time of EV also in highly dense traffic conditions. To evaluate performance of commercial applications, the authors investigate mean throughput with respect to the number of communication vehicles.

Performance of Intersection Collision Warning and Forward Collision Warning is specifically investigated in [50], [24], [108] and [21]. Authors in [50] develop a simulation environment to evaluate performance of ICW. The vehicle traffic simulator is realized with MATLAB, where the authors are able to vary vehicle classification, size, speed, origin and destination as well as flow rate. Furthermore, they are able to vary the number of lanes in the intersection, traffic light management and specify different intersection collision scenarios. However, network scalability aspects were not investigated in detail in this study, as during each simulation scenario only 20 vehicles were present. The authors in [24] make use of findings in [50] and present simulation architecture for the evaluation of the ICW systems. The study investigates the effect of the buildings in the intersection, repeater in the intersection center,

vehicle density and packet transmission interval on the experienced packet collisions and latency. However, to decide which vehicles in the scenario will be able to receive warnings successfully, the authors obtain experienced packet collisions as a statistical average of a large set of different simulations scenarios. Furthermore, maximum message generation frequency, which was investigated in the scenarios is equal to 4 Hz, the transmission power was set to 10 dBm and antenna height of 25 cm above the vehicle roof. The authors in [108] also evaluate performance of Intersection Collision Warning in high density network conditions, however the network is limited by only 100 transmitters, packet size is equal to 128 bytes, nodes remain stationary and hidden node problem is not considered as well.

The authors in [127] conduct a simulation study, where they evaluate the performance of inter-vehicle communication systems and connected with it reliability of V2V safety messages. The study takes the following operation conditions into account: vehicular speed, transmission power, driver reaction time and vehicular traffic density. The authors evaluate two vehicles which move towards each other in the cross-traffic and obtain mean distance from the calculated crash point (intersection center) when the driver manages to stop the vehicle.

The authors in [21] select *zero amount of false positive/negative warnings* issued by Forward Collision Warning as key performance metric. In this study the authors define maximum node density when requirement of zero false positive/negative warnings can always be fulfilled. Further, they define to what extent this idealistic application requirement can be relaxed to achieve a balance between network scalability and cooperative awareness accuracy. The simulations are based on the empirical model presented in [80].

The study in this chapter has partly been inspired by the research described above. However, we focus on using more precise set of application requirements and more realistic application simulation approach.

5.2 Simulation Setup and Scenario Description

The following section provides the reader with the information about simulation setup and scenario description and additionally gives details on specific features and assumptions, which are used in the following simulation study.

Simulation Environment

To conduct our research we use the simulation environment and setup which have been presented in [66]. We investigate urban intersection scenarios, where the road traffic network is realized with SUMO (Simulation of urban mobility) tool and communication network is built with OMNeT++ simulation framework. The OMNeT++ communication model is compatible with the ITS-G5 specifications and includes a detailed representation of the frame collisions due to co-channel interferences, including physical layer capture (PLC). Transmission of CAMs via periodic single-hop

broadcast is realized with the Outside the Context of a Basic Service Set (OCB) mode. The implemented path loss models are obtained based on measurements in [125]. Additionally, the utilized simulation model includes Nakagami fading model and several shadowing models.

Parameter	Value	Parameter	Value
P_t	23 dBm	f_c	5.9 GHz
G_t, G_r	1.0	h_t, h_r	1.5 m
f_g	5, 10, 15 Hz	CW	15
Message size	400 Bytes	MAC frame size	480 Bytes
R_b	3, 6 Mbps	N	-100 dBm
SIR_{th}	12, 9 dB	$P_{r,th}$	-91 dBm
$P_{r,cs}$	-93 dBm	Fading model	Nakagami-m

Table 5.1: Simulation parameters [66]

Table 5.1 summarizes the simulation parameters, which were used in the following scenarios. P_t stands for the transmission power, f_c is the carrier frequency, G_t and G_r are gains of the transmitter and receiver antennas, h_t and h_r are the heights of the antennas at Tx and Rx, f_g represents the message generation rate, CW is the size of the contention window, R_b denotes the data rate and N is the noise floor. Furthermore, SIR_{th} stands for SNR threshold, after exceeding which the frame cannot be decoded. The receiver sensitivity is depicted with $P_{r,th}$ and $P_{r,cs}$ is the carrier sense threshold (for more details refer to [66]).

Scenario Topology

The simulation study utilizes Manhattan traffic road network, which consists of 9 idealized symmetrical intersections, where each side of the building block is equal to 300 m and each street has a width of 40 m (Fig. 5.1a). All streets in the scenario are two-laned and cross each other at 90° angle.

To avoid boundary effects and ensure realistic communication conditions, we conduct our evaluation in a specific ROI: intersection in the middle of the simulation network, surrounded by the buildings F, G, J and K (Fig. 5.1a). Furthermore, we specifically consider three scenario topologies: *close*, where all four buildings are present in the ROI; *half-open*, with only two buildings and *open*, with no buildings in the ROI (Figs. 5.1a - 5.1c). This allows us to investigate how different placement of the buildings will impact achievable application reliability, given that each time the same intersection under the same combination of the network parameters is considered.

Penetration Rate

The total number of all vehicles in the simulation network is equal to 1250, which corresponds to the traffic density of 82.5 veh/km/lane with inter-vehicle distance of approximately 7.12 m. This traffic density is fixed and stays constant through the

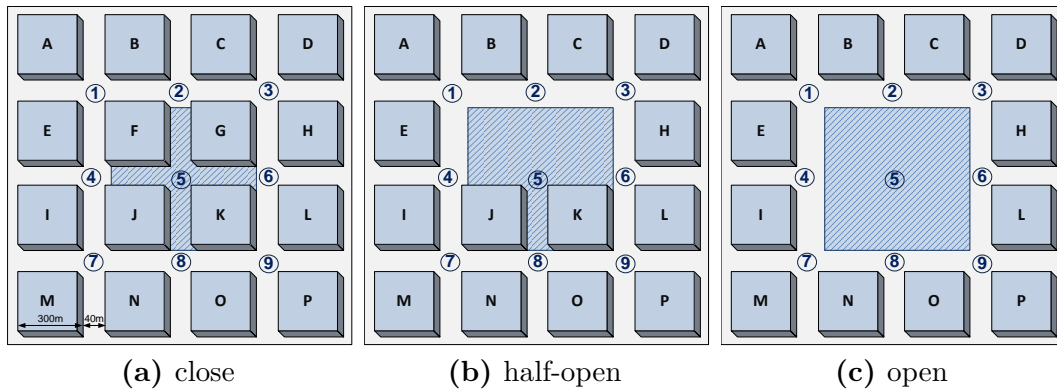


Figure 5.1: Intersection topologies: close, half-open, open

complete simulation study. Instead, the communication density (number of vehicles in the network which are able to broadcast and receive awareness messages) varies by changing different penetration rates. Such approach allows us to investigate application reliability in different network saturation conditions and simultaneously ensures the homogeneous distribution of the vehicles in the scenario.

For further investigation we consider three different penetration rates: $p = 5\%$, $p = 10\%$ and $p = 25\%$ from the maximum number of the vehicles in the communication network. According to [130] and [60] these penetration rates are comparable with *free flow*, *normal* and *high density* traffic classes respectively. The *free flow* describes sparse traffic conditions, where the vehicles are able to follow their routes without additional delays due to other traffic participants. The *normal* traffic class corresponds to the normal traffic flow with still short waiting times. The *high density* represents a very busy but still stable traffic (rush hour but not a traffic jam yet). Traffic density k and the average distance between vehicles d_v for each traffic class are given in Table 5.2.

Table 5.2: Traffic classes

	$p = 5\%$ <i>free flow</i>	$p = 10\%$ <i>normal</i>	$p = 15\%$ <i>high density</i>
k [veh/km/lane]	4.13	8.23	43.43
d_v [m]	237.13	116.5	20.65

TTC Zones

As it has already been explained in chapter 2, according to driver notification concept there are two time-to-collision (TTC) zones, in which the driver will be informed or warned: *Information* and *Awareness Warning*. Since the boundaries between these two zones are not strictly fixed, this study treats them as one. In the third *Automatic*

Pre - Post Crash zone automatic braking or steering will take place in the event of the inevitable collision. Figs. 5.2a-5.2c illustrate TTC zones I and II with a blue area and zone III is denoted with a red area.

Transmitter - Receiver Position Combinations

Analogically to [127], for further evaluation we select one specific Tx-Rx pair from a total number of network nodes instead of obtaining reception probabilities by taking each node in the network into account. In such case other communication nodes will act as a source of interferences, which affect the selected Tx-Rx pair but are not included into evaluation directly. This aids to address the use cases specifically and make the simulation approach situation aware.

In each simulation scenario Tx is fixed at a certain position before the intersection center and the receiver Rx is moving towards the intersection center with a constant speed of 50 km/h despite a possible obstruction due to other traffic participants. Such abstraction from real traffic situations allows for comparability of the results between different simulation runs and scenarios.

In our study we consider three Tx-Rx position combinations: *cross traffic*, *intersection center* and *opposite sides*, which address ICW (Fig. 5.2a) and FCW (Fig. 5.2c) use cases or both of them simultaneously (Fig. 5.2b). We select such position combinations to investigate how different placement of Tx and Rx within the same intersection scenario and under the same network load conditions will impact application reliability. Based on this we aim to prove that even within the same scenario and under the same communication conditions different V2V applications will perform in a different way.

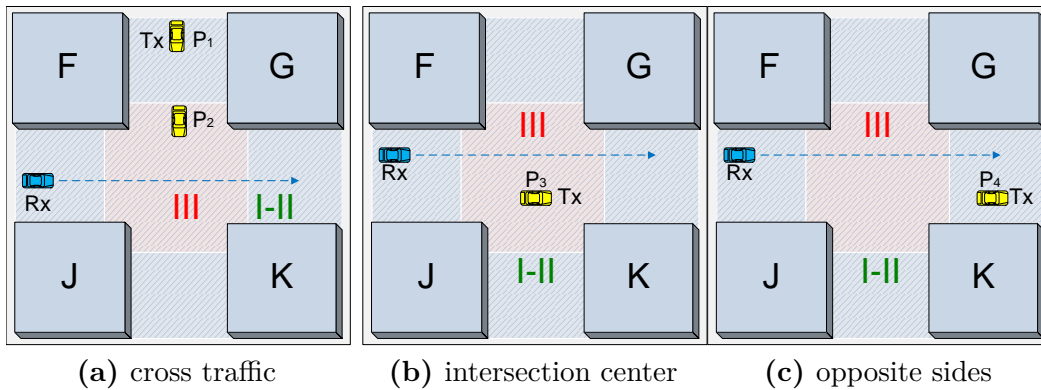


Figure 5.2: Combinations of Tx-Rx positions

In case of the *cross traffic* Tx is fixed in the orthogonal to Rx street $P_1 = 75$ m and $P_2 = 35$ m before the intersection center (Fig. 5.2a). In case of the *intersection center* transmitter is positioned directly in the middle ($P_3 = 0$ m) and by *opposite sides* transmitter is located $P_4 = 70$ m before the intersection center in the opposite to the Rx street (Figs. 5.2b and 5.2c). These position combinations reflect the situations

when Tx vehicle is positioned within TTC zones I-II or III.

5.3 Parameter Study

In this parameter study we investigate how message generation rate f_g , data rate R_b , penetration rate p , Tx-Rx position combinations and different intersection topologies can affect achievable application reliability.

5.3.1 Effect of Message Generation Rate

The following investigates the effect of different message generation rates on the achievable information freshness in the condition of close intersection topology and different penetration rates. We consider $f_g = [5, 10, 15]$ Hz message generation rates and $p = [5, 10, 25]$ % penetration rates.

Generally, the losses in the far-field of the intersection are mainly caused by the path loss due to the buildings and distance between the transmitter and the receiver. In the near-field they are caused by the interferences due to the hidden node stations and packet drop due to overload, as in the intersection center Tx and Rx will "hear" from all the stations within the intersection.

Figs. 5.3a - 5.3c demonstrate that for the penetration rate $p = 5\%$ interferences are minor, thus all obtained probability functions offer near to perfect communication conditions in the far- and near-field intersection areas: P_{RIFs} reach 0.99 at approx. 250 m and start to fall at $d_{deg} = 5 - 10$ m before the intersection center (LOS).

Starting from $p = 10\%$ the interference level increases and packet loss in the far- and near-field of the intersection start to grow. Furthermore, at $p = 10\%$ all probability functions demonstrate the so called "safety zone": P_{RIFs} experience noticeable degradation in the near- and far-field areas, however they always reach 0.99 at the specific area of the intersection, mostly 100-150 m before the center. This is due to the fact that signal strength degradation caused by the interaction of the transmitter signal with the surrounding buildings prevents Rx to suffer from a certain number of interferences due to stations, which are positioned orthogonally to Rx. Thus, in higher network load scenarios signal degradation due to shadowing results in a positive "guarding" effect against the interferences.

With an increase of the penetration rate the interferences in the far- and near-field intersection areas grow considerably. At $p = 25\%$ in the near-field area packet collisions are caused by the interferences due to the communication stations which are positioned within the intersection FGJK (Fig. 5.1a). In the far-field the total number of Rx collisions is caused by the interferences due to the path loss and additional interferences due to the terminals within the neighboring intersection EFLJ (Fig. 5.1a).

The high number of interferences leads to two interesting effects, which can be seen at each message generation rate: 1) narrowing of the "safety zone" and 2) shifting of the "safety zone" towards the intersection center. From the application perspective the second effect exhibits a great advantage, as for safety use cases it is of more importance

to provide high application reliability shortly before the envisioned collision point than in the far-field area. For instance, P_{RIF} , which is obtained for $f_g = 10$ Hz and penetration rate $p = 25\%$ (Fig. 5.3b) reaches 0.99 at 60 m before the intersection center and then starts to degrade again at $d_{deg} = 10$ m, as the effect of the "safety zone" is finished. Despite the fact that 60 m might not be a sufficient forewarning distance for all V2V use cases to gradually realize all available driver notification levels, the reliable communication range of $d_{0.99} = 60$ m before potential crash point still allows the driver to perform a safe braking maneuver (Fig. 3.7). Furthermore, at 10 m before the intersection center LOS is mostly available, which implies the active operation of other ADAS that are based on the onboard environmental sensors.

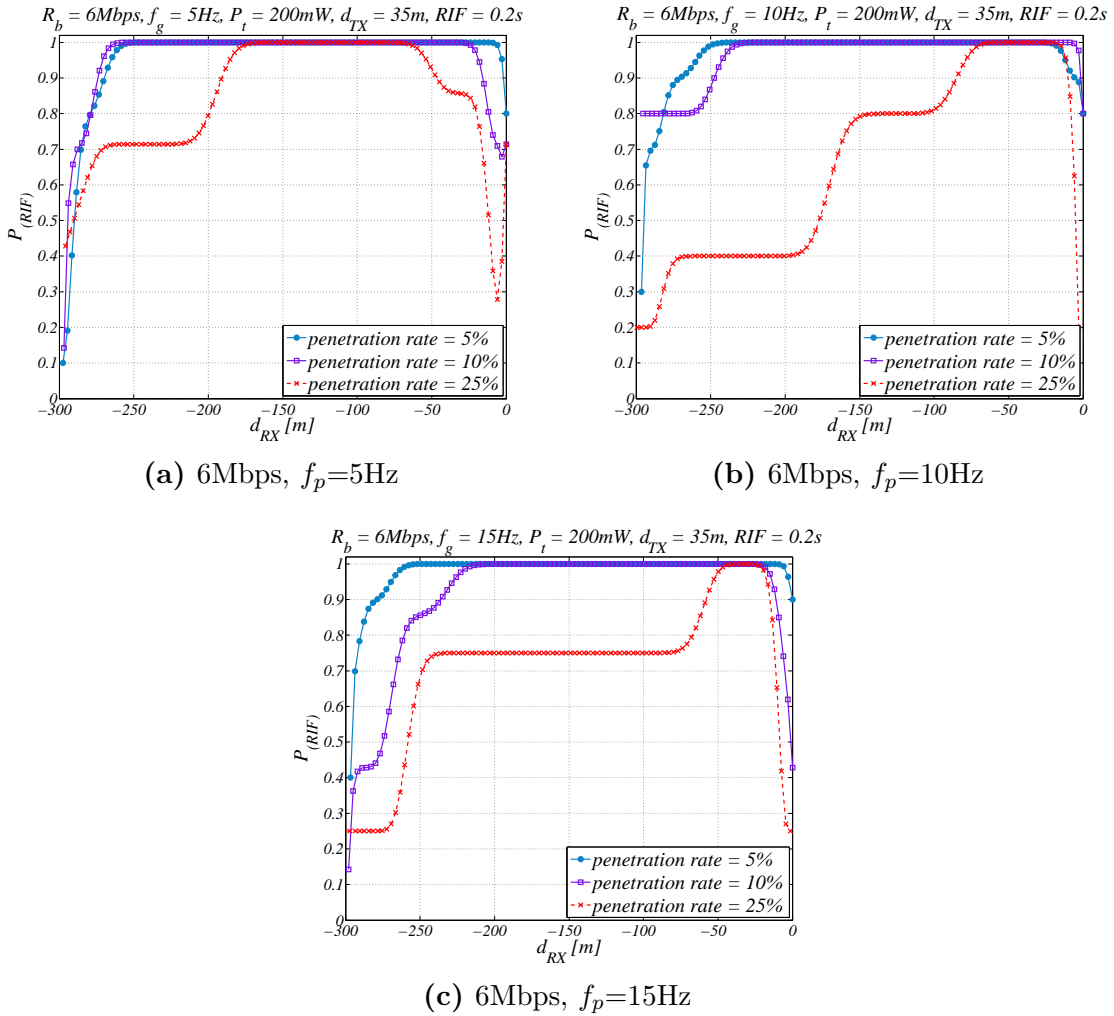


Figure 5.3: Effect of the message generation rate on the P_{RIF} for different penetration rates at close intersection

Interestingly, the P_{RIF} obtained for $f_g = 5$ Hz, $p = 25\%$ and by $RIF = 0.2$ s starts to degrade in the near-field area as early as $d_{deg} = 60$ m before the intersection center

(Fig. 5.3a). The reason is that at $f_g = 5$ Hz each transmitted packet has to be received to fulfill the reliability requirement and this is challenging in urban environment and high network load conditions. Therefore, P_{RIF_s} obtained for $f_g = 10$ Hz and $f_g = 15$ Hz outperform probability function obtained for $f_g = 5$ Hz even at higher penetration rates, considering the fact that achieving $P_{RIF} = 0.99$ in the near-field intersection area is of more importance than in the middle area. This allows us to conclude, that the message generation frequency must always be higher than the required RIF interval in order to provide sufficient reliability.

The results also show that the increase of the update frequency does not bring additional benefits in terms of P_{RIF} . In case of $p = 25\%$ the P_{RIF_s} at $f_g = 10$ Hz and $f_g = 15$ Hz degrade at approximately same distance d_{deg} before the intersection center, however the length of the "safety zone" is shorter at $f_g = 15$ Hz (Figs. 5.3b - 5.3c). Thus, message generation rate of $f_g = 10$ Hz is optimal to support V2V safety applications in selected scenarios. In case of the close topology it is valid for all three penetration rates. The half-open and open topologies can generate acceptable P_{RIF_s} until $p = 10\%$, if congestion control technics are not used. For more details refer to section 5.3.4.

5.3.2 3 Mbps vs. 6 Mbps

The following investigates the effect of the data rate on achievable application reliability. Currently, 6 Mbps is assumed to be default for the DSRC communications due to its robustness in the presence of noise and simultaneous provision of the higher throughput. This allows for effective operation of V2V applications in high network load scenarios. However, $R_b = 3$ Mbps (the lowest data rate, which is specified in IEEE 802.11p) with the most robust BPSK modulation scheme implies lower receiver sensitivity, which can result in lower packet error ratios at greater communication ranges. This, however, does not stand true by higher penetration rates, where faster coding rates are required. Thus, the following investigates achievable application reliability when operating at 3 Mbps and 6 Mbps and considers $f_g = [5, 10, 15]$ Hz message generation rates and $p = [5, 10, 25]\%$ penetration rates. Our goal is to determine whether there are scenarios, where $R_b = 3$ Mbps can outperform $R_b = 6$ Mbps.

Figs. 5.4a - 5.4c demonstrate a general tendency at each message generation rate: by lower penetration rates ($p = 5\%$) the difference between achieved P_{RIF_s} is minor both at 3 Mbps and 6 Mbps data rates. On the other hand, already by $p = 10\%$ the $R_b = 6$ Mbps noticeably outperforms $R_b = 3$ Mbps and by $p = 25\%$ the difference in the achieved P_{RIF_s} is extreme. This effect also grows with the increase of the message generation rate. For instance, at $f_g = 15$ Hz the P_{RIF} achieved at 3 Mbps and $p = 10\%$ never reach 0.99 (Fig. 5.4c), whereas for $f_g = 10$ Hz the same parameter combination offers much better performance in terms of P_{RIF} (Fig. 5.4b). This is due to the fact that receiver sensitivity of -93 dBm by $R_b = 3$ Mbps induces a bigger cell, which in its turn decreases collisions due to the hidden stations but also results in more nodes which attempt to access the channel simultaneously. This causes extremely low P_{RIF}

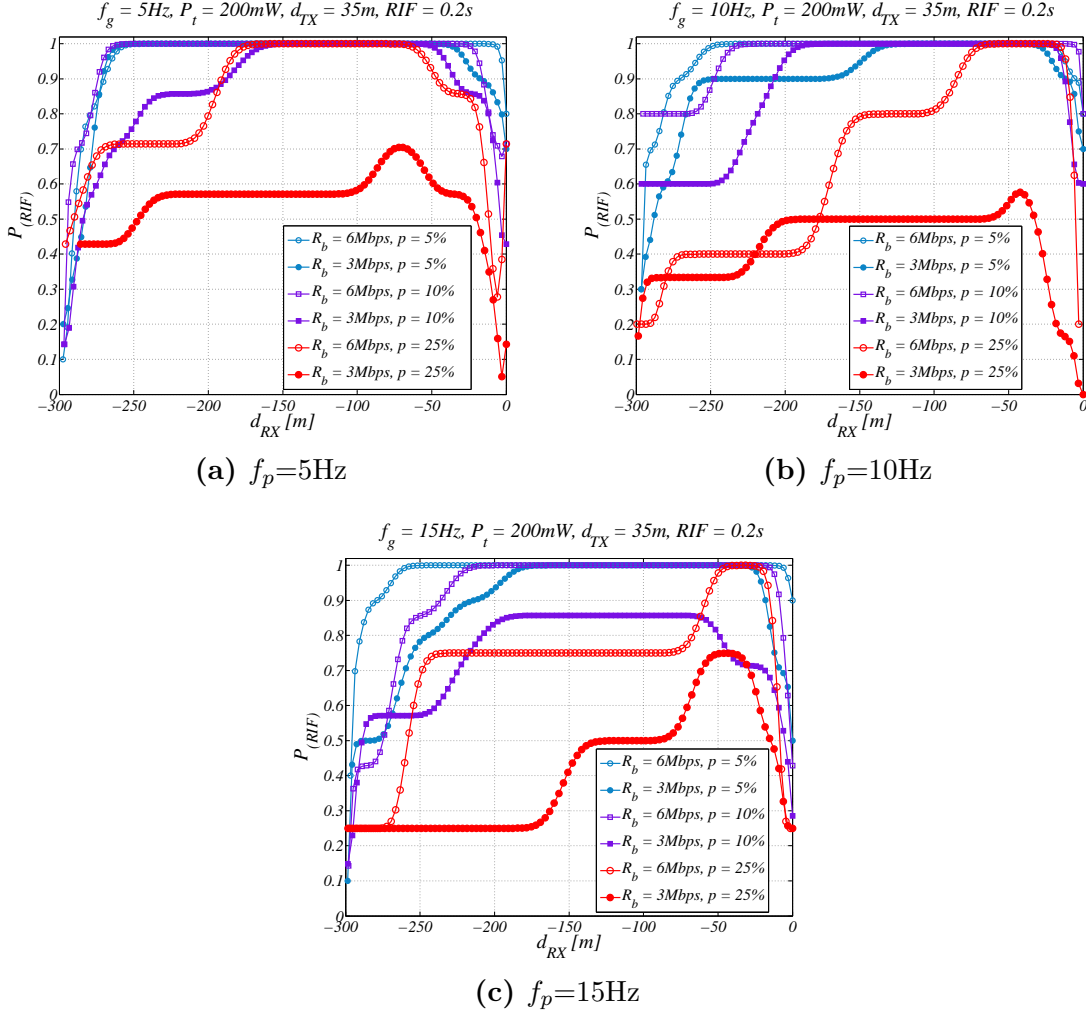


Figure 5.4: Effect of the data rate on the P_{RIF} for different f_g and p

at higher channel loads at $R_b = 3\text{Mbps}$.

Presented results clearly show that with the increase of the message generation frequency $R_b = 6\text{Mbps}$ always outperforms $R_b = 3\text{Mbps}$. The results also allow us to conclude that the less penetration rate is, the less influence the data rate has on the application reliability. Moreover, the usage of lower data rates by low channel load does not bring additional advantage in the urban environment.

5.3.3 Effect of the Transmitter Position

The following investigates the effect of the transmitter position at P_{RIF} when Tx is placed at $d_{TX} = 75\text{m}$ and $d_{TX} = 35\text{m}$ relatively to the intersection center. This represents the situation when Tx is situated in the TTC zones I-II and III respectively. The analysis of the data has shown that by $p = 5\%$ both $d_{TX} = 75\text{m}$ and $d_{TX} = 35\text{m}$

provide almost equally good results by each message generation rate, thus Figs. 5.5a-5.5c present obtained probability functions for penetration rates $p = 10\%$ and $p = 25\%$.

Fig. 5.5a demonstrates that for $f_g = 5$ Hz and $p = 10\%$ the P_{RIFs} in the near-field area are almost identical to each other, despite the fact that Tx is positioned first at 35 m and then at 75 m before the intersection center. As expected, in the far-field area the P_{RIF} , which is obtained by $d_{TX} = 35$ m outperforms the one when d_{TX} is equal to 75 m due to less path loss. A similar tendency can be observed for $f_g = 10$ Hz and $p = 10\%$ in Fig. 5.5b. However, the probability functions generally outperform those at $f_g = 5$ Hz. This confirms the already made conclusion that $f_g = 5$ Hz is too unstable for the requirement of $RIF = 0.2$ s. As expected, the P_{RIFs} obtained for $f_g = 15$ Hz and $p = 10\%$ demonstrate greater number of packet collisions due to the increase of interferences in both near-field and far-field intersection areas (Fig. 5.5c). We can also observe that the P_{RIFs} that were obtained at $d_{TX} = 35$ m and $d_{TX} = 75$ m show similar performance in the near-field area. However, in the far-field area P_{RIF} at $d_{TX} = 75$ m has a considerably constricted "safety zone".

This allows us to conclude, that in case of $p = 10\%$ for all message generation rates the probability functions demonstrate identical behavior: P_{RIF} at $d_{TX} = 35$ m always outperforms the one at $d_{TX} = 75$ m in the far-field area due to less path loss. However, the difference between both P_{RIFs} in the near-field is minor and position of Tx does not play a significant role in this case. This implies that for moderate penetration rates the number of packet collisions due to interferences is approximately the same in the center ($d_{TX} = 35$ m) and in the middle area of the intersection ($d_{TX} = 75$ m). Generally, for $p = 10\%$ the number of packet collisions in both intersection areas increases proportionally to the number of interferences, which start to dominate communication channel with the increase of message generation rates.

A different picture can be observed for $p = 25\%$ when Tx is positioned at $d_{TX} = 75$ m before the intersection center. Even at $f_g = 10$ Hz P_{RIF} reaches 0.99 only shortly at approx. $d_{RX} = 70$ m before the intersection center and then falls (Fig. 5.5b). Moreover, the P_{RIF} obtained for $f_g = 15$ Hz never exceeds 0.8 even in the "safety zone" (Fig. 5.5c). This is the evidence that at higher penetration rates Tx suffers from interferences due to communication stations which are positioned not just within the intersection FGJK, but also partially from the ones within the area of the intersection BCFG (Fig. 5.1a). This causes Tx to drop additional packets and thus increases a total experienced packet loss at Rx.

From the application perspective this allows us to conclude that by higher penetration rates transmitter position to the intersection center has a significant impact on the achievable application reliability. We can see that if congestion control technics are not used the P_{RIF} at $d_{TX} = 75$ m is not acceptable for V2V applications either by lower message generation rates nor by higher ones. This additionally confirms the fact that near-field intersection area is of more relevance for safety applications, not only in the sense of application design, but also from the communication reliability perspective.

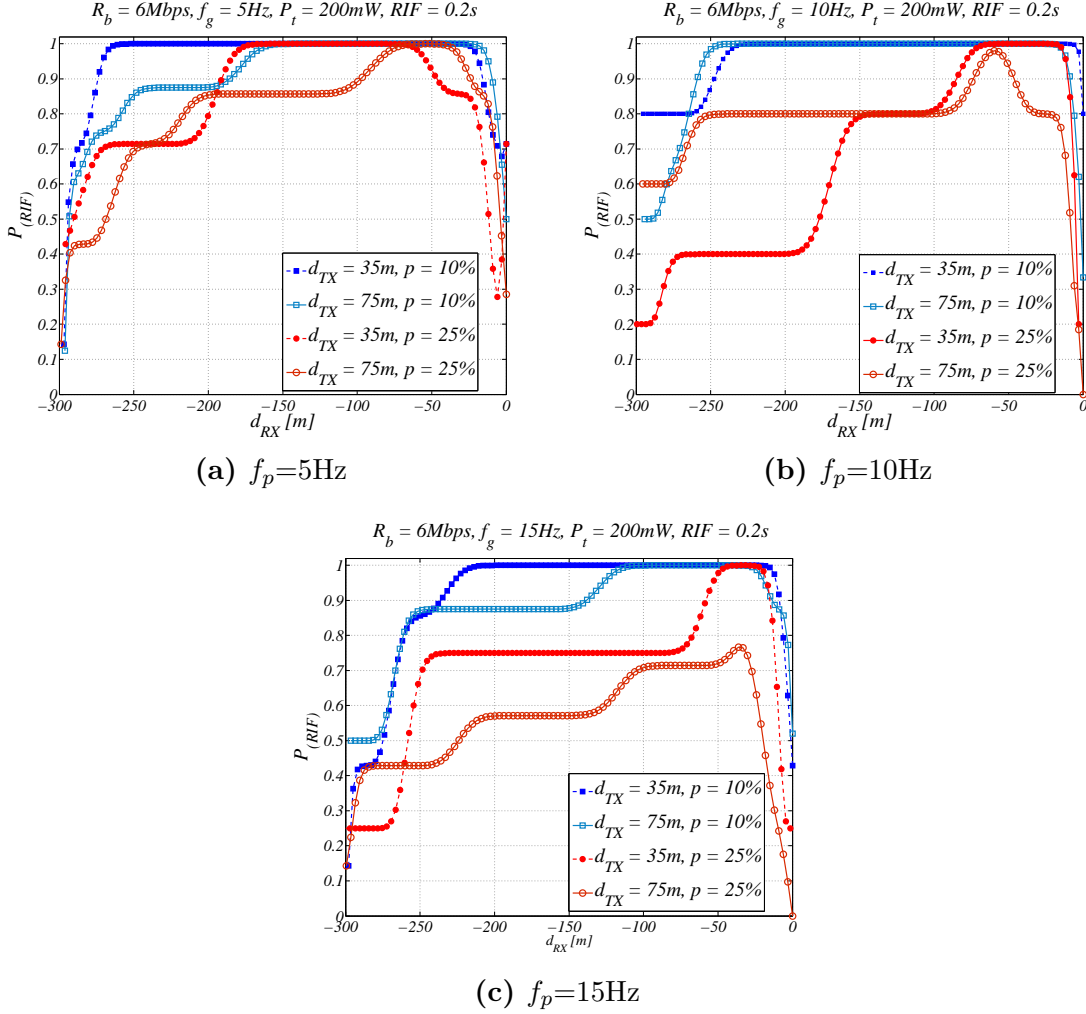


Figure 5.5: Effect of different Tx positions relative to the intersection center on the P_{RIF} for different f_g and p

5.3.4 Effect of the Intersection Topology and Tx - Rx Positions

The following investigates how different intersection topologies (close, half-open, open) and combination of Tx-Rx positions (*cross traffic*, *intersection center*, *opposite sides*) can affect application reliability. The analysis of the simulation data has shown that at low and moderate penetration rates ($p = 5\%$, $p = 10\%$) all P_{RIF} s offer a long "safety zone" and perform equally well in the near-field area by each combination of the network parameters. Thus, we show here results for $f_g = 10\text{Hz}$ and $f_g = 15\text{Hz}$ message generation rates and $p = 25\%$ penetration rate only, as in high channel load scenarios these P_{RIF} s show different behavior in each scenario. Further only data rate $R_b = 6\text{Mbps}$ is considered, as results in section 5.3.2 have demonstrated its advantage over $R_b = 3\text{Mbps}$.

Cross Traffic

In case of *cross traffic* Tx-Rx position combination the transmitter is located $d_{TX} = 35$ m inside of the intersection canyon and Rx is driving towards the intersection center in the orthogonal street (Fig. 5.2a). Further we do not consider $d_{TX} = 75$ m, as the results in section 5.3.3 have demonstrated that $d_{TX} = 35$ m is more favorable in terms of application reliability in *cross traffic* scenarios.

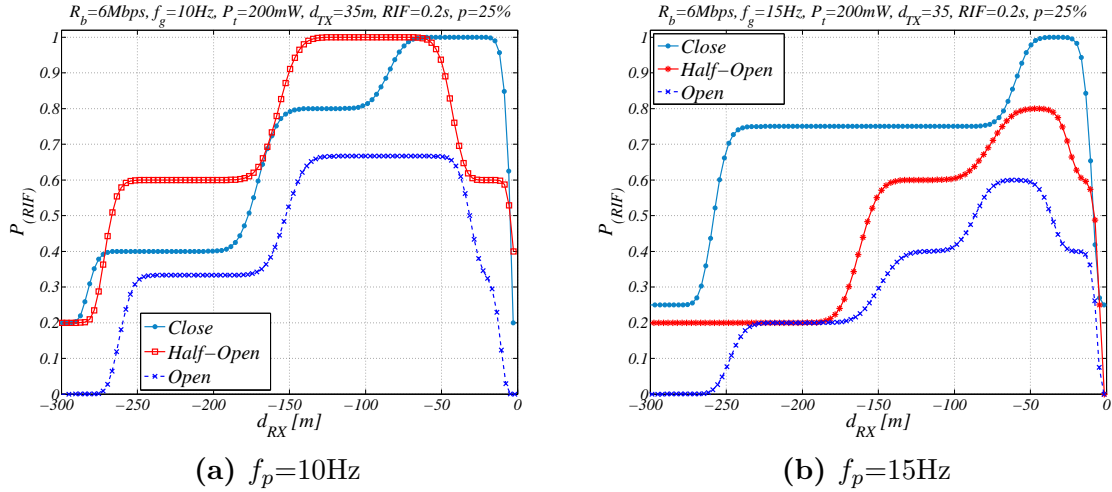


Figure 5.6: Effect of different intersection topologies and cross traffic Tx-Rx position combination on the P_{RIF} for $f_g = 10$ Hz, 15 Hz and $p = 25\%$

The results in Figs. 5.6a - 5.6b demonstrate how buildings affect application reliability in the high network load scenarios. In case of close intersection and $f_g = 10$ Hz P_{RIF} progresses slower than for the half-open topology due to NLOS between Rx and Tx. On the other hand, only close topology generates P_{RIF} of 0.99 in the area $d_{RX} = [50 \dots 0]$ m before the intersection center, where the collision point is assumed. The "safety zone" in this case is equal to 62 m and $d_{deg} < 15$ m. The half-open topology also has a "safety zone" due to the shadowing effect of houses "J" and "K" (Fig. 5.1b), which protect Rx from some of the interferences. It is approximately twice as long as the one of the close intersection. However, due to a high number of interferences in the intersection center and absence of buildings "F" and "G" P_{RIF} starts to degrade as early as 55 m before the intersection center ($d_{deg} = 55$ m). In case of open topology the number of interferences is the largest, thus the P_{RIF} demonstrates the worst performance and does not exceed 0.67 in its highest point.

Naturally, with the increased channel load probability functions degrade more intensively. For $f_g = 15$ Hz only the close intersection topology results in the P_{RIF} , which is able to reach 0.99 at the near-field intersection area (Fig. 5.6b). However, the "safety zone" in this case is narrower and approximately equals to 25 m. Nevertheless, this is an important result, which again confirms the significance of the buildings and

the positive effect of shadowing in the high channel load scenarios. Due to a high number of packet collisions the half-open topology results in maximal P_{RIF} of 0.8 and open topology reaches the maximum at $P_{RIF} = 0.6$.

Intersection Center

The following presents the results, which were obtained when Tx was positioned directly in the intersection center (Fig. 5.2b). Fig. 5.7a demonstrates that by this Tx-Rx position combination and for $f_g = 10$ Hz the packet loss in the near-field area is much higher than in *cross traffic* for all intersection topologies. Since Tx is positioned in the middle of the intersection, it is exposed to interferences from all four sides of the intersection. In case of the close topology this causes the P_{RIF} to degrade as early as $d_{deg} = 50$ m before the intersection center, when in *cross traffic* scenario the effect of the "safety zone" is finished only in the intersection center. On the other hand, packet collisions in the far-field area due to path loss are less, as a strong LOS component is present during the whole simulation time: P_{RIF} reaches 0.99 at already $d_{RX} = 170$ m before Tx. The increased number of interferences by this Tx-Rx position combination causes considerably worse P_{RIF} also in the half-open topology. The "safety zone" is extremely narrow and P_{RIF} reaches 0.75 only for a short period of time. On average packet collisions due to the interferences result in the P_{RIF} degrading to 0.4. Due to the same reasons open topology results in the probability function which shortly reaches the maximum value of 0.64 and is stable at approx. $P_{RIF} = 0.33$.

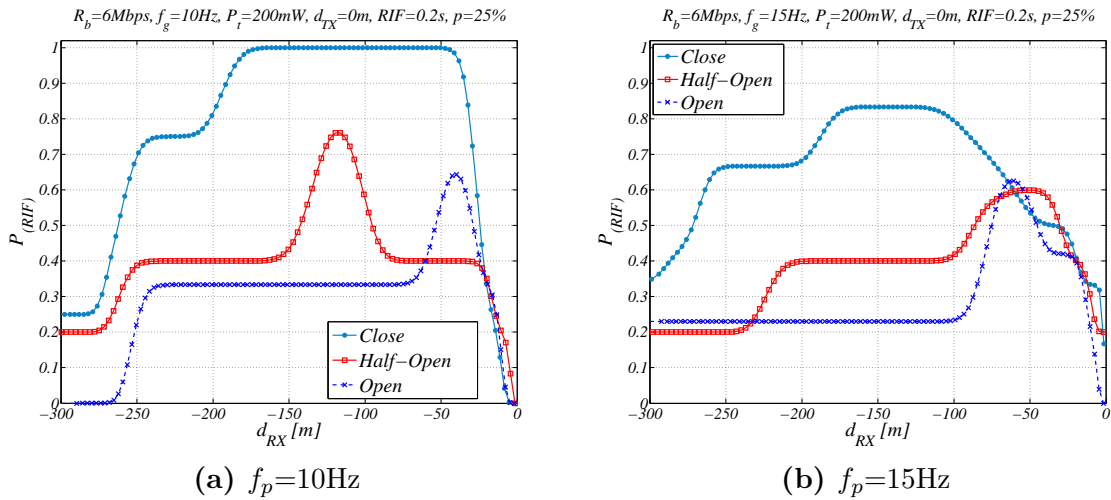


Figure 5.7: Effect of different intersection topologies and intersection center Tx-Rx position combination on the P_{RIF} for $f_g = 10$ Hz, 15 Hz and $p = 25\%$

For $f_g = 15$ Hz the P_{RIF} in the close topology does not exceed 0.82 and degrades at approximately $d_{deg} = 130$ m before the intersection center (Fig. 5.7b). This is another evidence that buildings play a major role towards ensuring reliable communication in urban scenarios under high network load conditions. Moreover, the shift of the "safety

zone" towards intersection center with the increasing channel load, characteristic to the close topology, was not confirmed in *intersection center* scenario both for $f_g = 10$ Hz and $f_g = 15$ Hz. The half-open and open topologies demonstrate a similar behavior: due to exposure of Tx to the interferences from all sides of the intersection the P_{RIF_s} does not exceed 0.61.

Generally, we can conclude that the placement of Tx in the intersection center can cause challenging communication conditions in each intersection topology.

Opposite Sides

In contrast to other scenarios in this chapter or in chapter 4, here we depict P_{RIF_s} relatively to d_{RX-TX} : the distance between Rx and statically positioned transmitter Tx. Further we investigate the case when the transmitter is positioned $d_{TX} = 70$ m away from the intersection center (Fig. 5.2c).

Fig. 5.8a demonstrates that for $f_g = 10$ Hz all P_{RIF_s} show a considerable improvement, when compared to those in the *intersection center* case. In fact, by close topology the probability functions demonstrate near to perfect communication conditions, which was never the case in any other *cross traffic* or *intersection center* scenario. This is the result of positioning Tx in the "safety zone" of buildings "G" and "K", when at the same time Rx benefits from the shadowing due to buildings "F" and "J" while approaching the intersection center (Fig. 5.2c). Interestingly, the P_{RIF} strongly degrades between 100 m and 50 m before the intersection center with its lowest point at approximately $d_{RX-TX} = 70$ m. This corresponds to the intersection center area, since Tx is positioned at $d_{TX} = 70$ m away from it and opposite to Rx. This again confirms the fact that P_{RIF} degrades the most in the intersection center, where the interference level is the highest.

The half-open intersection also results in a degradation of P_{RIF} in the intersection center and, similarly to the close topology, a better application reliability when compared to the one in the *intersection center* case. Interestingly, it also outperforms P_{RIF} by *cross traffic* in the near-field area, despite the fact that there probability function reaches 0.99 and by *opposite sides* does not exceed 0.8. In case of the open topology the interferences are too high, thus P_{RIF} does not exceed 0.25 during the whole simulation time and degrades to 0 in the intersection center.

Fig. 5.8b demonstrates that the P_{RIF_s} for $f_g = 15$ Hz exhibit similar behavior to those for $f_g = 10$ Hz: considerable degradation at $d_{RX-TX} = 100 - 50$ m (intersection center). However, due to the increased number of interferences P_{RIF_s} progress much slower than they did for $f_g = 10$ Hz, regardless of the intersection topology. Furthermore, the probability function at close topology reaches 0.99 only shortly at $d_{RX-TX} = 120$ m and after passing the intersection center area P_{RIF} does not reach 0.99 again, as it occurs for $f_g = 10$ Hz. The P_{RIF} which was obtained in the half-open intersection reaches the maximum of 0.75. This allows to assume that in this case the losses are caused not just by interferences due to the effect of the intersections FGJK and EFIJ, but also by those due to the influence of intersection GHKL, since Tx is placed at $d_{TX} = 70$ m away from the intersection center (Fig. 5.1a).

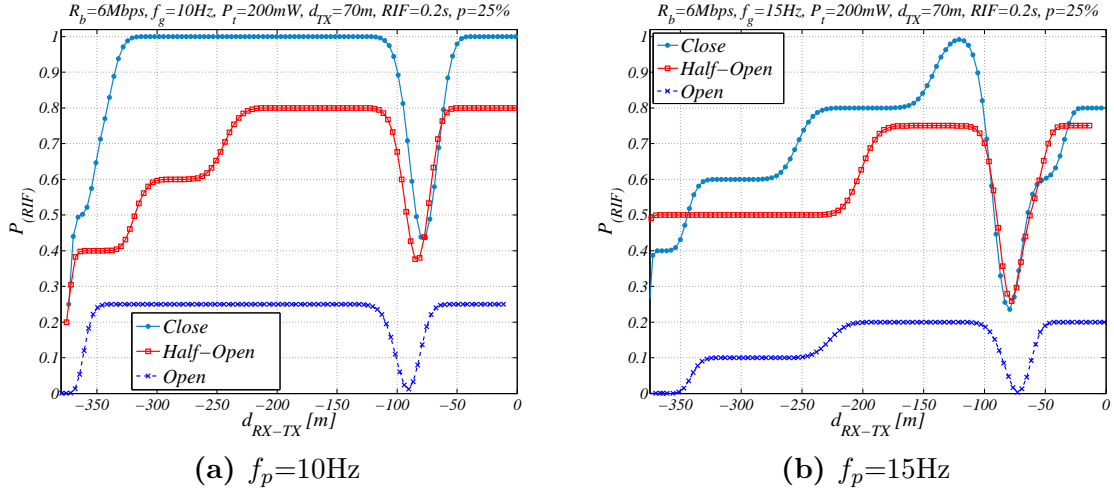


Figure 5.8: Effect of different intersection topologies and intersection center Tx-Rx position combination on the P_{RIF} for $f_g = 10, 15$ Hz and $p = 25\%$

The results of the parameter study confirm a major importance of buildings towards providing a sufficient level of application reliability by isolating relevant nodes from some of the communication stations in other areas of the network. Furthermore, they demonstrate that by all investigated topologies and position combinations of Rx and Tx the message generation rate of $f_g = 15$ Hz does not bring additional benefit in terms of the application reliability. Thus, $f_g = 10$ Hz represents a good trade-off between the required information freshness and induced network load, which is valid in all investigated intersection topologies and for all Tx-Rx position combinations.

Furthermore, the analysis of the simulation data has shown that a close intersection topology leads to acceptable application reliability in most of the investigated scenarios, even under high channel load conditions. The exception is *intersection center* scenarios, which result in challenging communication conditions even in close intersection topology.

5.4 Feasibility Analysis

This section investigates to what extent it is possible to support safety-related V2V applications in the high-load communication scenarios. Towards this objective we first obtain numerical values of application requirements, based on the concept which has been described in chapter 3. In the next step we evaluate the discussed simulation scenarios against these requirements and draw a conclusion which communication parameter combinations together with spatial factors are feasible to support ICW and FCW.

5.4.1 Assumptions

In the following study we assume that in case of ICW TTC zone I starts at 80 m before the collision point. This is considered to be a trade-off between a dynamic urban environment and the comfort of the driver, assuming that the average driving speed is equal to 50 km/h. FCW implies shorter forewarning distances due to the constant change of LOS/NLOS conditions while driving in urban canyons and the fact that the application should react only at potential collision objects in a relevant lane. Thus, we assume TTC zone I to start at 60 m before envisioned collision point.

In zone III minimum required communication range has to be taken into account in case of both applications. It is equal to the stopping distance, thus $d_{min} = 35$ m for the dry asphalt state if the velocity of the vehicle is 50 km/h. The details for the definition of the stopping distance for the velocity range $\in [50 \text{ km/h} - 100 \text{ km/h}]$ are given in Fig. 3.7a.

Furthermore, the degradation distance d_{deg} is assumed to be 15 m, which corresponds to the maximum LOS between two vehicles, which can be guaranteed in the urban environment. This is due to the fact that average vehicle length is assumed to be 5 m, thus $d_{deg} = 15$ m includes the length of Rx and Tx positioned in the same lane next to each other and the maximum separation distance when no other vehicle can be located between them and obstruct LOS.

5.4.2 Use Case Requirements

In the following feasibility study we make use of the metrics, which have been suggested in chapter 3: probability of the information freshness P_{RIF} , reliable communication range $d_{0.99}$, minimum required communication range d_{min} , degradation distance d_{deg} , the earliest and the latest driver notification times $t_{TTC(F)}$ and $t_{TTC(L)}$. Numerical values of these metrics in each TTC zone are derived having in scope ICW and FCW use cases.

Intersection Collision Warning: as it has already been defined in section 3.4 in the far-field of the intersection the information freshness requirement is relaxed and $RIF = 1$ s. Thus, the target P_{RIF} in TTC zone I-II is equal to 20% of the one when RIF is 0.2 s. This stems from the fact that by $RIF = 0.2$ s and $n=1$ condition the application would require 5 successful packet receptions per second and in case of $RIF = 1$ s only one successful reception per second.

Reliable communication range $d_{0.99}$ reflects available forewarning distance when communication is reliable. Thus, in good communication link conditions $d_{0.99}$ can be greater than the length of the TTC zone I-II. This implies that communication conditions are better than it is required by the application. When conditions are sufficient, $d_{0.99}$ can be less than the length of TTC zone I-II but cannot be shorter than the one of III TTC. By insufficient communication link conditions $d_{0.99}$ is less than the length of zone III. Therefore,

$$\begin{cases} d_{0.99} > 80 \text{ m}, & \text{good} \\ 80 \text{ m} \leq d_{0.99} \leq 35 \text{ m}, & \text{sufficient} \\ d_{0.99} < 35 \text{ m}, & \text{insufficient} \end{cases}$$

The earliest driver notification time $t_{TTC(F)}$ is calculated with Eq. 3.1 and is equal to $t_{TTC(F)} = 5.8 \text{ s}$.

In TTC zone III the $RIF = 0.2 \text{ s}$ due to the increased probability of emergency braking maneuvers and automatic safety systems intervention ($E_{pred} = 0.25 \text{ m}$, see Tables 3.1-3.3). The target P_{RIF} in this case is equal to 99%.

Reliable communication range $d_{0.99}$ has to be considered in TTC zone III even if it has already been achieved in zone I-II. Unlike interference-free scenarios, where after achieving 0.99 P_{RIF} stays constant, in the high channel load scenarios the information freshness can get worse in the intersection center due to the higher number of interferences. In TTC zone III the reliable communication range $d_{0.99}$ has to be at least equal to $d_{min} = 35 \text{ m}$. Due to the same reasons the degradation distance d_{deg} is also of great importance in TTC zone III. The latest driver notification time $t_{TTC(L)}$ is obtained with equation Eq. 3.2 and belongs to the interval $\in [3.2...0] \text{ s}$.

Forward Collision Warning: the FCW will impose similar requirements as ICW and the values of $d_{0.99}$, d_{min} , d_{deg} , $t_{TTC(F)}$, $t_{TTC(L)}$ in TTC zones I-II and III are defined following the same logic. The information freshness requirement in TTC zone I-II is not relaxed as it is in case of the ICW due to the shorter notification distances and higher vehicle dynamics. Thus, $RIF = 0.2 \text{ s}$, as it has already been defined in section 3.4. The target P_{RIF} in both TTC zones is equal to 0.99. Furthermore, as it has been explained above in this section, the reliable communication range is equal to $d_{0.99} = 60 \text{ m}$. And communication link quality conditions are defined as follows:

$$\begin{cases} d_{0.99} > 60 \text{ m}, & \text{good} \\ 60 \text{ m} \leq d_{0.99} \leq 35 \text{ m}, & \text{sufficient} \\ d_{0.99} < 35 \text{ m}, & \text{insufficient} \end{cases}$$

Table 5.3 summarizes the obtained numerical values of the ICW and FCW requirements.

5.4.3 Evaluation Results

In the following we present a summary of the feasibility analysis in Tables 5.4 - 5.7. The results are calculated by evaluating the obtained P_{RIF_s} against the requirements given in Table 5.3.

Table 5.3: Application requirements

TTC zone:	ICW		FCW	
	I-II	III	I-II	III
$P_{RIF}[\%]$	20	99	99	99
$RIF[s]$	1	0.2	0.2	0.2
$d_{0.99}[m]$	80	-	60	-
$t_{TTC(F)}[m]$	5.8	-	4.3	-
$d_{min}[m]$	-	35	-	35
$d_{deg}[m]$	-	15	-	15
$t_{TTC(L)}[m]$	-	3.2	-	1.7

Intersection Collision Warning

While evaluating ICW we choose $d_{TX} = 35$ m and $d_{TX} = 0$ m Tx positions, as they both correspond to the relevant driving situations for this use case. The assumed crash point is located in the intersection center. To define whether reliability requirements are met in TTC zone I-II, we evaluate if the required level of $P_{RIF} = 0.2$ is achieved in $d_{0.99} = [80...35]$ m range for each specific combination of communication parameters. Similarly, reliability requirements are met in TTC zone III if P_{RIFs} reach the required level of 0.99 at $d_{0.99} \geq 35$ m before the crash point and simultaneously d_{deg} does not exceed 15 m (see Table 5.3).

Table 5.4 demonstrates that in the far-field intersection area (TTC zone I-II) and by $d_{TX} = 35$ m the reliability requirements are fulfilled by all communication parameter combinations and in case of all three intersection topologies. Moreover, the achieved communication link quality is generally much higher than the specified threshold of $P_{RIF} \geq 0.2$. In the close topology the lowest P_{RIF} value in the $[80...0]$ m range is equal to 0.75, in the half-open one it does not exceed 0.68 and in case of open topology it is equal to 0.6 (Fig. 5.6b). Reliable communication range is considerably higher than minimum stopping distance ($d_{0.99} > d_{stop}$) and falls in the range of $[250...300]$ m in all topologies. Thus, $t_{TTC(F)}$ considerably exceeds the required value as well.

In the near-field intersection area (TTC zone III) most of the communication parameter combinations also result in good to sufficient application reliability. For instance, for $f_g = 5$ Hz, $p = 5\%$ and close intersection topology the reliable communication range is equal to $d_{0.99} = 293$ m and latest driver notification time $t_{TTC(L)}$ is equal to 18.5 s. In the same topology $d_{0.99}$ is equal to 151 m and $t_{TTC(L)} = 8.33$ s for $f_g = 15$ Hz and $p = 10\%$. Even at $p = 25\%$ and $f_g = 10$ Hz $d_{0.99}$ is 63.5 m and $t_{TTC(L)} = 1.98$ s, which is more than sufficient to satisfy reliability requirements.

Table 5.4 also demonstrates that several communication parameter combinations cannot provide the required communication link reliability by the ICW. Yet, this is

Table 5.4: Feasibility analysis summary for ICW by $d_{TX} = 35$ m

f_g	p	TTC zone I-II			TTC zone III		
		Close	H.-Open	Open	Close	H.-Open	Open
5 Hz	5 %	+	+	+	+	+	+
	10 %	+	+	+	+	+	+
	25 %	+	+	+	-	+	+
10 Hz	5 %	+	+	+	+	+	+
	10 %	+	+	+	+	+	+
	25 %	+	+	+	+	-	-
15 Hz	5 %	+	+	+	+	+	+
	10 %	+	+	+	+	+	+
	25 %	+	+	+	-	-	-

only the case by very high penetration rate ($p = 25\%$). For instance, by combination of $f_g = 5$ Hz and $p = 25\%$ the requirements cannot be fulfilled in close intersection topology, whereas half-open and open topologies provide acceptable results. As it has already been explained in the previous section, this is due to the fact that $f_g = 5$ Hz cannot provide a stable P_{RIF} when RIF is set to 0.2 s and $p = 25\%$. Taking into account greater path loss, in this case the close topology is worse compared to the other two topologies, where a strong LOS component is available during the whole simulation time. This leads to the degradation of the probability function as early as $d_{deg} = 56$ m before the intersection center, when the allowed threshold lies by $d_{deg} = 15$ m. With the increase of message generation rate the building profile starts to play a protecting role and close topology offers better performance in terms of P_{RIF} than other two topologies at $f_g = 10$ Hz and $f_g = 15$ Hz for $p = 25\%$ penetration rate. Furthermore, comparing the P_{RIFs} which were obtained at $f_g = 10$ Hz and $f_g = 15$ Hz for $p = 25\%$ we can observe that they are quite similar and in both cases $d_{0.99} > d_{min}$ (Figs. 5.6a and 5.6b). However, the P_{RIF} at $f_g = 15$ Hz starts to degrade as early as $d_{deg} = 18$ m, which is greater than the allowed threshold of 15 m. This demonstrates the limits of protecting effect of the buildings in high network load scenarios.

Table 5.5 summarizes the results for Intersection Collision Warning when Tx is positioned directly in the intersection center ($d_{TX} = 0$ m). Similarly to the previous case ($d_{TX} = 35$ m), all obtained P_{RIFs} demonstrate sufficient communication link quality conditions in the TTC zone I-II, with reliable communication range $d_{0.99}$ and earliest driver notification time $t_{TTC(L)}$ considerably exceeding required threshold values (Table 5.3).

However, the P_{RIFs} in the TTC zone III, show considerable worsening, due to the increased number of interferences. As a result, by penetration rate $p = 25\%$ no P_{RIF} is able to meet reliability requirements which are imposed by ICW on the communication link, even in case of the close intersection topology. The P_{RIF} at

$p = 10$ Hz and by $p = 25\%$ is the only probability function which reaches a target value of 0.99. Despite this fact $d_{deg} = 50$ m is considerably higher than the allowed threshold (Fig. 5.7a).

Open intersection topology exhibits the worst application reliability by moderate and high network loads. The analysis of the measurement data has shown that in these cases the application reliability suffers the most in the intersection center and d_{deg} requirement is not going to be fulfilled more likely than the one imposed on reliable communication range. For instance, by $p = 10\%$ and at $f_g = 10$ Hz open topology results in $d_{0.99}$ of 245 m, which is considerably greater than the required value but d_{deg} in this case is equal to 15 m, which lies on the boarder of the allowed threshold. With the increase of the channel load ($f_g = 15$ Hz and $p = 10\%$) the open topology results in $d_{0.99} = 47$ m, which is less than specified reliable communication range but still more than required $d_{min} = 35$ m. However, degradation distance d_{deg} in this case equals to 19 m.

Table 5.5: Feasibility analysis summary for ICW by $d_{TX} = 0$ m

f_g	p	TTC zone I-II			TTC zone III		
		Close	H.-Open	Open	Close	H.-Open	Open
5 Hz	5 %	+	+	+	+	+	+
	10 %	+	+	+	+	+	+
	25 %	+	+	+	-	-	-
10 Hz	5 %	+	+	+	+	+	+
	10 %	+	+	+	+	+	+
	25 %	+	+	+	-	-	-
15 Hz	5 %	+	+	+	+	+	+
	10 %	+	+	+	+	+	-
	25 %	+	+	+	-	-	-

Forward Collision Warning

In the following we present the results, which are obtained for the Forward Collision Warning when transmitting vehicle is positioned 1) directly in the intersection center ($d_{TX} = 0$ m) and 2) inside of the intersection canyon ($d_{TX} = 70$ m).

Table 5.6 summarizes the results for the case when envisioned collision point is located in the intersection center. Since information freshness requirement is not relaxed in TTC zone I-II as it is in case of the ICW, we observe that by penetration rate of $p = 25\%$ and message generation rates of $f_g = 10$ Hz and $f_g = 15$ Hz the application reliability requirements are not satisfied even in TTC zone I-II. In zone I-II the application reliability is sufficient only for $f_g = 5$ Hz and $p = 25\%$. However, the analysis of the data has shown that the reliable communication range $d_{0.99}$ by open intersection topology is equal to only 60 m, which still reflects sufficient communication

link conditions but lies on the limit of the required value (Table 5.3). Comparison of Tables 5.5 and 5.6 demonstrates how the same communication conditions can be translated by different V2V safety applications in a different way.

For $p = 10\%$ the application reliability requirements are fulfilled by all parameter combinations in TTC zone I-II. For instance, for close intersection topology and $f_g = 10\text{ Hz}$ the reliable communication range is equal to $d_{0.99} = 284.92\text{ m}$ and the latest time to collision is $t_{TTC(F)} = 20.5\text{ s}$.

Naturally, in TTC zone III more parameter combinations are not able to satisfy application reliability requirements of the FCW. Since the requirements of the ICW and FCW in this zone are identical (see Table 5.3) as well as Tx position in this situation, the evaluation results are the same for both applications.

Table 5.6: Feasibility analysis summary for FCW by $d_{TX} = 0\text{ m}$

f_g	p	TTC zone I-II			TTC zone III		
		Close	H.-Open	Open	Close	H.-Open	Open
5 Hz	5 %	+	+	+	+	+	+
	10 %	+	+	+	+	+	+
	25 %	+	+	+	-	-	-
10 Hz	5 %	+	+	+	+	+	+
	10 %	+	+	+	+	+	+
	25 %	-	-	-	-	-	-
15 Hz	5 %	+	+	+	+	+	+
	10 %	+	+	+	+	+	-
	25 %	-	-	-	-	-	-

Table 5.7 represents the case when Tx is positioned in a street canyon, between two significant interacting objects (buildings "G" and "K", Fig. 5.2c). Regardless of the TTC zone all combinations of $f_g = 5\text{ Hz}$ and $f_g = 10\text{ Hz}$ for penetration rates of $p = 5\%$ and $p = 10\%$ deliver stable P_{RIFs} in the range of $d_{TX-RX} \in [50...0]\text{ m}$, which fulfills the reliability requirements in terms of $d_{0.99}$ and d_{deg} .

In the III zone the open topology again shows the worst performance in terms of P_{RIF} . For instance, at $f_g = 15\text{ Hz}$ and $p = 10\%$ the probability function never reaches 0.99, which is not the case by half-open and close topologies.

For $p = 25\%$ and all message generation rates the P_{RIFs} , which are obtained in open and half-open intersection topologies, never reach 0.99 both in TTC zones I-II and III (Figs. 5.8a - 5.8b). Only close topology is able to deliver sufficient P_{RIFs} with all parameter combinations, except when P_{RIF} is obtained for $f_g = 15\text{ Hz}$ and $p = 25\%$ (the highest network load). In this case the probability function reaches 0.99 for a short period of time and does not recover to 0.99 afterwards.

Results in Tables 5.4-5.7 allow us to make an important observation: penetration rate of $p = 10\%$, which corresponds to normal traffic conditions in the urban environment,

Table 5.7: Feasibility analysis summary for FCW by $d_{TX} = 70$ m

f_g	p	TTC zone I-II			TTC zone III		
		Close	H.-Open	Open	Close	H.-Open	Open
5 Hz	5 %	+	+	+	+	+	+
	10 %	+	+	+	+	+	+
	25 %	+	-	-	+	-	-
10 Hz	5 %	+	+	+	+	+	+
	10 %	+	+	+	+	+	+
	25 %	+	-	-	+	-	-
15 Hz	5 %	+	+	+	+	+	+
	10 %	+	+	-	+	+	-
	25 %	-	-	-	-	-	-

provides sufficient application reliability for the ICW and FCW in majority of evaluated scenarios. The exception is open topology, which is rare in urban environment [89]. Naturally, utilization of congestion control mechanisms will considerably improve communication link quality, and will promote application reliability by $p = 25\%$.

5.5 Summary

This chapter has investigated achievable application reliability in urban intersections in high-load conditions based on simulations. We discussed how message generation rate f_g , data rate R_b , penetration rate p , Tx position relatively to the intersection center and to the Rx position can affect achievable application reliability. Furthermore, we showed the effect of different intersection topologies (close, half-open, open). Next, we have conducted the feasibility analysis of discussed scenarios in the scope of Intersection Collision Warning and Forward Collision Warning applications.

We have demonstrated that message generation rate of $f_g = 15$ Hz does not bring additional benefit in terms of the application reliability and $f_g = 10$ Hz represents a good trade-off between the required information freshness and network load. Furthermore, we have shown that message generation rate is to be always set higher than the RIF interval to provide sufficient application reliability. The analysis of P_{RIFs} for data rates $R_b = 6$ Mbps and $R_b = 3$ Mbps allowed us to conclude, that data rate $R_b = 3$ Mbps does not outperform $R_b = 6$ Mbps in any of the investigated scenarios.

We have also demonstrated a major importance of buildings towards providing a sufficient level of application reliability by isolating Tx and Rx from irrelevant nodes in the communication network. We have shown that in close intersection and *cross traffic* scenarios, P_{RIFs} exhibit a "safety zone", which shifts to the intersection center with the increased channel load. This is advantageous for V2V use cases, as it is

important to provide high application reliability shortly before the collision point.

Furthermore, we have found out that sufficient application reliability can be achieved in the majority of scenarios when $p = 5\%$ and $p = 10\%$ in half-open and opened topologies. Closed topology, on the other hand, results in acceptable application reliability even for $p = 25\%$, which is advantageous, taking into account that closed intersections constitute 90% of all intersections in the typical urban environment [89]. The study has also shown that *intersection center* Tx-Rx position combination is the most challenging by all intersection topologies and by moderate and high network load results in P_{RIFs} , which cannot satisfy requirements of V2V safety applications. On the other hand, we showed that when Rx and Tx vehicles are both located within the "safety zone" and a strong LOS-component between the vehicles exists most of the time, V2V safety applications exhibit high application reliability (*opposite sides* scenarios).

The analysis of reliability requirements of ICW and FCW has shown that in high-load scenarios degradation distance requirement d_{deg} is more challenging to fulfill than the requirements, which are imposed on the reliable communication range $d_{0.99}$. We also showed that these applications will be able to reliably operate at the majority of urban intersections, given reasonable size of the *RIF* interval and moderate penetration rates ($f_g = 10\%$). Not sufficient application reliability by $p = 25\%$ is considered to be uncritical in the scope of this research, since we expect future V2V communications to profit from congestion control algorithms.

It is also worth noting that requirements in section 5.4.2 are specified rather strictly, as the aim was to investigate the limits of V2V communication and identify potentially challenging scenarios, which will need special attention from the side of the congestion control protocol and application developers. From the perspective of the application design the graceful degradation methods can be envisioned, where application can temporarily deliver only a part of its functionality but instead can operate with more relaxed P_{RIF} , $d_{0.99}$ and d_{deg} requirements. For that the application has to be aware of the current and future communication link quality in the real time, which is discussed in the next chapter. There we present two frameworks for prediction of the communication link reliability in real-time modus.

6 Real-Time Prediction of the Communication Link Quality

"Ordinary mortals know what's happening now, the gods know what the future holds because they alone are totally enlightened. Wise men are aware of future things just about to happen." (C. P. Cavafy) [39]

V2V communication channels represent a communication environment with intermittent link conditions, where not all network nodes will be able to have the same level of communication link quality in a given time instant or maintain it through equally long periods of time. Moreover, due to a high node mobility and a complexity of the vehicle routes in VANETs, the severity of communication channel impairments has a random character. Thus, to ensure reliable operation of safety applications it is essential to possess sustained and accurate information about the current level of cooperative awareness between the relevant network nodes.

Traditionally, in V2V communications the information about the communication link quality is used at the transmitter to realize dynamic rate and power adaptive control strategies and QoS ad-hoc routing algorithms. However, to make the operation of the V2V applications more robust against failures, it is of great significance to make the receiver aware of the changes in communication link quality as well. In the moment of successful packet reception the application at the receiver side will immediately update the tracking information about the neighboring nodes and will not require additional feedback about the past communication link quality. Thus, the following suggests a novel method, which predicts whether a predefined application-specific QoS will be maintained in the near future.

Due to the short-term behavior of the V2V network, the prediction must be also performed at a short time scale. This can be achieved through the already presented information freshness metric. In contrast to multimedia or other streaming applications, the fact that a V2V safety application requires a defined number of successfully received packets within an information freshness interval is advantageous, as this leads to more relaxed requirements on the communication medium. Unlike the post processing phase, where it has to be defined whether the condition of the information freshness is fulfilled in the $[t_i - RIF, t_i]$ time interval (Fig. 3.1), the following method predicts whether this condition will be fulfilled in the next $[t_i, t_i + RIF]$ time interval. This is especially relevant for the autonomous driving applications, as in the event of a predicted communication link failure the control can be given back to the driver earlier, which ensures additional reaction time.

6.1 Related Work

Currently the VANET-related research activities on the link reliability estimation are mainly concentrated on the prediction of the link availability for QoS ad-hoc routing algorithms. The authors in [35] describe different methods of link reliability estimation in VANETs and propose a model for estimation of expected transmission success ratios, which can be used to provide different quality levels to various services in VANETs. Sofra et al. in their series of works [136], [135], [134] develop and evaluate a cross-layer design where the received power metric is logged at the physical layer and used to estimate the residual lifetime of the communication links in VANETs. Other prediction-based approaches are presented in [58] and [99]. A routing protocol for multimedia communications, which utilizes a link reliability model is presented in [101]. The authors stress that traffic parameters are vital towards accurate prediction of link reliability. Furthermore, the authors in [29] show that link quality estimation can be used to improve multi-hop packet forwarding in VANETs and propose an approach to estimate the link quality by the receiver, while taking transmission parameters of each vehicle into consideration.

In [102] the author addressed link availability prediction at the transmitter side in low power wireless sensor network based on the packet reception history. The authors in [30] introduce a method for short-term communication link estimation to characterize dynamics of unstable links at a high resolution in time and predict their reliability. An in depth analysis of the reasons for the packet delivery success and failure is given in [138]. The authors show that packet losses are highly correlated over short period of time and not correlated over long time periods. Additionally, a comprehensive survey of general online failure prediction techniques in computer science is given in [117].

In our study we consider the link reliability estimation at the receiver side and present two approaches, which realize short-term predictions of the future reception status based on the packet reception history as the main context information. To the best of our knowledge the following study is the first to present a completely feedback-free estimation of the short-term link quality at the receiver.

This chapter is structured as follows: section 6.2 gives details of experimental data which has been used as the basis for the further studies. Section 6.3 presents an algorithm, which is based on machine learning approach, gives the implementation details and presents the results. Furthermore, this section investigates possible optimization methods of the algorithm for better prediction. Section 6.4 presents design and implementation details of the model-based estimation and provides numerical results. Finally, section 6.5 conducts a measurement study and evaluates the performance of both approaches against the measurement data.

6.2 Experimental Data

Both algorithms have been developed and evaluated using the measurement data, which was gathered over the 5.5 months of the sim^{TD} field trials (1.07.12 - 14.12.12). During this time up to 120 vehicles drove fixed routes in urban, highway and rural environments and in application-specific scenarios. This approximately corresponds to 43000 vehicle hours and 1650000 km travelled distance.

The vehicles were continuously sending CAM messages and when events were triggered, they additionally sent DENM messages. During the measurement, the CAM generation rate was set to 5 Hz (driving state) and 2 Hz (standstill state). Whenever a vehicle received a packet in the MAC layer, a log entry was created, containing alongside other information the current timestamp and an identifier of the sending vehicle. This is the only information used by the algorithms.

In the following sections we describe both algorithms in detail. The first algorithm uses a look-up table (LUT) whereas the second uses a model-based approach.

6.3 Algorithm 1: LUT-Based Estimation

LUT-Based algorithm predicts in real time the communication quality between a specific vehicle and the host vehicle by learning from the context information available at the host vehicle. Specifically, the algorithm estimates how high is the probability that in the next *RIF* interval the host vehicle will be able to successfully receive n packets from a certain communication partner. Based on findings in chapters 3 - 5, this chapter makes use of the assumption that $n = 1$ and *RIF* = 0.3 s.

Fig. 6.1 depicts the concept of the algorithm. From the current point in time t_0 the algorithm predicts, if one or more packets from this communication partner will be received in the following interval $[t_0, t_{after}]$, where the size of this interval is equal to the *RIF* interval. To achieve this, the algorithm had monitored the recent communication at least starting at t_{start} . This interval is rasterized and a binary is computed. For each segment the dedicated bit in the pattern is set to 1 if one or more packets are received in this time frame. Otherwise it is set to 0.

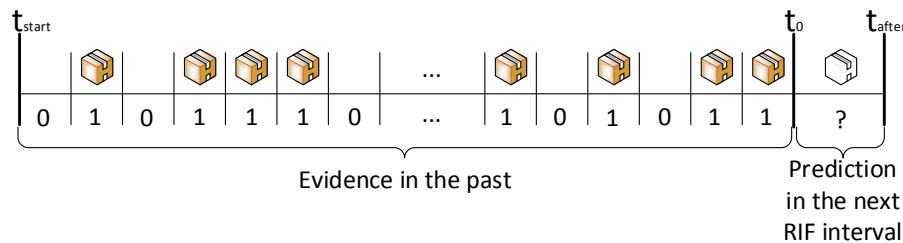


Figure 6.1: Concept of the LUT-Based algorithm

The pattern can now be used as an index to the look-up table. It has to be noted that the number of segments in the $[t_{start}, t_0]$ defines the number of bits in the pattern. As the look-up table has an entry for each pattern the table size is increased with the

pattern size. For pattern length of m bits the table will contain 2^m entries ranging from the binary values $0\dots 0$ to $1\dots 1$. Also the number of segments has to be tuned to the estimated maximum transmission frequency. Only this way it can be ensured that all the information in the reception history can be gathered. This leads to a trade-off between memory consumption and possible prediction accuracy. The look-up takes place in two different modes: 1) the learning mode and 2) the evaluation mode.

Learning mode: in this mode the algorithm gathers communication patterns and corresponding packet followup statistics for each specific pattern. For each pattern the number of successful (*goodCount*) and failed (*badCount*) followup receptions is stored into the table. Similarly to the pattern, the *goodCount* and *badCount* are also defined as the dedicated bit in the time segment. But in this case the time segment is equal to the size of the *RIF* interval. Fig. 6.2 illustrates the learning process of the framework.

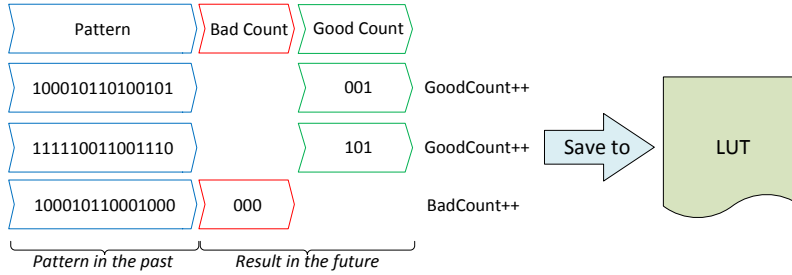


Figure 6.2: Learning mode

Since the required number of successfully received packets in the $[t_0, t_{after}]$ is $n = 1$, by $f_g = 5$ Hz only the combination with all zeros is treated as *badCount*, all other combinations will be treated as *goodCount*. Further the algorithm goes through the measurement data which was selected for learning and fills the table of the 2^m size. Fig. 6.3 illustrates the table after completing the learning process.

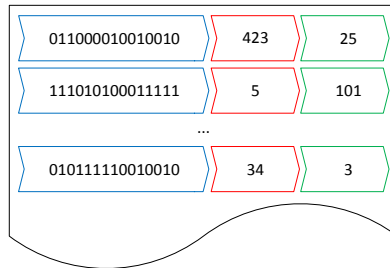


Figure 6.3: LUT structure

The learning process of the framework was based on the maximum of 4.5 months of the field trials. When one specific vehicle is in focus, it corresponds to 391.9 driving hours or 77.8% of measurement data for this vehicle.

Evaluation mode: in this mode the algorithm estimates the success probability of receiving at least 1 packet within the next $[t_0, t_{after}]$ interval based on the data obtained during a learning phase. The success probability P_s for each specific pattern is calculated as follows:

$$P_s = \frac{N_{goodCount}}{N_{goodCount} + N_{badCount}} \quad (6.1)$$

where P_s is the success probability, $N_{goodCount}$ is the number of successful receptions for a specific pattern and $N_{badCount}$ is the number of failed receptions for the same pattern.

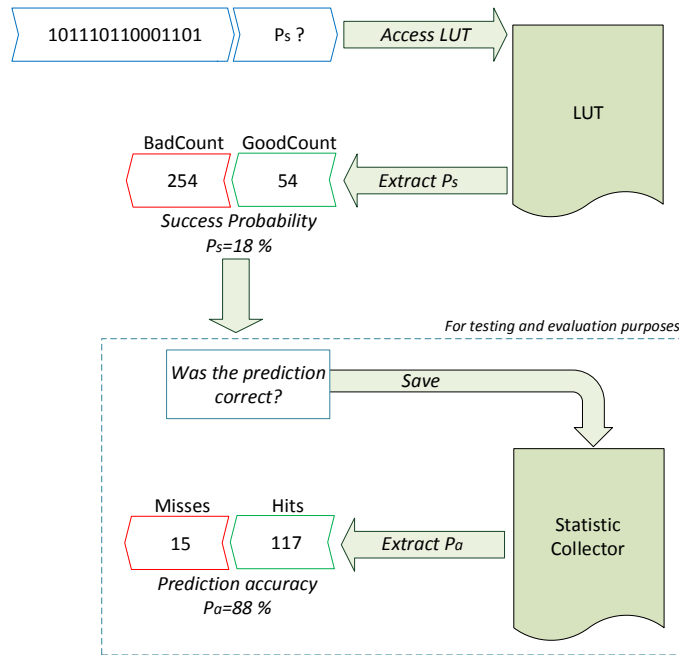


Figure 6.4: Evaluation mode

Fig. 6.4 demonstrates the operation of the LUT-Based algorithm in the evaluation mode. For the testing and optimization purposes not only the success probability of the prediction is calculated but also statistics of the accuracy of the algorithm. Obviously, the efficiency of the algorithm depends on the number of times when the algorithm made a correct prediction (*hit*) and when it made an erroneous one (*miss*). These values are defined as follows:

$$\begin{aligned} P_s > thresholdYes & \quad \text{and at least } n = 1 \text{ packets is received} & \rightarrow Hit \\ P_s \leq thresholdYes & \quad \text{and at least } n = 1 \text{ packets is not received} & \rightarrow Hit \\ P_s > thresholdYes & \quad \text{and at least } n = 1 \text{ packets is not received} & \rightarrow Miss \\ P_s \leq thresholdYes & \quad \text{and at least } n = 1 \text{ packets is received} & \rightarrow Miss \end{aligned}$$

Where *thresholdYes* is a defined by the application value, after which the application

should expect a packet in the next *RIF* interval. This threshold is required because after the learning phase some of the patterns might have P_s around 50% which means that for these patterns no reliable prediction can be made. This problem can be solved by introducing cut-off lines to define positive, negative and unsure predictions. Further we refer to the accuracy of the algorithm as to *prediction accuracy* P_a and it is the ratio of successful predictions and failures:

$$P_a = \frac{N_{hit}}{N_{hit} + N_{miss}} \times 100\% \quad (6.2)$$

where P_a is the prediction accuracy, N_{hit} is the total number of *hits* for a specific pattern and N_{miss} is the number of *misses* for the same pattern.

The evaluation process was based on 1 month of field trials, which correspond to 22.2% of the measurement data or 111.8 driving hours. Naturally, when the algorithm is running in the control device of a vehicle only prediction P_s will be calculated.

If the host vehicle receives messages from multiple vehicles at the same time, the process above is performed in parallel for each vehicle. When the pattern for a vehicle consists only of zeros (i.e. no packets were received for some time) the algorithm stops tracking this vehicle, assuming that it is out of the communication range. In case new packets are received from this vehicle again, the algorithm resumes the calculation. It is also important to notice, that for series-oriented implementations it is not necessary to separate learning and evaluation modes. The algorithm is able to perform prediction and learn at the same time. The separation was implemented purely to achieve reproducible and comparable results for the evaluation of the algorithm.

The main advantages of this approach are that it does not require much memory and can be calculated at high speed due to the absence of complex and time consuming runtime computations. This allows for an implementation of this algorithm in the vehicle control device, where it will continue to learn with further context information and will be able to adapt itself to the surroundings of a specific vehicle over time. This adaptation could be helpful when the daily route of the driver changes from urban to rural or highway areas or when market penetration of V2X rises.

6.3.1 Implementation Details

Fig. 6.5 depicts the main functional components of the proposed algorithm, which will be described in this section.

LogFileParser

Due to the big amount of information constantly exchanged by the vehicles, *sim*^{TD} system makes use of the logging mechanism. It saves different payload and service data assigned to the specific *LogIDs*, which are represented by not repeating real numbers.

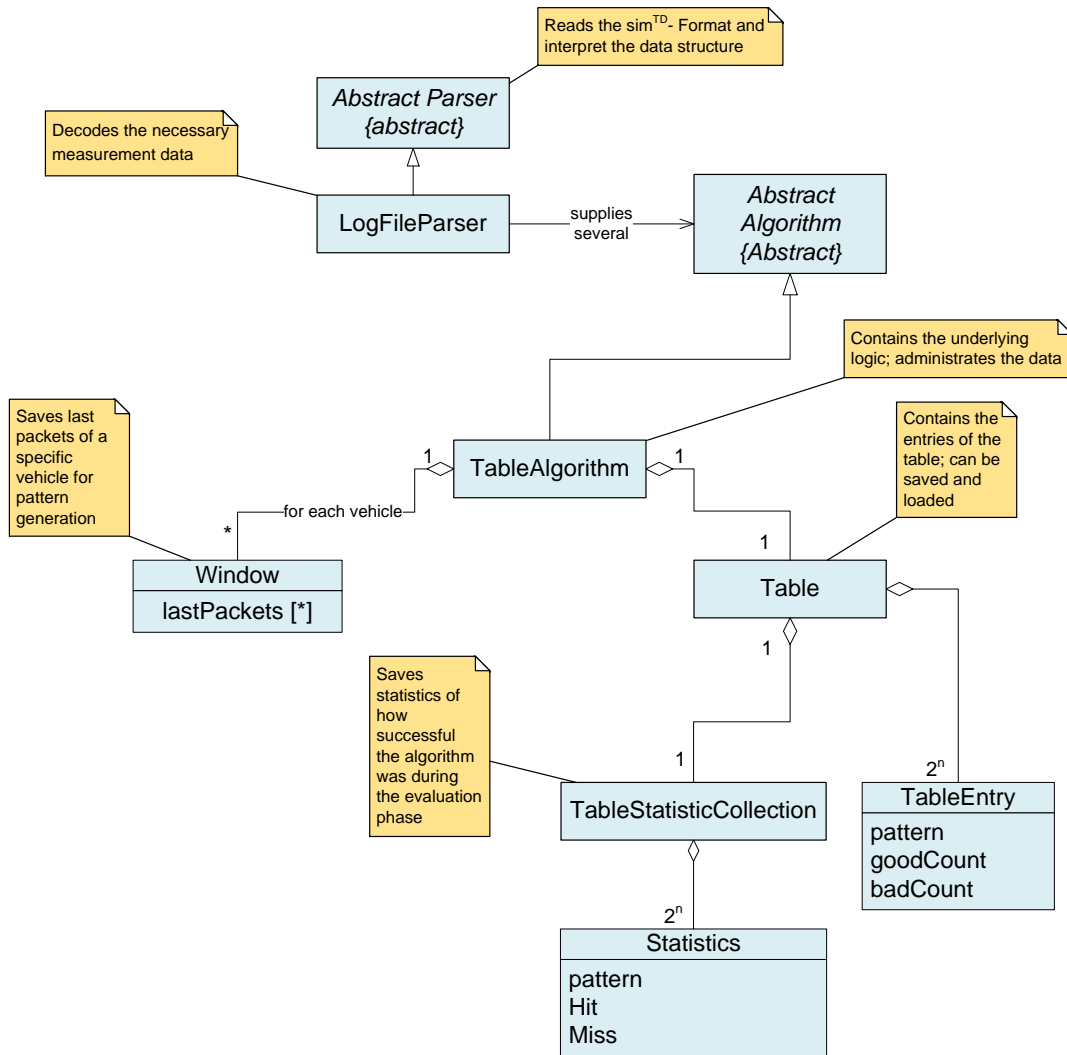


Figure 6.5: Main functional components of the LUT-Based algorithm

The logging is performed at the application unit (AU) and has direct connection to the MAC layer over TCP/IP (Fig. 6.6)³.

LogFileParser reads the log files line by line, searches for *LogID* used for packet reception and then extracts the required information, such as:

- *packet timestamp* is the time in ms, when a packet is saved in the logging system.
- *action* is a parameter that contains the information whether a packet is received or transmitted. This parameter has two values: "1" when a packet is received and "0" when a packet is transmitted.

³ According to the sim^{TD} terminology CCU is a name of the OBU (on-board unit), which was utilized in the project.

- *senderID* is a specific ID of a transmitting vehicle. If pseudonym option at the vehicle is activated, the SenderID will be changed after exceeding a certain time interval, which is approximately equal to 10 min.
- *sourceID* is a specific ID of the vehicle that initially generated the packet. If pseudonym option at the vehicle is activated, the sourceID will also be changed after exceeding a certain time interval, which is approximately equal to 10 min.

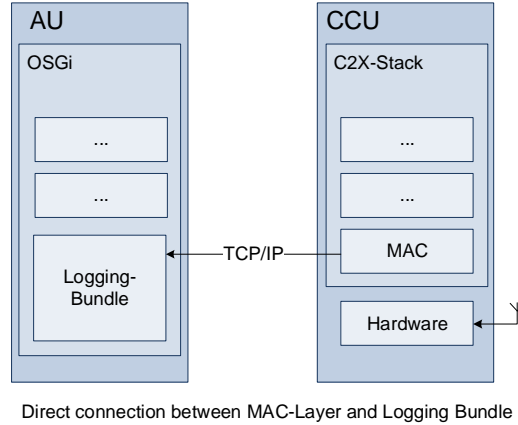


Figure 6.6: sim^{TD} logging system

Class *LogFileParser* filters each line of the log file first according to relevant *logIDs*, then according to *action == 1* and *senderID == sourceID*, as the algorithm is only interested in the evaluation of the received packets without multi-hopping. For the better correspondence to the reality the DENMs are not filtered out and evaluated together with CAMs. After the filtering *LogFileParser* sends senderID and timestamp of the packet to *newPacket* function to process the data.

Context Window

The framework realizes prediction by observing packet reception in the Context Window of a certain length, which is defined in class *Window*. It is updated with the simulation time t_{sim} . Time t_0 is equal to $t_0 = t_{sim} - t_{after}$, where t_{after} relatively to t_0 reflects the size of the interval for which the prediction has to be made (*Result*) and is equal to the size of the *RIF* interval. The time of the beginning of the window t_{start} is equal to $t_{start} = t_0 - t_{before}$, where time t_{before} relatively to t_0 reflects the time for which the context information is observed (*Pattern*). This is illustrated in Fig. 6.8.

The class *Window* contains three functions which are further used by *TableAlgorithm* class: *addPacket*, *isPacketStillRelevant*, *calculateForCurrentTime*.

TableAlgorithm

Fig. 6.7 illustrates the main steps of the *TableAlgorithm* class. To perform the prediction per vehicle, *TableAlgorithm* creates a separate Context Window of a $[t_{start},$

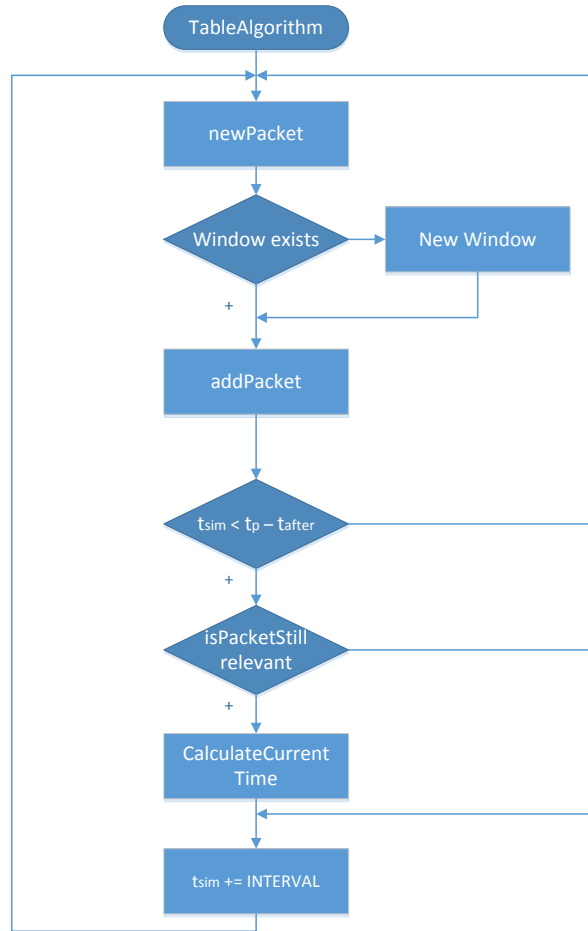


Figure 6.7: Structure of the TableAlgorithm

$t_{sim}]$ size for each SenderID which is currently available in the communication range of the host vehicle. During the field trials the security option was activated. Thus, when a vehicle changes its pseudonym, *TableAlgorithm* treats it as a new vehicle and creates a new Context Window for it. When a new packet is received from a vehicle, *TableAlgorithm* checks if the Context Window for current vehicle already exists or creates a new window in case of the first packet. Further function *addPacket* saves timestamp t_p of each received packet into *lastPackets* array.

To update the Context Window, *TableAlgorithm* defines simulation time t_{sim} . In case of the first packet t_{sim} will become equal to its timestamp and further it increases with $INTERVAL = 200\text{ms}$ steps. This relies on the assumption that maximum message generation rate is $f_g = 5\text{Hz}$, as it is a default frequency in the diving state of the vehicle during sim^{TD} field trials. To ensure synchronizing of the simulation time with the timestamp of the current packet, simulation time should not exceed a time limit $t_{sim} < t_p - t_{after}$. In this way if t_{sim} exceeds the timestamp of a current packet and a new packet is not received yet (i.e. $t_{sim} > t_p - t_{after}$) the simulation time

will stop until the timestamp of a new packet is available (Fig. 6.8). Also if a larger time gap between two received packets occurs, the algorithm makes sure that the simulation time does not directly jump to the timestamp of the received packet, but increases step by step. This ensures a correct processing flow regardless of the fact that implementation is log file based and the algorithm is only triggered by packet reception.

Further, *TableAlgorithm* calls the function *isPacketStillRelevant* which checks if there is still at least one relevant packet in the window. When the whole pattern is filled with zeros, *TableAlgorithm* stops calculation for this senderID and waits for a new packet, as it is assumed that a current remote vehicle is out of the communication range of the host vehicle. If the data is still present for the current simulation time, the *TableAlgorithm* goes into the next step, where it calls the function *calculateForCurrentTime*.

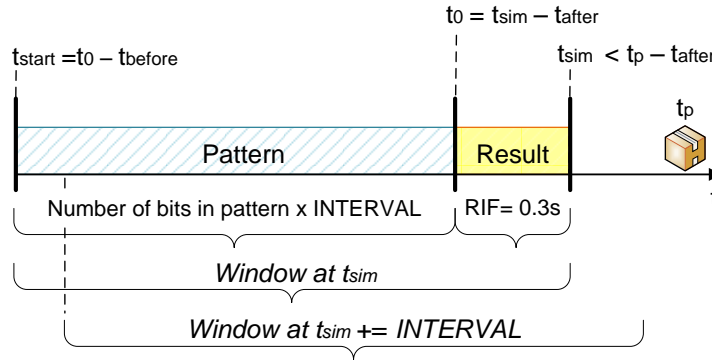


Figure 6.8: Context Window

calculateForCurrentTime

Function *calculateForCurrentTime* first initializes the size of the pattern as $\frac{t_{before}}{INTERVAL}$. In the next step it calculates the pattern in $[t_{start}, t_0]$ interval of the Context Window and prediction result in the next $[t_0, t_{sim}]$ based on the information available in the *lastPackets* array. In the *Pattern* the received and lost packets will be saved as a Boolean with "true" (if received) and "false" (if lost). If there is at least one packet received in the $[t_0, t_{sim}]$ interval the *Result* will be saved as "true" and "false" if otherwise. The decision about packet reception/loss in $[t_{start}, t_0]$ interval is based on the comparison of the timestamp of the packet t_p and the t_{start} : in each simulation step a packet is received if $t_{start} \leq t_p < t_{start} + INTERVAL$ and lost if otherwise. The *Result* in each simulation step is set as "true" if the condition $t_0 \leq t_p < t_{sim}$ is fulfilled.

Further *calculateForCurrentTime* calls *updateWithResult* function, which either updates success probability P_s in the *Table* class (learning mode) or uses it for the evaluation (evaluation mode).

updateWithResult

In the first step function *updateWithResult* transforms the pattern from a Boolean to binary number. Further it can operate in the learning or evaluation modes (Fig. 6.9):

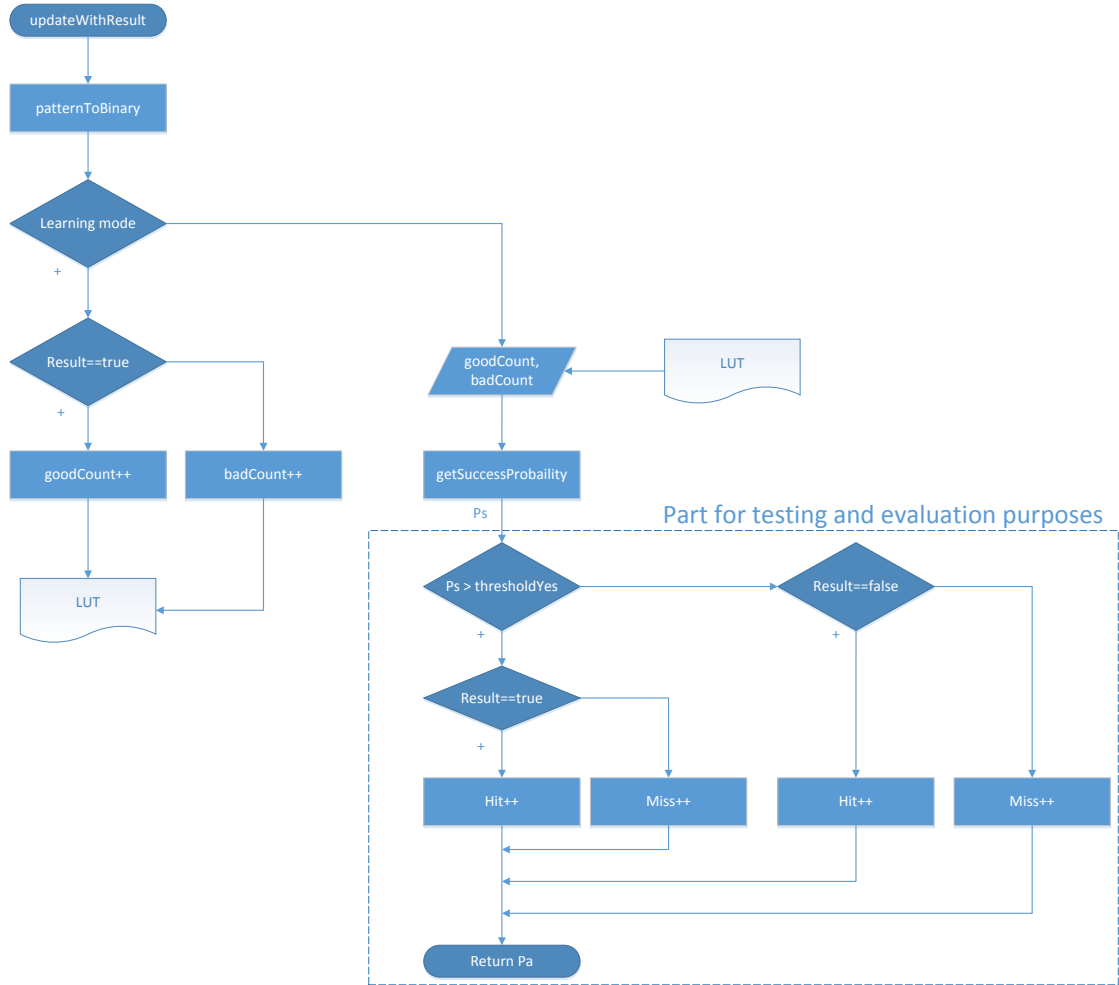


Figure 6.9: Structure of updateWithResult

- Learning Mode: in the learning mode *updateWithResult* gathers and updates the packet reception statistics for each specific pattern. If *Result* in the $[t_0, t_{after}]$ time interval is "true", the *updateWithResult* increments the *goodCount* counter and in case of "false", the *badCount* counter. The values of both counters are then saved in the look-up table.
- Evaluation Mode: in the first step *updateWithResult* accesses the LUT and extracts the values of *goodCount* and *badCount* counters, which correspond to the current pattern and then calls *getSuccessProbability*, which computes success probability P_s . In case of the implementation variant where the algorithm is running in the control device of a vehicle the function *calculateForCurrentTime*

will only return the value of P_s . Since we want to maintain efficiency statistics of the algorithm *calculateForCurrentTime* also obtains prediction accuracy P_a as a ratio of successful (*hit*) and erroneous (*miss*) predictions. The values of the cut-off line are flexible and will be set manually in *thresholdYes* and *thresholdNo* variables. Where *thresholdYes* is the value of P_s after which an application should expect a packet in the next *RIF* interval and *thresholdNo* is a cut-off line before which application should not expect a successful reception. Based on the number of made *hits* and *misses* *updateWithResult* returns prediction accuracy P_a . To capture a complete range of values the *thresholdYes* = *thresholdNo* = 50 % by default.

6.3.2 Results

In this section we analyze achievable values of prediction accuracy P_a under different parameter combinations and select those, which deliver the best trade-off between the prediction accuracy and the algorithm performance.

Optimal Pattern Size

Due to the memory limitations in the vehicle control device it is important to define the best combination of the pattern size and prediction accuracy P_a . Fig. 6.10 illustrates that the prediction accuracy does not significantly improve after 10-bit pattern and the curve goes into saturation after 18-bit pattern. Here we make an assumption that pattern size of 15-bit is a good trade-off between the required memory and prediction accuracy of the algorithm.

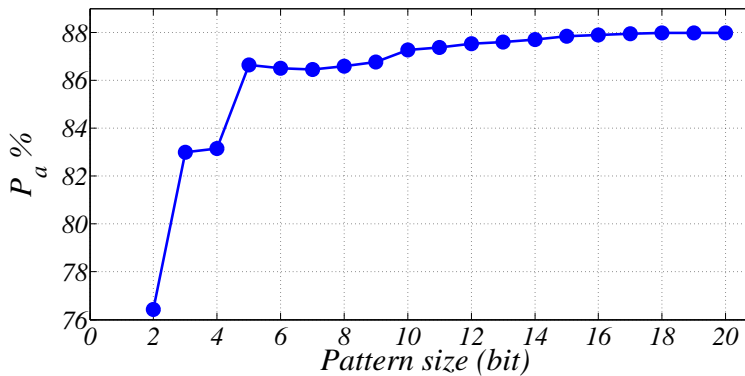


Figure 6.10: Optimal pattern size

Duration of the Learning Phase

In the beginning of this chapter this research made an assumption that the more data the framework has for learning, the higher prediction accuracy P_a it will be able to achieve. Fig. 6.11 illustrates the improvement of P_a according to different amount of learning information. The difference between the achieved P_a is minor over

a whole range of learning phase and after 4 months of learning P_a stays approximately constant. It allows us to conclude that the data, which is available after 4.5 month of field trials, is already sufficient to achieve the maximum possible P_a and the further learning would not lead to a significant improvement. Further this research uses the LUT with 4.5 month of learning phase, except for the cases where it is specifically highlighted otherwise.

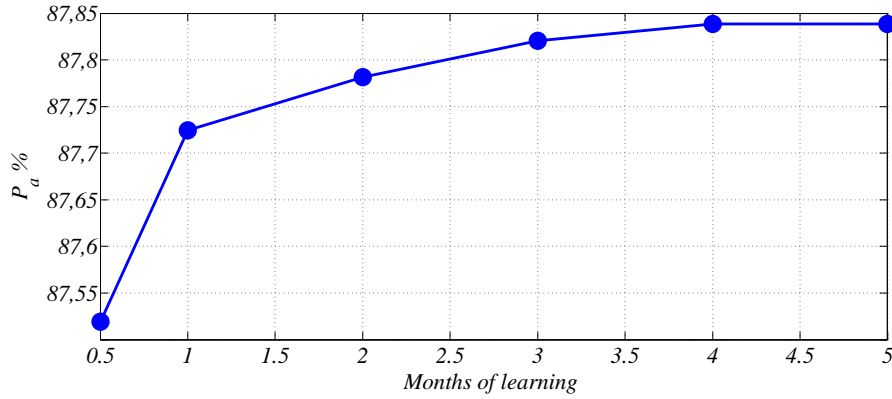


Figure 6.11: Benefit of the learning phase duration

Cut-off Line 50 %

First we conduct the analysis of a complete range of the evaluation data (111.8 driving hours) and obtain prediction accuracy P_a for the case when $thresholdYes = thresholdNo$. Therefore, $hits$ and $misses$ are obtained as:

$$\begin{aligned}
 P_s > 50\% & \quad \text{and } n = 1 \text{ packets is received} & \rightarrow Hit \\
 P_s \leq 50\% & \quad \text{and } n = 1 \text{ packets is not received} & \rightarrow Hit \\
 P_s > 50\% & \quad \text{and } n = 1 \text{ packets is not received} & \rightarrow Miss \\
 P_s \leq 50\% & \quad \text{and } n = 1 \text{ packets is received} & \rightarrow Miss
 \end{aligned}$$

In this case the algorithm makes 30196258 $hits$ and 4180823 $misses$ and prediction accuracy according to Eq. (6.2) is equal to $P_a = 87.838\%$. Further this research uses this value as a baseline for P_a , when no additional optimization is performed.

Fig. 6.12a depicts the frequency distribution of P_s when the framework had different amount of data for learning (from 2 weeks to 4.5 months) and 1 month of measurement data for the evaluation. In case of 2 weeks learning there are 3 peaks, due to a high number of patterns, which occurred only once or twice during the evaluation phase. With the increase of learning data P_a values at all bins are close to those in case of 4.5 months learning, where mean $\mu = 63.07$, median $x_{0.5} = 67$ and mode $\hat{x} = 76$. Standard deviation $\sigma = 20.3$ shows that the values are relatively highly scattered. The distribution is asymmetric and shifted to the right (skewness $\chi = -0.63$ and $\mu < x_{0.5} < \hat{x}$).

Fig. 6.12b additionally depicts the frequency distribution of P_a when the framework had from 2 weeks to 4.5 months learning phase duration and 1 month of measurement

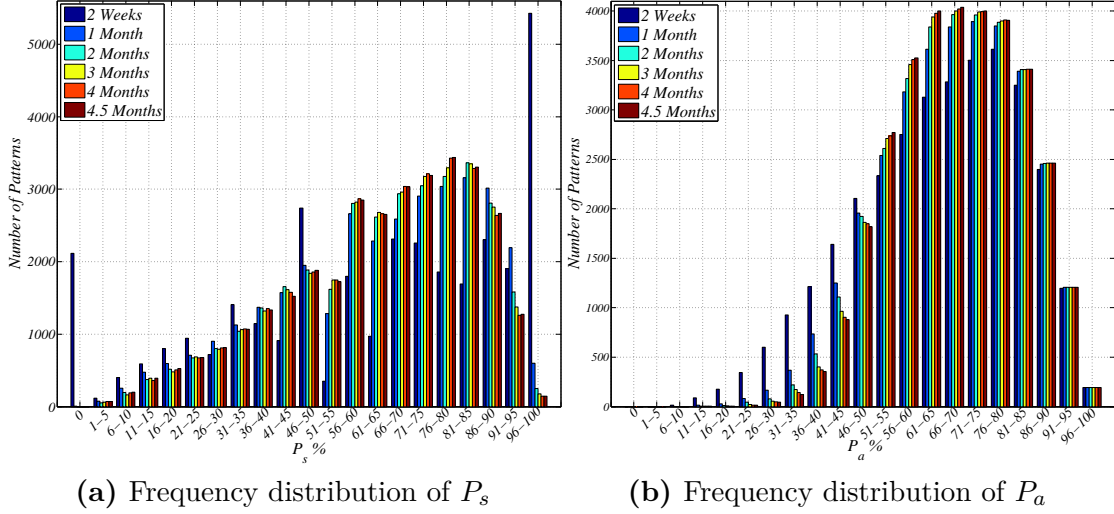


Figure 6.12: Frequency distribution of P_s and P_a

data for the evaluation. In case of 4.5 months of learning, the P_a distribution is also shifted to the right ($\chi = -0,18$) but significantly less scattered ($\sigma = 13.57$). When the framework had only 2 weeks for learning the number of P_a values below 50 % is high. With the increase of the learning phase duration, the majority of P_a values lie in 60-85 % area. The duration of the learning phase does not play a significant role when comparing the number of P_a values in 86-100 % area. It additionally confirms the conclusion that the learning phase does not necessarily have to be long.

Optimisation

Due to the nature of the safety applications the maximum achievable $P_a \approx 87\%$ will not be sufficient to apply the prediction algorithm alone. Therefore, in the following we investigate possible optimizations of the framework by applying different types of data filtering, which would enhance P_a but simultaneously not result in the loss of a significant amount of data. Namely, these are:

- Cut-off line filtering: moving *thresholdYes* and *thresholdNo* values out of 50 %-area of P_s and therewith reaching better P_a but ignoring all the values in the area between *thresholdYes* and *thresholdNo*
- Information amount filtering: ignoring the patterns, which did not gather enough information (*hits* and *misses*) after learning phase. This is based on the assumption that such patterns will deliver poor P_a .

While evaluating the performance of the algorithm, a key aspect is how often the framework can deliver a useful prediction value. Thus, we make use of the *prediction interval* t_p , a performance metric which depicts how frequently the algorithm is able

to make a prediction. It is defined by the simulation time of the framework t_{sim} and is equal to 200 ms by default.

Further we will analyze two cases: when the framework had 2 weeks of learning time and 4.5 months (minimum and maximum duration of the learning phase). Tables 6.1 - 6.2 report achievable P_a as well as the amount of lost data l in % and corresponding t_p in ms in case of different types of filtering. The lost data l represent the number of *hits* and *misses* which are lost due to filtering when compared to their total number in case when no filtering is applied. Due to the constantly changing vehicle pseudonyms during the field trials it is possible to evaluate the size of t_p only for a total number of vehicles (HV performs a prediction for all senderIDs in its range). Therefore, t_p reported in Tables 6.1 - 6.2 is a statistical average. All parameters in Tables 6.1 - 6.2 with index "1" correspond to the case when the LUT is based on 2 weeks of learning and those with index "2" correspond to the case of 4.5 months learning phase.

Cut-off Line Filtering Due to the high requirements imposed on the data accuracy, V2V safety applications will not be able to use a complete range of P_s values, making the 50%-area of minor significance. Obviously, the more distant the values of P_s are from the 50%-area, the higher the values of P_a will be, but simultaneously the more patterns will be ignored and the less frequent the framework will be able to make a prediction.

Since safety applications vary in their purposes, design and requirement on the data accuracy, Table 6.1 reports the values of P_a for different combinations of *thresholdNo* and *thresholdYes*. For instance, cut-off line 10-90 % correspond to the case, when an application requires highly precise prediction results and have to ignore all the patterns within $P_s \in [9.99..89.99]\%$ interval. In such case the values in this interval will be treated by the algorithm as "no value available".

Table 6.1: Cutt-off line filtering, 2 weeks and 4.5 months learning phase

No, %	Yes, %	2 Weeks			4.5 Months		
		P_{a1} , %	l_1 , %	t_{p1} , ms	P_{a2} , %	l_2 , %	t_{p2} , ms
50	50	87.519	0	200	87.838	0	200
45	55	88.386	2.40	204.91	88.694	2.35	204.81
40	60	89.135	4.69	209.85	89.613	5.07	210.68
35	65	90.118	8.11	217.65	90.850	9.18	220.22
30	70	91.012	11.32	225.52	91.992	13.27	230.59
25	75	92.097	15.31	236.15	93.237	18.47	245.30
20	80	93.206	20.08	250.24	94.572	24.70	265.62
10	90	95.605	32.99	298.45	96.647	36.97	317.33
5	95	96.663	41.42	341.44	97.797	47.60	381.70

Table 6.1 demonstrates that the algorithm based on 4.5 month learning phase duration offers a better performance by means of P_a , however, the difference is minor and does not exceed 1 %. We can also see that before 25 - 75 % cut-off line in case of 4.5

months of learning t_{p_2} does not exceed 250 ms and $l_2 \approx 20\%$ of information is lost. The maximum P_{a_2} is equal to 93.2% and t_{p_2} is 1.23 times greater than default $t_{p_2} = 200$ ms. It allows us to assume, that in case of ignoring the P_s values $\in [24.99...74.99]\%$ interval, the framework would not suffer from a significant degradation of the performance by means of t_p . Starting from the cut-off line 20% for *thresholdNo* and 80% for *thresholdYes* the prediction accuracy reaches $P_{a_2} = 95 - 98\%$, but the value of t_{p_2} exceeds 250 ms. Since t_p in Table 6.1 is a statistical average obtained for all vehicles, its increase implies the possibility of the large time gaps between each prediction. To understand whether higher values of t_p can be acceptable by V2V applications, more detailed analysis should be done for two specific vehicles (see section 6.5).

Figs. 6.13a - 6.13b illustrate the distribution of P_a when different cut-off lines are applied. The values at the NaN bin represent the number of ignored patterns. We can observe that with the increasing distance between *thresholdYes* and *thresholdNo* from each other the low P_a values are disappearing and only the values which exceed 50% are present. This effect, however, is clearly seen only when the framework has had enough data available for learning: in case of 4.5 months learning almost all P_a values lie above 50%, which does not hold true when the framework had only two weeks for learning. While comparing Figs. 6.12b and 6.14b we see that when cut-off line filtering is applied, the highest P_a values lie in the 70-80% area, which is a significant improvement.

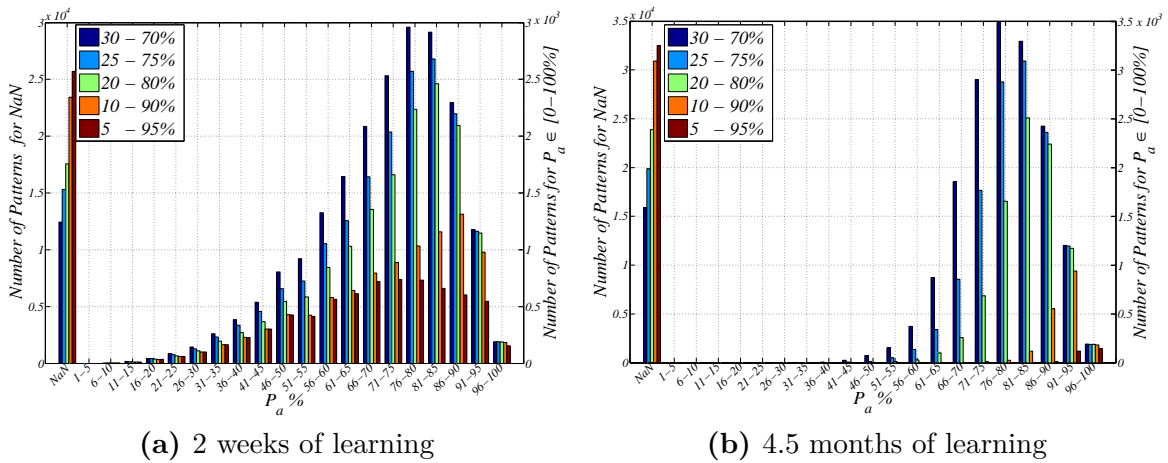


Figure 6.13: P_a by different cut-off lines, 2 weeks and 4.5 months learning phase

Information Amount Filtering Another type of filtering is according to the total number of *hits* and *misses* per pattern. Further we refer to it as to information amount per pattern m . The analysis of the data had shown that *hits* and *misses* are not uniformly distributed over the whole range of patterns, since some of them occurred more frequently than the other. It allows us to make an assumption that the patterns, which do not offer a certain amount of accumulated information, do

not offer a good prediction result either and their exclusion will enhance prediction accuracy P_a . However, it may also decrease the performance of the algorithm, as in this case the algorithm will ignore some patterns and, thus, will not be able to deliver a prediction value every 200 ms. To understand how high the benefit of this approach in relationship to the negative impact is we document P'_a , l' and t'_p values when patterns, which contain less than m of accumulated information are ignored by the algorithm. Similarly to the cut-off filtering case, here we also analyze performance of the algorithm when it had 2 weeks and 4.5 month learning phase and t_p is a statistical average (Table 6.2).

The values of parameter m in case of 4.5 month learning phase are found empirically and lie in the range $\in [500\dots 1000000]$, which corresponds to $m \in [3\% - 50\%]$ of filtered data. Naturally, when the framework has 2 weeks learning phase the amount of information per pattern will be different. For instance, after 2 weeks of learning $m = 3\%$ corresponds to $m_1 = 25$, $m = 50\%$ to $m_1 = 14508$ *hits* and *misses*.

Table 6.2: Information amount filtering, 2 weeks and 4.5 months learning phase

$m, \%$	2 Weeks				4.5 Month			
	m_1	$P'_{a_1}, \%$	$l'_1, \%$	t'_{p_1}, ms	m_2	$P'_{a_2}, \%$	$l'_2, \%$	t'_{p_2}, ms
100	all data	87.519	0	200	all data	87.838	0	200
> 3	> 25	89.182	6.5	213.85	> 500	88.725	4.1	208.61
> 5	> 60	89.934	10.2	222.67	> 1000	89.249	6.9	214.74
> 9.4	> 200	91.060	16.7	240.01	> 3000	90.193	12.2	227.71
> 11	> 280	91.437	18.8	246.32	> 4000	90.460	13.9	232.08
> 12	> 375	91.665	20.6	251.41	> 5000	90.650	15.1	235.63
> 13	> 455	91.816	21.8	255.61	> 6000	90.860	16.2	238.79
> 13.83	> 516	91.921	22.7	258.56	> 7000	91.042	17.3	241.77
> 14.68	> 600	92.114	23.7	262.06	> 8000	91.193	18.3	244.75
> 16	> 730	92.424	25.5	268.62	> 10000	91.419	20	250.00
> 24.3	> 1188	92.881	28.4	279.40	> 50000	92.937	30.1	286.19
> 31.55	> 2972	93.508	34.3	304.60	> 100000	93.808	37.6	320.27
> 45.58	> 8691	95.470	46	370.34	> 500000	96.604	53.1	426.82
> 50	> 14508	96.060	48.7	389.57	> 1000000	96.903	54.9	443.79

Table 6.2 demonstrates that when the patterns which accumulated less than 7000 of *hits* and *misses* are ignored, P'_{a_2} reaches 91% by $l'_2 = 17.3\%$ and $t'_{p_2} = 241.77$ ms. Comparing it to the equivalent lost data l_2 in case of the cut-off filtering, P_{a_2} outperforms P'_{a_2} by approximately 2% ($P_{a_2} = 93.237\%$) and t_{p_2} is almost equal to t'_{p_2} ($t_{p_2} = 245.30$ ms). When LUT had 2 weeks for learning this dependence is the same. For instance, in case of information amount filtering $l'_1 = 20.6\%$, $P'_{a_1} = 91.665\%$ and $t'_{p_1} = 251.41$ ms and by cut-off line filtering by equivalent amount of lost data P_{a_1} is equal to 93.206% and t_{p_1} is 250.24 ms.

Results in Table 6.2 also show that P'_{a_1} outperforms P'_{a_2} in several cases. The difference, however, is minor and does not exceed 1%. This fluctuation can be

explained by only approximate match of information amount for filtering m_1 and m_2 in case of 2 weeks and 4.5 months learned LUT.

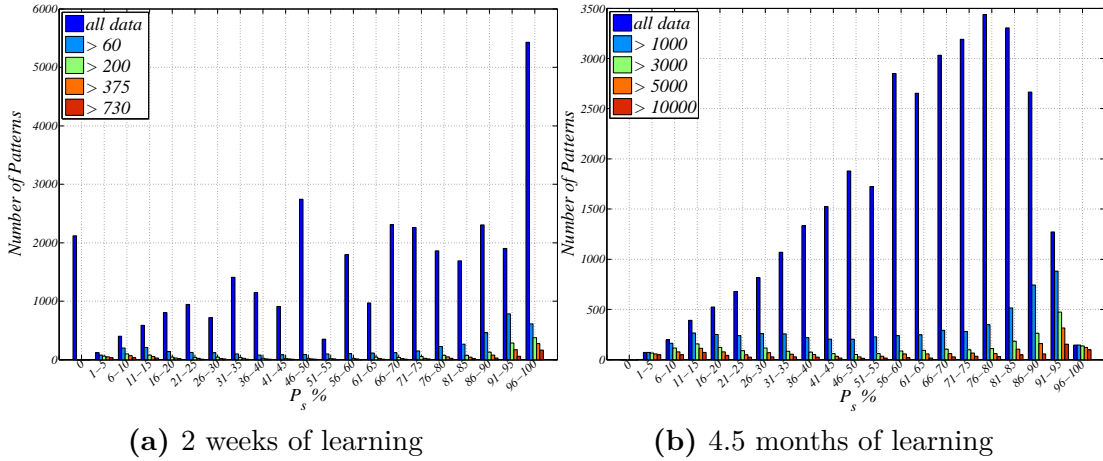


Figure 6.14: P_s when information amount filtering is applied, 2 weeks and 4.5 months learning phase

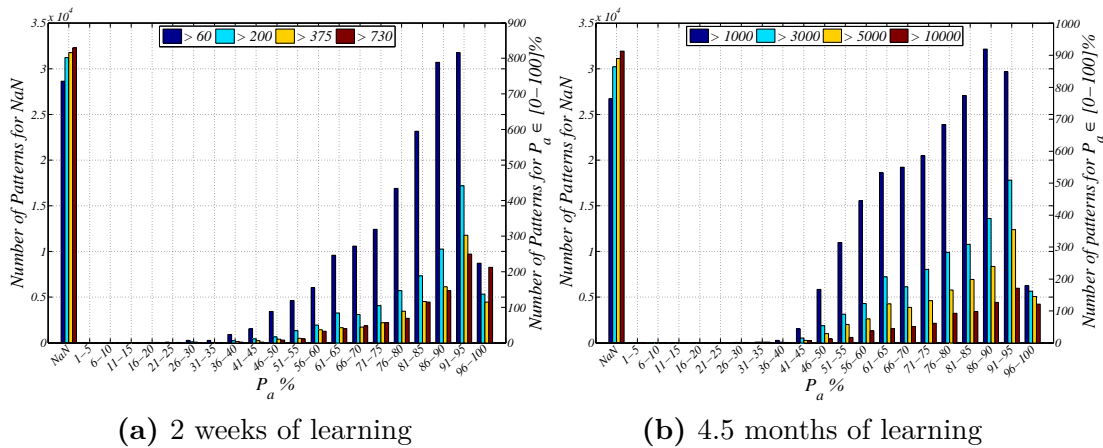


Figure 6.15: P_a when information amount filtering is applied, 2 weeks and 4.5 months learning phase

Figs. 6.14a - 6.14b demonstrate the distribution of P_s after applied filtering. In case of 4.5 month learned LUT it is to observe that when the patterns which have accumulated less than 1000 *hits* and *misses* have to be filtered out, the majority of patterns in the middle area of the histogram will be lost. However, when $P_s \in [90 - 100 \%$] or $\in [1 - 30 \%$] relatively small number of patterns will be ignored. Similar effect is observed when the LUT had 2 weeks for learning. Absence of peaks at P_s equal to 0%, 50%, 100% after filtering indicates that these patterns occurred only several times and, therefore, did not gather sufficient amount of information.

Figs. 6.15a - 6.15b demonstrate the P_a distribution when the filtering is applied.

Similarly to Figs. 6.13a - 6.13b the values at the NaN bin represent the number of ignored patterns. Generally we can observe, that by information amount filtering more information will be ignored, leaving, therefore, considerably smaller number of useful patterns. Comparing Fig. 6.13b and Fig. 6.15b we can see that the scattering of P_a by information amount filtering is more than by cut-off filtering, thus, considerably less values lie in the desired 75-100% area.

Best Trade-off

As it has already been stated in this section, it is important to find a threshold between prediction accuracy and required frequency of the algorithm outputs $f_p = \frac{1}{t_p}$. Fig. 6.16 depicts the values of P_a and t_p , which have already been reported in Tables 6.1 - 6.2 and demonstrates how they are related when different filtering is applied. Additionally, we give an example where both methods are combined. For this we have selected the case of 4.5 month learning phase and performed cut-off line filtering but ignored all patterns that gathered less than $m = 5000$ hits and misses. This information amount value is chosen exemplarily from Table 6.2 as a good threshold between prediction accuracy P'_{a2} and t'_{p2} .

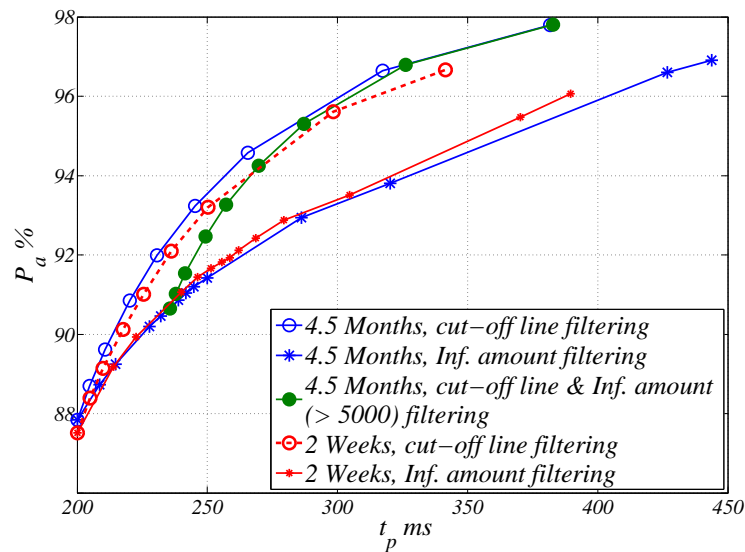


Figure 6.16: P_a by different types of filtering

We can observe that ignoring values in a specific area of P_s (cut-off filtering) gives a better performance by means of t_p and P_a than ignoring the patterns, which did not accumulated enough information after learning phase. Fig. 6.16 additionally demonstrates that combining both methods does not offer the improvement of P_a but results in the increase of t_p .

6.4 Algorithm 2: Model-Based Estimation

This algorithm predicts whether there will be at least $n = 1$ packet received in the $[t_0, t_{after}]$ time interval omitting the learning process by means of the LUT and trains a model instead. Similarly to the LUT-Based approach, this algorithm takes packet reception history as an input and additionally takes into account the RSSI values. The evaluation process shown in Fig. 6.4 is used for *Algorithm 2* as well, with the only difference that P_s is calculated with the model instead of using LUT.

6.4.1 Implementation Details

Algorithm 2 inherits all main functional components of the LUT-Based algorithm (see Fig. 6.5). Due to the absence of the LUT the class *Table* does not contain table entries anymore. However *StatisticCollector* still saves success/failure statistics for each pattern. The *LogFileParser* class additionally extracts RSSI values from the corresponding *LogIDs* and performs the same filtering as it has already been described in section 6.3.1.

CalculateCurrentTime

Function *CalculateCurrentTime* in *Algorithm 2* is depicted in Fig. 6.17. After the pattern is completed the algorithm estimates the average value of the RSSI for it. Further the algorithm uses each bit of the pattern and corresponding RSSI value as inputs for the model, which calculates P_s based on the logit model. To realize it *CalculateCurrentTime* uses two new functions: *getReceivedPowerAverage*, *getProbability*.

Estimation of RSSI

The function *getReceivedPowerAverage* calculates average RSSI value based on the pattern information:

if a packet is received ("1" in the pattern) → take a real measured RSSI value
 if a packet is lost ("0" in the pattern) → take the last measured RSSI value

Further the algorithm sums up the values of RSSI and returns an average RSSI value per pattern:

$$RSSI_{average} = \frac{\sum_{i=0}^n RSSI}{pattern\ length} \quad (6.3)$$

In case of the first packet the average RSSI for such pattern is set to -120 dBm, which corresponds to the lowest RSSI recorded during the measurement.

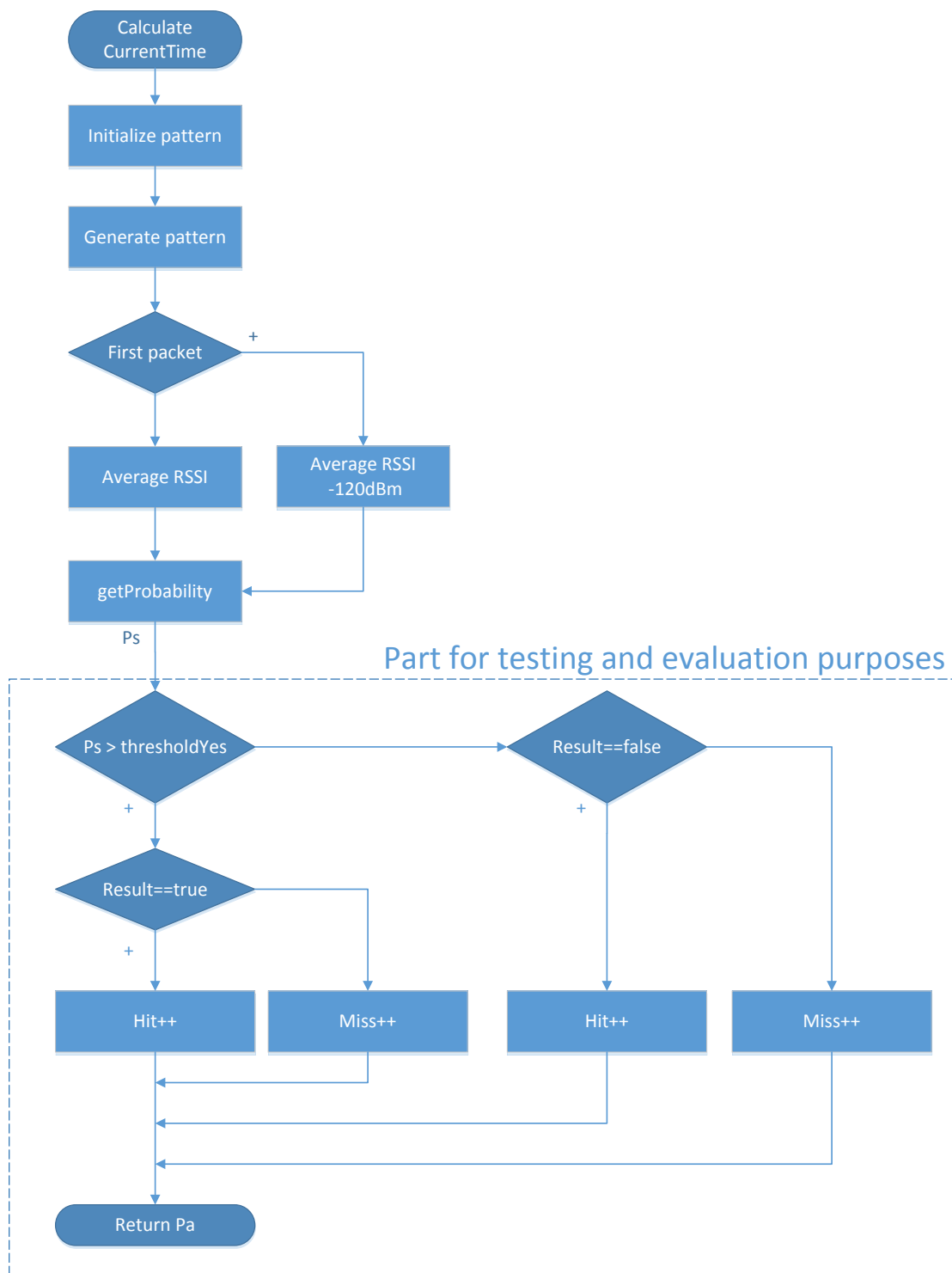


Figure 6.17: Structure of the CalculateCurrentTime in Algorithm 2

Logit Model

Algorithm 2 makes use of the multinomial logistic regression model (logit model) to predict the probability of receiving at least $n = 1$ packet in the $[t_0, t_{after}]$ time interval according to a set of predictors x_1, x_2, \dots, x_q , where q stands for the total number of independent observations. Thus, the success probability P_s is a dependent variable y which takes the value $\in [0..1]$ interval, where 1 indicates that the event has occurred (case) and 0 - that event has not occurred (noncase). The probability of y to take the value of 1 is given as:

$$P\{y = 1 \mid x\} = f(z) \quad (6.4)$$

where $z = \theta_0 + \theta_1 \times x_1 + \dots + \theta_q \times x_q$ and x_1, \dots, x_q are the vectors of values of independent variables, $\theta_1, \dots, \theta_q$ are the regression coefficients, q is the number of observations. The $f(z)$ is the logistic function:

$$f(z) = \frac{e^z}{e^z + 1} = \frac{1}{1 + e^{-z}} \quad (6.5)$$

For the selection of the regression parameters $\theta_0, \dots, \theta_q$ we create a training set of learning pairs $(x^{(1)}, y^{(1)}), \dots, (x^{(q)}, y^{(q)})$, where $x^{(i)} \in R^n$ - vector of values of the independent variables, and $y^{(i)} \in \{0,1\}$ - the corresponding value of y . The training set is based on approx. 4000000 training pairs.

The $x^{(i)}$ vector is represented by 15 bits of the pattern entries, which is a given sequence of zeros and ones and a corresponding to this specific pattern $RSSI_{average}$ value. Thus, the function *getProbability* obtains success probability P_s as:

$$P_s = F(\text{Pattern}, RSSI_{average}) = \frac{1}{1 + e^{-z}} \quad (6.6)$$

$$\begin{aligned} z = & \theta_0 + \theta_1 \times x_1 + \theta_2 \times x_2 + \theta_3 \times x_3 + \theta_4 \times x_4 + \theta_5 \times x_5 + \theta_6 \times x_6 \\ & + \theta_7 \times x_7 + \theta_8 \times x_8 + \theta_9 \times x_9 + \theta_{10} \times x_{10} + \theta_{11} \times x_{11} + \theta_{12} \times x_{12} \\ & + \theta_{13} \times x_{13} + \theta_{14} \times x_{14} + \theta_{15} \times x_{15} + \theta_{16} \times x_{16} \end{aligned}$$

where P_s is a success probability that in the next $[t_0, t_{after}]$ time interval there will be at least $n = 1$ packet received; the independent variables from x_1 to x_{15} corresponds to 15 bits of the pattern and independent variable x_{16} correspond to $RSSI_{average}$. The regression coefficients $\theta_1, \dots, \theta_{16}$ are found with maximum likelihood method:

$$\begin{aligned}
\theta_0 &= 0.79789126533 & \theta_1 &= -0.43192984191 & \theta_2 &= 0.14571818237 \\
\theta_3 &= -0.13694956650 & \theta_4 &= -0.60646378889 & \theta_5 &= 0.07629370099 \\
\theta_6 &= -0.71639401891 & \theta_7 &= -0.03998230807 & \theta_8 &= 0.00034864404 \\
\theta_9 &= -0.42715307949 & \theta_{10} &= -0.32546945263 & \theta_{11} &= -1.89632592172 \\
\theta_{12} &= -0.71751373920 & \theta_{13} &= -0.37755223163 & \theta_{14} &= -0.64243565119 \\
\theta_{15} &= 1.02098246556 & \theta_{16} &= -0.01103842151 & &
\end{aligned}$$

6.4.2 Results

This section presents the obtained values of P_a and corresponding l and t_p values when Model-Based approach is applied. To ensure the comparability of the results, the same measurement data is used for evaluation as in case of the LUT-Based approach. Since learning process with LUT is omitted in this method, this section considers only cut-off line filtering.

Table 6.3: P_a and t_p by cut-off line filtering when Model-Based approach is used

No, %	Yes, %	Model-Based Approach		
		P_a , %	l , %	t_p , <i>ms</i>
50	50	86.633	0	200
45	55	87.982	3.97	208.27
40	60	89.004	7.2	215.53
35	65	89.961	10.88	224.42
30	70	91.281	16.52	239.58
25	75	92.608	22.31	257.45
20	80	93.903	28.93	281.43
10	90	92.828	80.22	1011.06
5	95	94.771	88.75	1777.66

Table 6.3 demonstrates that the values of P_a are generally comparable to those, which are achieved with the LUT-Based approach by all cut-off lines (see Table 6.1). However, the values of t_p in case of 10-90 % and 5-95 % cut-offs are extremely high, which indicates that the logit model outputs P_s higher than 90 % or lower than 10 % rarely with the used set of data.

Fig. 6.18 depicts the frequency distribution of P_a when Model-Based approach is applied. The distribution has the following parameters: mean $\mu = 65.18$, median $x_{0.5} = 66.67$, mode $\hat{x} = 50$, standard deviation $\sigma = 16.99$, skewness $\chi = -0.38$. It is more scattered than the P_a distribution obtained with the LUT-Based approach ($\sigma_{LUT} = 13.57$) and less shifted to the right ($\chi_{LUT} = -0.18$). The mean and the median are comparable ($\mu_{LUT} = 63.07$, $x_{0.5_{LUT}} = 67$), the mode, however, exhibits a big difference in favor of the LUT-Based approach ($\hat{x}_{LUT} = 76$). Comparing Figs. 6.13b and 6.18 we can also observe that logit model produces more P_a values equal to 100 % when cut-off filtering is applied than LUT-Based method. However, due to the greater scattering LUT-Based approach outperforms the one based on logit model in

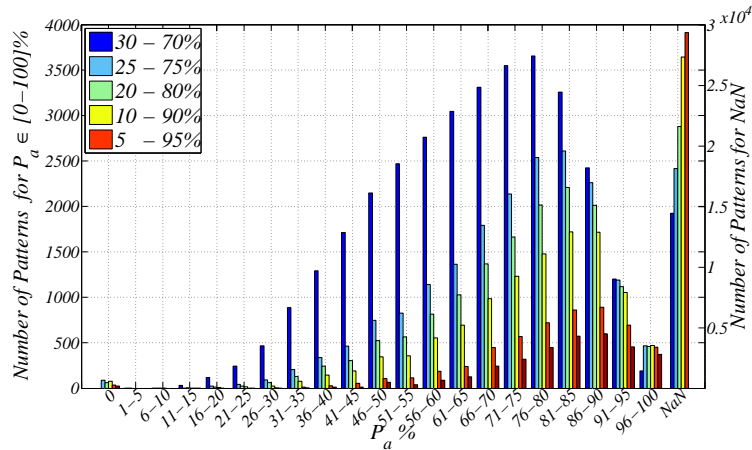


Figure 6.18: Prediction accuracy P_a by cut-off filtering by Model-Based approach

terms of P_a .

Fig. 6.19 compares P_a values achieved when using LUT-Based and Model-Based approaches are used. We can see that before 10-90% the LUT-Based algorithm outperforms the Model-Based estimation in terms of both P_a and t_p . The values of P_a after 10-90% cut-off cannot be used in the real time by the application due to their rare occurrence ($t_p > 1$ s).

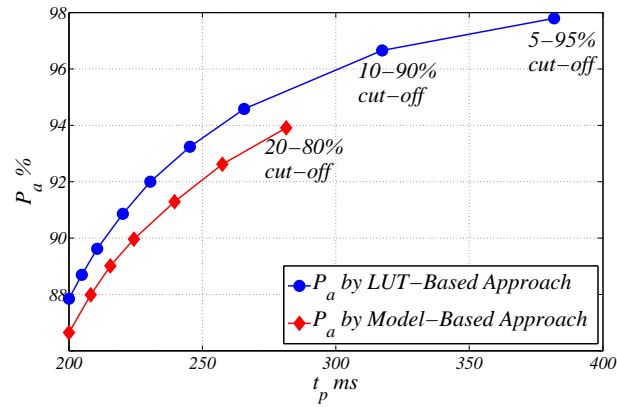


Figure 6.19: Prediction interval t_p when LUT- and Model-Based approaches are applied

6.5 Testing

In the following section we use LUT- and Model-Based algorithms, which were developed and trained based on the sim^{TD} data. To prove that these frameworks are effectively applicable for the future V2V safety applications, we generate independent measurement data for the evaluation phase, further referred to as BS-WOB data set. It was obtained with 2 vehicles driving in the cities of Braunschweig and Wolfsburg,

on highways A39 and A2 and rural road L295 in the surroundings of Braunschweig. The urban environment includes driving in the narrow street canyons, main roads as well as multiple intersection scenarios. To ensure the reproducibility of the experiment the vehicle models, hardware and software remained the same as by sim^{TD} field trials. The total duration of this measurement is 4.11 hours and it covered approximately 107 km. The amount of data available for the evaluation per vehicle is equal to 20 MB.

This section reports the obtained values of P_a and corresponding t_p , when LUT and Model-Based approaches are applied. The fact, that in this measurement campaign there were only two participating vehicles allows us to ignore the aspect of constantly changing pseudonyms and to obtain precise knowledge of t_p during the whole measurement period.

6.5.1 Results

Table 6.4 reports the number of *hits* and *misses* per different groups of patterns when LUT- or Model-Based algorithms are applied and compares the BS-WOB data set (4.11 hours) and the sim^{TD} data (111.8 driving hours, which are standardly used for evaluation). Pattern "0" corresponds to 15-bit pattern which contains all zeros, pattern 32767 corresponds to 15-bit pattern which contains all ones and "others" stands for all patterns between them.

Table 6.4: Information amount per different groups of patterns

Pattern	Information amount m	
	BS-WOB data set	sim^{TD} data set
0	1165	11185914
other	21426	22561968
32767	23639	629208

The analysis has shown that in BS-WOB data set information amount per 0 and 32767 patterns is in sum greater than for all other patterns (1.15 times), which is not the case in the sim^{TD} data set. Such distribution of *hits* and *misses* could result in a better P_a . To evaluate it we first obtain prediction accuracy for BS-WOB data set with the LUT approach when all data is considered ($P_a = 96.517\%$) and then we obtain P_a in case when 0 and 32767 patterns are excluded ($P_a = 93.368\%$). The small difference between these two values ($\Delta P_a \approx 3\%$) implies that considerably better P_a is not artificially achieved due to the frequency of 0 and 32767 patterns. Performing the same calculations for sim^{TD} data results in P_a equal to 87.838% in the first case and 82.109% in the second case. It leads to the conclusion that BS-WOB measurement data is comparable to sim^{TD} data. The considerably lower P_a achieved with the sim^{TD} data can be explained with the averaging of P_a for all vehicles. Due to constantly changing pseudonyms it was not possible to separate specific vehicle for a long enough period of time. The same tendency can be observed when the Model-Based approach is used.

It should be stressed that the fact that during BS-WOB measurement in 50 % of cases we observed 0 and 32767 patterns is an important finding. Since the driving situations, covered within this measurement campaign were realistic for the future V2V applications, we can assume that such distribution of *hits* and *misses* will be realistic in the future as well. At least we can assume it for an early deployment stage of V2V technology when penetration rates are not high. Furthermore, the fact that by all other patterns the framework achieved a good P_a confirms that it can be effectively utilized for envisioned applications. High P_a obtained with sim^{TD} and BS-WOB data sets also allows us to assume that the frameworks will also be efficient under high and low network density conditions.

Table 6.5: P_a achieved by cut-off line filtering when LUT- and Model-Based approaches are applied for BS-WOB data set

No, %	Yes, %	LUT-Based approach			Model-Based approach		
		$P_{a_{LUT}}$, %	l_{LUT} , %	$t_{p_{LUT}}$, ms	P_{a_M} , %	l_M , %	$t_{p_{LUT}}$, ms
50	50	96.517	0	200	95.353	0	200
45	55	96.750	0.62	201.25	95.689	0.83	201.67
40	60	97.043	1.33	202.71	95.98	1.61	203.27
35	65	97.735	4.3	209	96.43	2.65	205.45
30	70	97.497	3.04	206.27	96.828	4.74	209.95
25	75	97.798	4.50	209.42	97.336	8.32	218.16
20	80	98.189	9.01	219.8	97.682	9.81	221.76
10	90	98.794	14.44	233.76	98.374	25.06	266.88
5	95	99.094	24.51	264.95	98.956	33.9	302.55

Due to relatively small amount of data available for the evaluation in BS-WOB data set the graphical interpretation of the frequency distribution of P_a values is omitted. Table 6.5 reports the values of P_a , l and t_p when LUT-Based and Model-Based approaches are applied to BS-WOB data set. The results are comparable with each other. The LUT-Based approach outperforms the one with the model in terms of P_a and t_p by all cut-off lines to minor degree only. It is important to notice, that with BS-WOB data set the Model-Based approach also offers good performance with the 10-90 % and 5-95 % cut-offs, which was not the case with the sim^{TD} data (see Table 6.3). It can be explained with less noisy measurement data in the BS-WOB data set due to more controlled execution of the field trials.

Fig. 6.20 depicts the achieved P_a and corresponding t_p when LUT- and Model-Based approaches are applied to the sim^{TD} and the BS-WOB data sets. Generally, the tendency is the same: the LUT-Based approach outperforms the Model-Based in terms of P_a and t_p . Furthermore, the Model-Based approach also shows good performance in terms of t_p by 10-90 % and 5-95 % cut-offs when the BS-WOB data is evaluated. This indicates that the suggested model can be effective when future V2V safety applications are deployed.

To analyze to what extent the algorithm is able to deliver prediction value every

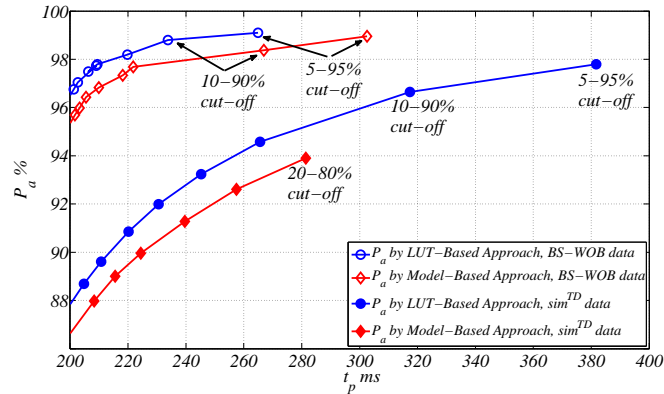


Figure 6.20: P_a vs. t_p when LUT- and Model-Based approaches are applied for sim^{TD} and BS-WOB data sets

200 ms and how big the time gaps between two useful predictions can be Tables 6.6 and 6.7 present frequency distribution of t_p when LUT- and Model-Based approaches are applied. To illustrate it we make use of parameter N , which is a number of times when algorithm made a prediction.

Table 6.6: Frequency distribution of t_p when LUT-Based approach is applied

t_p	N for LUT-Based Approach						
	all data	35-65 %	30-70 %	25-75 %	20-80 %	10-90 %	5-95 %
200	45168	43512	43084	42007	38685	35738	29560
400	0	511	463	755	2099	2312	3909
600	0	91	138	150	188	347	667
800	0	32	65	72	64	86	15
1000	0	22	26	32	35	35	9
1200	0	6	19	13	26	35	13
1400	0	5	11	21	13	54	31
1600	0	3	6	10	22	23	34
1800	0	2	6	7	2	13	59
2000	0	1	2	5	3	1	0
2200	0	0	1	3	4	8	4
2400	0	0	2	6	5	9	18
2600	0	0	0	6	8	9	21
2800	0	0	0	4	10	2	37
3000	0	0	0	1	3	8	12
More	0	0	0	4	19	56	85

Table 6.6 demonstrates that in case of LUT-Based approach N is comparable at all t_p bins until 20-80 % cut-off. We can see that at 200 ms bin N is high and close to the value which is obtained when no filtering is applied ($N = 45168$). Furthermore,

at 400 ms bin N does not exceed 755 before 20-80 % cut-off and stays low at bins ≥ 600 ms. This means that the algorithm will mostly be able to make a prediction every 200 ms before 20-80 %.

Starting with the cut-off line 20-80 % we observe that N at 400 ms bin increases considerably and at bin 200 ms, on the other hand, decreases greatly. It allows us to conclude that if an application will require high level of accuracy to meet "yes" or "no" decision ($thresholdYes > 80\%$, $thresholdNo < 20\%$), the algorithm will not always be able to deliver prediction value every 200 ms. High peaks at 400 ms and 600 ms bins ($N = 3909$ and $N = 668$ respectively) by 5-95 % cut-off line suggest that the framework will be able to output prediction value by this cut-off line only sporadically.

Table 6.7: Frequency distribution of t_p when Model-Based approach is applied

t_p	N for Model-Based Approach						
	all data	35-65 %	30-70 %	25-75 %	20-80 %	10-90 %	5-95 %
200	45168	42978	41360	38560	37706	28632	22798
400	0	548	1340	2246	2244	2490	964
600	0	59	250	449	549	1843	141
800	0	12	37	66	81	100	36
1000	0	6	16	40	64	399	1452
1200	0	0	13	24	33	29	241
1400	0	0	3	8	19	23	48
1600	0	0	5	9	12	21	23
1800	0	0	1	2	12	10	5
2000	0	0	0	1	5	14	143
2200	0	0	0	1	3	15	11
2400	0	0	0	0	3	11	44
2600	0	0	0	0	0	12	145
2800	0	0	0	0	1	7	10
3000	0	0	0	0	0	5	16
More	0	0	0	0	0	29	149

Table 6.7 demonstrates frequency distribution of t_p when Model-Based approach is applied. We can observe the same tendency as in the previous case, however, the negative effect of filtering starts earlier. By 30-70 % cut-off line N at 200 ms bin is considerably lower than it was in the previous case but at bin 400 ms it increases 2.89 times. Additionally, in case of 5-95 % cut-off line there are high peaks at 1000 ms bin and after it, which is not the case with the LUT-Based approach. Despite relatively minor difference in average t_p values when LUT- and Model-Based approaches are used (see Table 6.5), results above allow us to conclude that when Model-Based estimation is used there is a risk of big time gaps between two useful prediction values after 25-70 % cut-off line. Thus, if a V2V application imposes high requirements on "yes" and "no" decisions, the suggested model might be less effective than LUT-Based approach.

6.6 Summary

This chapter has developed and experimentally implemented two methods towards predicting the communication link quality: Look-Up Table (LUT) and Model-Based estimation. The LUT-Based estimation takes packet reception history as an input for the prediction. Based on the received and lost packets the framework generates a binary string (communication pattern), where "1" corresponds to a successfully received packet and "0" to a lost packet. The number of successes and failures after a specific string are saved in the LUT, which is called each time to make a prediction. To ensure good statistical average the framework observes success and failure statistics during a specific period of time (learning phase). The Model-Based approach takes packet reception history and average RSSI value as inputs and instead of using LUT trains a logit model to make a prediction. For the development of both algorithms we used the measurement data, which was gathered during the 4.5 months of the sim^{TD} project field trials.

Based on the data analysis we have found that the optimal length of the communication pattern is equal to 15-18 bits. Furthermore, our research has shown that the required duration of the learning phase is relatively short: after 4 month of learning the prediction accuracy of the framework was approximately constant.

The results have also shown that the prediction accuracy of the framework can be enhanced significantly if a filtering of the information is applied. We have investigated two filtering possibilities: 1) information amount filtering: ignoring the communication patterns which did not gather enough information during the learning phase (only for the LUT-Based approach) and 2) cut-off line filtering: ignoring the communication patterns, which results in success probability close to the 50 % area. The analysis has shown that the second method provides significantly better performance than the first filtering approach.

To prove that the suggested algorithms can be effectively used by future V2V applications, we have performed additional real-world measurements, independent from the sim^{TD} trials. We find out that LUT- and Model-Based methods can both provide prediction accuracy of 93-95 % if no filtering is applied and 97 % in case of ignoring the communication patterns which result in success probabilities close to the 50 % area. However, if the envisioned safety application will impose high requirements on the true positive and false positive decisions, the LUT-Based approach offers better performance.

Generally, the main advantages of both developed methods compared with the existing work is their completely generic nature and simultaneously high performance in urban, rural and highway environments as well as low to no memory requirements.

7 Conclusion and Outlook

The main purpose of this thesis was to evaluate different aspects of communication link reliability for V2V safety applications and to analyze to what extent DSRC communication is feasible to satisfy reliability requirements of these applications. Furthermore, the effectiveness of the proposed assessment metrics for real-time communication link reliability prediction have been studied.

Towards this objective this thesis has first proposed an effective set of metrics to characterize the application reliability. Further, we have evaluated these metrics using the data which was obtained in extensive real-world measurement campaigns in different NLOS scenarios. The focus was to identify the most significant environmental factors, which can affect the reliability of the V2V applications. Moreover, we have analyzed in detail how adequately classical network performance metrics can address application reliability and compared them with the metrics proposed in this thesis. Afterwards, a simulation study has been performed where achievable application reliability in congested network scenarios has been analyzed. Additionally, we have identified the most favorable combinations of the network parameters to support reliable V2V communication in these scenarios. Finally, this thesis has developed and implemented two algorithms which enable real-time short-term prediction of the communication link reliability and evaluated their effectiveness based on real-world measurements.

7.1 Contributions

The following section summarizes the main contributions of this thesis. They are listed as follows:

- This thesis has developed an effective method for communication link reliability assessment in the context of V2V safety applications. We have proposed a novel metric the probability of the information freshness P_{RIF} as well as expanded the definition of the reliable communication range. This allowed for more precise evaluation of communication link reliability and therewith decreased the possibility of erroneous interpretation of measurement or simulation data.
- This thesis has provided an elaborate measurement analysis of communication influencing factors due to the environment for different intersection scenarios under NLOS conditions. We have analyzed the effect of different intersection topologies, traffic conditions and transmitter positions relatively to the intersection center. Furthermore, in this work we have investigated the effects of

the vegetation when it obstructs LOS between a transmitter and a receiver. Additionally, the relationship between the achievable application reliability and vegetation types, densities and seasonal effects has been analyzed.

- In this thesis we have compared effectiveness of the suggested P_{RIF} metric and classical network performance metrics, specifically packet delivery ratio, for the application reliability assessment. We have shown that PDR alone is not always enough to precisely characterize reliability of V2V applications and confirmed this conclusion with examples, which were obtained through the real-world measurements.
- This thesis has provided a detailed theoretical analysis of weather conditions on V2V communications. It quantified the attenuation amount due to rain, dry and wet snow, fog, hail, atmospheric gases, dust and sandstorms.
- This thesis has performed a network parameter study in high network load scenarios based on the simulations. It has analyzed how the data rate, message generation rate, penetration rate, intersection topology, Tx position relatively to the intersection center and relatively to Rx position contribute to the application reliability. It has also derived optimal combinations of these parameters towards ensuring reliable communication. Moreover, each parameter combination has been evaluated in the context of reliability requirements of Intersection Collision Warning and Forward Collision Warning. This was followed by the conclusion to what extent V2V safety applications can effectively operate under congested network conditions.
- This thesis has developed, implemented and tested two algorithms for short-term predictions of the communication link reliability in real time. It evaluated the advantages and disadvantages of each approach and confirmed their effectiveness based on the measurement study.

7.2 Open Issues and Future Work

In this thesis we have presented the results of extensive measurement and simulation studies and analyzed how reliable V2V applications can operate under different environmental and network conditions. Furthermore, we have developed a method for the short-term prediction of the communication link reliability in real time. As usual, there is still room for improvement and further research. Ideas towards extending this research are summarized in the following sections.

7.2.1 Measurement Study

- The focus of this research were mainly intersection scenarios. However, it is also useful to investigate application reliability while driving in the urban street

canyons and at highways. Due to different channel properties in these scenarios the results obtained at intersections may not be necessarily applicable for them.

- Moreover, the future work would be to study the information freshness probability under more dynamic conditions, for instance overtaking of trucks.
- This research has investigated vegetation effect on the communication link reliability only in dry weather conditions. It would be useful to expand this study and compare the selected intersection scenarios in wet and snowy weather conditions.
- For the investigation of the vegetation effect three rural intersections were selected. It would be useful to expand the measurement study at more scenarios with other vegetation types and densities to provide better statistical average in terms of achieved communication ranges.
- Currently most of the existing measurement studies, including the measurements in this work, are performed using hardware not specified by ETSI. It would be useful to perform several reference measurements of investigated scenarios with the mass-production measurement equipment and compare the results.
- While investigating the impact of the weather conditions, this research has used theoretical data only. It would be useful to perform several real-world measurements to confirm available theoretical knowledge.

7.2.2 Simulation Study

- All simulations were performed with transmission power of $P_t = 23$ dBm. It would be useful to expand the study and investigate how other transmission powers can affect application reliability in congested scenarios.
- In high node density scenarios the effectiveness of a co-operative application is directly dependent on the number of nodes in the vehicle's vicinity which are able to receive a notification in the event of a possible collision. Thus, it would be useful to investigate in each scenario what is the maximum number of nodes in a relevant to the Rx intersection area, which are able to maintain the required level of the information freshness.
- Furthermore, it would also be useful to analyze highway scenarios under various network load conditions. Thereby, the positions of Tx and Rx are of great importance (same lane, different lanes, distance from each other).
- During the simulation study the antenna characteristic was assumed to be isotropic. However, in reality the power radiated in a frontal direction will be different from the one, which is radiated to the back. Thus, it would be useful to bring this data in the simulation environment to ensure more realistic results.

7.2.3 Communication Link Reliability Prediction

- This thesis has evaluated the effectiveness of the proposed LUT- and Model-Based methods for one set of the real-world measurement data. To confirm the effectiveness of the developed approaches it would be useful to apply them on additional measurement data, which is obtained at other driving routes.
- The methods for communication link reliability prediction at the receiver side were found to be highly effective. It would be useful to investigate whether these approaches can be adapted for the prediction at the transmitter side.
- The LUT, if implemented at the control unit, can update the success/failure statistics during the driving and adapt itself to the new routes. It would be useful to parameterize the model with the adaptive coefficients as well.
- Evaluation of the algorithm performance has been made based on all data, which was gathered during BS-WOB measurement. It would be useful to define several application-relevant scenarios and separately evaluate specific effects, such as overtaking of trucks, lane change maneuvers, convoy driving with several vehicles, etc.
- Finally, it would be useful to implement both approaches at the control unit and conduct additional field trials.

Bibliography

- [1] Adaptive and Cooperative Technologies for Intelligent Traffic (ACTIVE). <http://www.aktiv-online.org/english/projects.html>. Last visited Nov. 2012.
- [2] Bundesministerium für Verkehr, Bau und Stadtentwicklung. Volkswirtschaftliche Kosten durch Straßenverkehrsunfälle für 2009 Jahr. http://www.bast.de/cln_015/nn_42254/DE/Publikationen/Forschung-kompakt/2011-2010/2011-04.html. Last visited Sept. 2013.
- [3] Communication for eSafety (COMeSafety). <http://www.comesafety.org>. Last visited Oct. 2012.
- [4] European Telecommunications Standards Institute (ETSI). <http://www.etsi.org/>. Last visited Sept. 2013.
- [5] Engineers Handbook: friction coefficients. <http://www.engineershandbook.com/Tables/frictioncoefficients.htm>. Last visited Oct. 2012.
- [6] Internet Engineering Task Force (IETF). <http://www.ietf.org/>. Last visited Oct. 2012.
- [7] Bundesministerium für Verkehr, Bau und Stadtentwicklung. Cooperative ITS Corridor, Joint deployment. http://www.bmvbs.de/SharedDocs/DE/Anlage/VerkehrUndMobilitaet/Strasse/flyer-eurokorridor-cooperative-its-corridor-in-deutsch.pdf?__blob=publicationFile. Last visited Sept. 2013.
- [8] Safety Pilot program overview. http://www.its.dot.gov/safety_pilot/spmd.htm. Last visited at Oct. 2012.
- [9] National Highway Traffic Safety Administration (NHTSA). <http://www.nhtsa.gov>. Last visited Mar. 2012.
- [10] Dedicated Short Range Communication (DSRC) Minimum performance requirements. Technical Report J2945, SAE.
- [11] Cooperative vehicles and road infrastructure for road safety (SAFESPOT). <http://www.safespot-eu.org>. Last visited Sept. 2013.
- [12] Safety Pilot. http://www.its.dot.gov/safety_pilot/index.htm. Last visited at Oct. 2012.

- [13] Sichere Intelligente Mobilität Testfeld Deutschland (sim^{TD}). <http://www.simtd.de/index.dhtml/deDE/index.html>. Last visited at Oct. 2012.
- [14] U.S. Department of Transportation. <http://www.dot.gov/>. Last visited Mar. 2012.
- [15] IEEE Standard for Information technology–Local and metropolitan area networks–Specific requirements–Part 11: Wireless LAN Medium Access Control (MAC) and Physical Layer (PHY) Specifications - Amendment 8: Medium Access Control (MAC) Quality of Service Enhancements. *IEEE Std 802.11e-2005 (Amendment to IEEE Std 802.11, 1999 Edition (Reaff 2003))*, 2005. doi: 10.1109/IEEESTD.2005.97890.
- [16] IEEE Standard for Information technology – Telecommunications and information exchange between systems – Local and metropolitan area networks – Specific requirements; Part 11: Wireless LAN Medium Access Control (MAC) and Physical Layer (PHY) Specifications. *IEEE Std 802.11-2007*, Dec. 2007. doi: 10.1109/IEEESTD.2007.373646.
- [17] IEEE Standard for Information technology – Telecommunications and information exchange between systems – Local and metropolitan area networks – Specific requirements; Part 11: Wireless LAN Medium Access Control (MAC) and Physical Layer (PHY) Specifications; Amendment 6: Wireless Access in Vehicular Environments. *IEEE Std 802.11p-2010*, July 2010. doi: 10.1109/IEEESTD.2010.5514475.
- [18] M.O. Al-Nuaimi and A. M. Hammoudeh. Measurements and predictions of attenuation and scatter of microwave signals by trees. *IEE Proceedings - Microwaves, Antennas and Propagation*, 141(2):70–76, Apr. 1994.
- [19] P. Alexander, D. Haley, and A. Grant. Cooperative Intelligent Transport Systems: 5.9-GHz Field Trials. *Proceedings of the IEEE*, 99(7):1213–1235, July 2011. doi: 10.1109/JPROC.2011.2105230.
- [20] N. An, T. Gaugel, and H. Hartenstein. VANET: Is 95% probability of packet reception safe? In *IEEE 11th International Conference on ITS Telecommunications (ITST '11)*, number 2, pages 113–119, St. Petersburg, Russia, 23–25 Aug. 2011. IEEE. doi: 10.1109/ITST.2011.6060037.
- [21] N. An, M. Maile, D. Jiang, J. Mittag, and H. Hartenstein. Balancing the requirements for a zero false positive/negative Forward Collision Warning. In *IEEE 10th International Conference on Wireless On-Demand Network Systems and Services (WONS '13)*, pages 191–195, Banff, AB, Canada, Mar. 2013.
- [22] M. Ando, M. M. Hasan, R. Jayawardene, T. Hirano, and J. Hirokawa. Localized behaviors of rain measured in Tokyo Tech millimeter-wave wireless network.

- In *5th European Conference on Antennas and Propagation (EuCAP'11)*, pages 1688–1692. IEEE, 11-15 April 2011.
- [23] M. Artimy. Local density estimation and dynamic transmission-range assignment in vehicular Ad Hoc networks. *IEEE Transactions on Intelligent Transportation Systems*, 8(3):400–412, Sept. 2007. doi: 10.1109/TITS.2007.895290.
- [24] A. Avila, G. Korkmaz, Y. Liu, H. Teh, E. Ekici, F. Ozguner, U. Ozguner, K. Redmill, O. Takeshita, K. Tokuda, M. Hamaguchi, S. Nakabayashi, and H. Tsutsui. A complete simulator architecture for inter-vehicle communication intersection warning systems. In *2005 IEEE International Conference on Intelligent Transportation Systems (ITSC '05)*, pages 461–466, Vienna, Austria, 13-15 Sept. 2005. IEEE. doi: 10.1109/ITSC.2005.1520092.
- [25] I. K. Azogu, M. T. Ferreira, and H. Liu. A security metric for VANET content delivery. In *2012 IEEE Global Communications Conference (GLOBECOM '12)*, pages 991–996, Anaheim, CA, USA, 3-7 Dec. 2012. IEEE. doi: 10.1109/GLOCOM.2012.6503242.
- [26] I. K. Azogu, M. T. Ferreira, J. A. Larcom, and H. Liu. A new anti-jamming strategy for VANET metrics-directed security defense. In *2013 IEEE Globecom Workshops (GC Wkshps '13)*, pages 1344–1349, Atlanta, GA, USA, 9-13 Dec. 2013. IEEE. doi: 10.1109/GLOCOMW.2013.6825181.
- [27] F. Bai and H. Krishnan. Reliability analysis of DSRC wireless communication for vehicle safety applications. In *2006 IEEE Intelligent Transportation Systems Conference (ITSC '06)*, pages 355–362, Toronto, ON, Canada, 17-20 Sept. 2006. IEEE. doi: 10.1109/ITSC.2006.1706767.
- [28] J.S. Baker. *Traffic Accident Investigation Manual*. Northwestern University Traffic Institute, USA, 1975.
- [29] R. Bauza, J. Gozalvez, and M. Sepulcre. Power-aware link quality estimation for vehicular communication networks. *IEEE Communications Letters*, 17(4): 649–652, Apr. 2013. doi: 10.1109/LCOMM.2013.022213.122554.
- [30] A. Becher, O. Landsiedel, G. Kunz, and K. Wehrle. Towards short-term wireless link quality estimation. In *5th ACM Workshop on Embedded Networked Sensors (Hot EmNetS '08)*, pages 1–5, Charlottesville, VA, USA, 2-3 June 2008. ACM.
- [31] R. Bhakthavathsalam, S. Nayak, and M. G. Srikumar. Expediency of penetration ratio and evaluation of mean throughput for safety and commercial applications in VANETs. In *2009 IEEE International Conference on Ultra Modern Telecommunications Workshops (ICUMT '09)*, pages 1–5, St. Petersburg, Russia, 12-14 Oct. 2009. IEEE. doi: 10.1109/ICUMT.2009.5345426.

- [32] J.J. Blum, A Eskandarian, and L. Hoffman. Challenges of intervehicle Ad Hoc networks. *IEEE Transactions on Intelligent Transportation Systems*, 5(4): 347–351, Dec. 2004. doi: 10.1109/TITS.2004.838218.
- [33] M. Boban, T. T. V. Vinhoza, M. Ferreira, J. Barros, and O. K. Tonguz. Impact of vehicles as obstacles in vehicular Ad Hoc networks. *IEEE Journal on Selected Areas in Communications*, 29(1):15–28, Jan. 2011. doi: 10.1109/JSAC.2011.110103.
- [34] S. V. Borodich, editor. *Reference Book for Radio-Relay Communication*. Radio and Communication, Moskow, Russia, 2nd edition, 1981.
- [35] A. Boukerche, C. Rezende, and R.W. Pazzi. A link-reliability-based approach to providing qos support for VANETs. In *IEEE 2009 International Conference on Communications (ICC '09)*, pages 1–5, Dresden, Germany, 14-18 June 2009. IEEE. doi: 10.1109/ICC.2009.5198623.
- [36] M. Burckhardt, H. Burg, R. Gnadler, R. Neumann, and G. Schiemann. Die Brems-Reaktionsdauer von PKW-Fahrern. In *Der Verkehrsunfall*, pages 224–236, 1981.
- [37] Car 2 Car Communication Consortium. CAR 2 CAR Communication Consortium Manifesto. Overview of the C2C-CC System. Technical Report V 1.1, 27 Aug. 2007.
- [38] Car2Car Communication Consortium. <http://www.car-to-car.org/>. Last visited Sept. 2013.
- [39] C. P. Cavafy. But the wise perceive things about to happen. In *Collected Poems*. G. Savidis, Ed. Princeton University Press, 1992.
- [40] CCIR. Radio Meteorological Data, volume 5. Technical Report 563-1, 1978.
- [41] CCIR. Attenuation by Atmospheric Gases. Technical Report 719, 1978.
- [42] CCIR. Attenuation and Scattering by Precipitation and Other Atmospheric Particles. Technical Report 721, 1978.
- [43] L. Cheng, B. E. Henty, D. D. Stancil, F. Bai, and P. Mudalige. Mobile Vehicle-to-Vehicle Narrow-Band Channel Measurement and Characterization of the 5.9 GHz Dedicated Short Range Communication (DSRC) Frequency Band. *IEEE Journal on Selected Areas in Communications*, 25(8):1501–1516, 2007. doi: 10.1109/JSAC.2007.071002.
- [44] Continental. Industrial Sensors. Datenblatt. ARS 30X /-2 /-2C/-2T/-21 Long Range Radar. http://www.conti-online.com/www/download/industrial_sensors_de_de/themes/download/ars_300_datenblatt_de.pdf. Last visited Sept. 2013.

- [45] CVIS D2.2. Use cases and system requirements. CVIS IST-4-027293-IP deliverable D2.2 version 1.0, IST CVIS Project, 2006.
- [46] R. D. De Roo, A. W. England, Y. C. Chung, E. Weininger, and K. M. Howell. Absorption at microwave frequencies in a moist metamorphic snow pack due to pendular ring accumulations of liquid water. In *2008 IEEE International Geoscience and Remote Sensing Symposium (IGARSS '08)*, volume 5, pages V – 41–V – 44, Boston, MA, USA, 7-11 July 2008. IEEE. doi: 10.1109/IGARSS.2008.4780022.
- [47] Delegation der Europäischen Union für die Schweiz und das Fürstentum Liechtenstein. EU-Kommission will Zahl der Verkehrstoten bis 2020 halbieren. http://ec.europa.eu/delegations/switzerland/press_corner/focus/focus_items/20100809_de.htm. Last visited July 2013.
- [48] L. Delgrossi. Part II 5.9 GHz DSRC PHY + MAC. In *5th IEEE International Symposium on Wireless Pervasive Computing (ISWPC '10)*, Modena, Italy, 5-7 May 2010. IEEE.
- [49] H. Derichs. Vergleich statistischer Auswerteverfahren der experimentell ermittelten Reaktionszeiten von PKW-Fahrern im Straßenverkehr. Master's thesis, Fachhochschule Köln, 1998.
- [50] A. Dogan, G. Korkmaz, Y. Liu, F. Ozguner, U. Ozguner, K. Redmill, O. Takeshita, and K. Tokuda. Evaluation of intersection collision warning system using an inter-vehicle communication simulator. In *7th International IEEE Conference on Intelligent Transportation Systems (ITSC '04)*, pages 1103–1108. IEEE, 3-6 Oct. 2004. doi: 10.1109/ITSC.2004.1399061.
- [51] T. ElBatt, S. K. Goel, G. Holland, H. Krishnan, and J. Parikh. Cooperative collision warning using Dedicated Short Range Wireless Communications. In *3rd ACM International Workshop on Vehicular Ad Hoc Networks (VANET '06)*, pages 1–9, Los Angeles, CA, USA, 24-29 Sept. 2006. ACM. doi: 10.1145/1161064.1161066.
- [52] ETSI. Intelligent Transport Systems (ITS); European profile standard for the physical and medium access control layer of Intelligent Transport Systems operating in the 5 GHz frequency band. Final draft ETSI ES 202 663 V1.1.0, ETSI Std., 2009.
- [53] ETSI. Intelligent Transport Systems (ITS); Vehicular Communications; Basic Set of Applications; Definitions. ETSI ITS Specification TR 102 638 V1.1.1, ETSI Std., June 2009.
- [54] ETSI. Intelligent Transport Systems (ITS); Vehicular Communications; Basic Set of Applications; Part 3: Specifications of Decentralized Environmental

- Notification Basic Service. ETSI ITS Specification TS 102 637-3 V1.1.1, ETSI Std., Sept. 2010.
- [55] ETSI. Intelligent Transport Systems (ITS); Vehicular Communications; Basic Set of Applications; Part 2: Specification of Cooperative Awareness Basic Service. ETSI ITS Specification TS 102 637-2 V1.2.1, ETSI Std., Mar. 2011.
- [56] Y. P. Fallah, C. L. Huang, R. Sengupta, and H. Krishnan. Analysis of information dissemination in vehicular Ad-Hoc networks with application to cooperative vehicle safety systems. *IEEE Transactions on Vehicular Technology*, 60(1): 233–247, Jan. 2011. doi: 10.1109/TVT.2010.2085022.
- [57] M. A. Fares, S. C. Fares, and C. A. Ventrice. Attenuation and phase shift of the electromagnetic waves due to moist snow. In *1997 IEEE SOUTHEASTCON '97: Engineering new New Century*, pages 109–112, Blacksburg, VA, USA, 12-14 Apr. 1997. IEEE. doi: 10.1109/SECON.1997.598621.
- [58] K. T. Feng, C. H. Hsu, and T. E. Lu. Velocity-assisted predictive mobility and location-aware routing protocols for mobile Ad Hoc networks. *IEEE Transactions on Vehicular Technology*, 57(1):448–464, Jan. 2008. doi: 10.1109/TVT.2007.901897.
- [59] A. Festag, G. Noecker, M. Strassberger, A. Lübke, B. Bochow, M. Torrent-Moreno, S. Schnauffer, R. Eigner, C. Catrinescu, and J. Kunisch. NoW: Network on Wheels: Project objectives, technology and achievements. In *5th International Workshop on Intelligent Transportation (WIT '08)*, pages 211–216, Hamburg, Germany, Mar. 2008.
- [60] Forschungsgesellschaft für Straßen- und Verkehrswesen e.V., editor. *HBS Handbuch für die Bemessung von Straßenverkehrsanlagen*. Number 299. FGSV Verlag GmbH, Köln, 2009.
- [61] N. I. Furashov and B. A. Sverdlov. Quasi-synchronous measurements of radiowave attenuation by falling snow at 138 and 247 GHz. In *3rd International Kharkov Symposium on Physics and Engineering of Millimeter and Submillimeter Waves (MSMW '98)*, volume 2, pages 472–473, 15-16 Sept. 1998. doi: 10.1109/MSMW.1998.755484.
- [62] G. Gärtner. Deliverable 13.2 - Anhang 1: Technische Test- und Versuchsfälle Gesamtsystem; Abschnitt 3.1 Tests und Versuche zur WLAN-Technologie. Technical report, Apr. 2010.
- [63] E. Giordano, R. Frank, G. Pau, and M. Gerla. CORNER: a realistic urban propagation model for VANET. In *IEEE 7th International Conference on Wireless On-demand Network Systems and Services (WONS '10)*, pages 57–60, Kranjska Gora, Slovenia, 3-5 Feb. 2010. IEEE. doi: 10.1109/WONS.2010.5437133.

- [64] J. W. F. Goddard and M. Thurai. Radar-derived path reduction factors for terrestrial systems. In *10th International Conference on Antennas and Propagation*, volume 2, pages 218–221. IET, 14-17 Apr. 1997. doi: 10.1049/cp:19970367.
- [65] C. Grover, I. Knight, F. Okoro, I. Simmons, G. Couper, P. Massie, , and B Smith. Automated Emergency Brake Systems: Technical requirements, costs and benefits. pages 1–109, 24 Jun. 2013. Project Report, TRL for DG Enterprise, European Commission.
- [66] H. Tchouankem, T. Zinchenko, and H. Schumacher. Impact of Buildings on Vehicle-to-Vehicle Communication at Urban Intersections. Technical report. <http://www.ikt.uni-hannover.de/fileadmin/institut/Publikationen/Impact-of-Buildings-on-Vehicle-to-Vehicle.pdf>.
- [67] A. Hirata, R. Yamaguchi, H. Takahashi, T. Kosugi, K. Murata, N. Kukutsu, and Y. Kado. Effect of rain attenuation for a 10-Gb/s 120-GHz-Band millimeter-wave wireless link. *2009 IEEE Transactions on Microwave Theory and Techniques*, 57(12):3099–3105, Dec. 2009. doi: 10.1109/TMTT.2009.2034342.
- [68] P. Hou, J. Zhuang, and G. Zhang. A rain fading simulation model for broadband wireless access channels in millimeter wavebands. In *IEEE 51st Vehicular Technology Conference: VTC2000-Spring*, volume 3, pages 2559–2563, Tokyo, Japan, 15-18 May 2000. IEEE. doi: 10.1109/VETECS.2000.851735.
- [69] C. L. Huang, Y. P. Fallah, and R. Sengupta. Analysis of aggregated power level and rate-power control designs for status update messages in VANETs. In *IEEE 6th International Conference on Mobile Adhoc and Sensor Systems (MASS '09)*, pages 615–620, Macau, China, 12-15 Oct. 2009. IEEE. doi: 10.1109/MOBHOC.2009.5336949.
- [70] C. L. Huang, Y. P. Fallah, R. Sengupta, and H. Krishnan. Information dissemination control for cooperative active safety applications in vehicular Ad-Hoc networks. In *2009 IEEE Global Telecommunications Conference (GLOBECOM '09)*, pages 1–6, Honolulu, HI, USA, Nov. 2009. IEEE. doi: 10.1109/GLOCOM.2009.5425750.
- [71] C. L. Huang, G. Xu, Y. P. Fallah, R. Sengupta, and H. Krishnan. Robustness evaluation of decentralized self-information dissemination control algorithms for VANET tracking applications. In *IEEE 70th Vehicular Technology Conference: VTC2009-Fall*, pages 1–5, Anchorage, AK, USA, 20-23 Sept. 2009. IEEE. doi: 10.1109/VETECF.2009.5378789.
- [72] R. A. Hulays and M. M. Z. Kharadly. Modeling of melting-snow particles for scattering and attenuation calculations. In *8th International Conference on Antennas and Propagation*, volume 2, pages 873–876, Edinburgh, Scotland, Mar. 1993. IET.

- [73] INTERSAFE-2 - An FP7 Project Funded By The EUROPEAN COMMISSION. User needs and operational requirements for a cooperative intersection safety system - Deliverable D3.1. pages 1–97, 2009.
- [74] G. G. Joshi, C. B. Dietrich, C. R. Anderson, W. G. Newhall, W. A. Davis, J. Isaacs, and G. Barnett. Near-ground channel measurements over line-of-sight and forested paths. *IEE Proceedings - Microwaves, Antennas and Propagation*, 2:589–596, Dec. 2005. doi: doi:10.1049/ip-map:20050013.
- [75] G. Karagiannis, R. Wakikawa, and J. Kenney. Traffic safety applications requirements draft-karagiannis-traffic-safety-requirements-00. <http://tools.ietf.org/html/draft-karagiannis-traffic-safety-requirements-00>, July 2009.
- [76] G. Karagiannis, O. Altintas, E. Ekici, G. Heijenk, B. Jarupan, K. Lin, and T. Weil. Vehicular Networking: A survey and tutorial on requirements, architectures, challenges, standards and solutions. *IEEE Communications Surveys Tutorials*, 13(4):584–616, Fourth Quarter 2011. doi: 10.1109/SURV.2011.061411.00019.
- [77] J. Karedal, F. Tufvesson, T. Abbas, O. Klemp, A. Paier, L. Bernadó, and A. F. Molisch. Radio channel measurements at street intersections for Vehicle-to-Vehicle safety applications. In *IEEE 71st Vehicular Technology Conference: VTC 2010-Spring*, pages 1–5, Taipei, Taiwan, 16-19 May 2010. IEEE. doi: 10.1109/VETECS.2010.5493955.
- [78] S. Kaul, M. Gruteser, V. Rai, and J. Kenney. Minimizing age of information in vehicular networks. In *8th Annual IEEE Communications Society Conference on Sensor, Mesh and Ad Hoc Communications and Networks (SECON '11)*, pages 350–358, Salt Lake City, UT, USA, 27-30 June 2011. IEEE. doi: 10.1109/SAHCN.2011.5984917.
- [79] R. Kiefer, D. LeBlanc, M. Palmer, J. Salinger, and M. Shulman. Development and validation of functional definitions and evaluation procedures for Collision Warning/Avoidance Systems. NHTSA Technical Report DOT HS 808 964, DOT, Aug. 1999.
- [80] M. Killat and H. Hartenstein. An empirical model for probability of packet reception in vehicular Ad Hoc networks. *EURASIP Journal on Wireless Communications and Networking*, 2009:4:1–4:12, Jan. 2009. doi: 10.1155/2009/721301.
- [81] B. Kloiber, T. Strang, M. Rockl, and F. de Ponte-Muller. Performance of CAM based safety applications using ITS-G5A MAC in high dense scenarios. In *2011 IEEE Intelligent Vehicles Symposium (IV '11)*, pages 654–660, Baden-Baden, Germany, 5-9 June 2011. IEEE. doi: 10.1109/IVS.2011.5940461.

- [82] P. Lahaie and M. Lecours. Attenuation by rain at 30 GHz: relationship between weather radar echoes and microwave attenuation. In *Canadian Conference on Electrical and Computer Engineering*, volume 2, pages 897–900, Montreal, QC, Canada, 05-08 Sept. 1995. IEEE. doi: 10.1109/CCECE.1995.526572.
- [83] H. Lu and C. Poellabauer. Analysis of application-specific broadcast reliability for vehicle safety communications. In *8th ACM International Workshop on Vehicular Inter-Networking (VANET '11)*, pages 67–72, New York, NY, USA, 2011. ACM. doi: 10.1145/2030698.2030709.
- [84] M. Lukuc. V2V Interoperability Project. In *USDOT ITS Connected Vehicle Workshop*. NHTSA Research, 25 Sept. 2012.
- [85] M. Lukuc. V2V Interoperability Project, USDOT ITS Connected Vehicle Workshop, NHTSA. http://www.its.dot.gov/presentations/CV_Safety_sept2012/pdf/Day%201%20-%20Interoperability%20-%20Lukuc.pdf, Sept. 2012.
- [86] M. Jerbi, S. M. Senouci, Y. Ghamri-Doudan, M. Cherif . *Next Generation Mobile Networks and Ubiquitous Computing*, chapter Vehicular Communications Networks: Current Trends and Challenges. Hershey, PA: Information Science Reference, 2010. doi: 10.4018/978-1-60566-250-3.ch023.
- [87] T. Mangel, O. Klemp, and H. Hartenstein. 5.9 GHz inter-vehicle communication at intersections: a validated non-line-of-sight path-loss and fading model. *EURASIP Journal on Wireless Communications and Networking*, 2011(1):1–11, 23 Nov. 2011. doi: 10.1186/1687-1499-2011-182.
- [88] T. Mangel, M. Michl, O. Klemp, and H. Hartenstein. Real-world measurements of non-line-of-sight reception quality for 5.9 GHz IEEE 802.11p at intersections. In *3rd International Conference on Communication Technologies for Vehicles (Nets4Cars/Nets4Trains '11)*, volume 6596/2011, pages 189–202, Oberpfaffenhofen, Germany, 2011. Springer Berlin/Heidelberg.
- [89] T. Mangel, F. Schweizer, T. Kosch, and H. Hartenstein. Vehicular safety communication at intersections: Buildings, Non-Line-Of-Sight and representative scenarios. In *IEEE 8th International Conference on Wireless On-Demand Network Systems and Services (WONS '11)*, pages 35–41, Bardonecchia, Italy, 26-28 Jan. 2011. IEEE. doi: 10.1109/WONS.2011.5720197.
- [90] C. F. Mecklenbrauker, A. F. Molisch, J. Karedal, F. Tufvesson, A. Paier, L. Bernadó, T. Zemen, O. Klemp, and N. Czink. Vehicular channel characterization and its implications for wireless system design and performance. *Proceedings of the IEEE*, 99(7):1189–1212, July 2011. doi: 10.1109/JPROC.2010.2101990.
- [91] R. Meireles, M. Boban, P. Steenkiste, O. Tonguz, and J. Barros. Experimental study on the impact of vehicular obstructions in VANETs. In *2010 IEEE*

- Vehicular Networking Conference (VNC '10)*, pages 338–345, Jersey City, NJ, USA, 13-15 Dec. 2010. IEEE. doi: 10.1109/VNC.2010.5698233.
- [92] Y. S. Meng, Y. H. Lee, and B. C. Ng. The effects of tropical weather on radio-wave propagation over foliage channel. *IEEE Transactions on Vehicular Technology*, 58(8):4023–4030, Oct. 2009. doi: 10.1109/TVT.2009.2021480.
- [93] P. Mirwaldt, A. Bartels, and K. Lemmer. Gestaltung eines Notfallassistenzsystems bei medizinisch bedingter Fahruntfähigkeit. In *5. Tagung Fahrerassistenz*, Munich, Germany, 15-16 May 2012.
- [94] J. Mittag, F. Schmidt-Eisenlohr, M. Killat, J. Härri, and H. Hartenstein. Analysis and design of effective and low-overhead transmission power control for VANETs. In *5th ACM International Workshop on Vehicular Inter-Networking (VANET'08)*, pages 39–48, San Francisco, CA, USA, 15 Sept. 2008. doi: 10.1145/1410043.1410051.
- [95] A. F. Molisch, F. Tufvesson, J. Karedal, and C. F. Mecklenbrauker. A survey on vehicle-to-vehicle propagation channels. *IEEE Wireless Communications*, 16(6):12–22, 2009. doi: 10.1109/MWC.2009.5361174.
- [96] A. F. Molisch, F. Tufvesson, J. Karedal, and C. F. Mecklenbrauker. Propagation aspects of vehicle-to-vehicle communications - an overview. In *2009 IEEE Radio and Wireless Symposium (RWS '09)*, pages 179–182, San Diego, CA, USA, 18-22 Jan. 2009. IEEE. doi: 10.1109/RWS.2009.4957315.
- [97] M. Müller. WLAN 802.11p Measurements for Vehicle to Vehicle (V2V) DSRC. Application Note. Rohde & Schwarz.
- [98] J. Muramatsu, N. Suzuki, Y. Ito, and T. Taga. Measurement of radio propagation characteristics for inter-vehicle communication in urban areas. In *2007 International Symposium on antennas and propagation (ISAP '07)*, Niigata, Japan, 20-24 Aug. 2007.
- [99] V. Namboodiri and G. Lixin. Prediction-based routing for vehicular Ad Hoc networks. *IEEE Transactions on Vehicular Technology*, 56(4):2332–2345, July 2007. doi: 10.1109/TVT.2007.897656.
- [100] M. Nekovee. Quantifying performance requirements of Vehicle-to-Vehicle communication protocols for Rear-End Collision Avoidance. In *IEEE 69th Vehicular Technology Conference: VTC2009-Spring*, pages 1–5, Barcelona, Spain, 26-29 Apr. 2009. IEEE. doi: 10.1109/VETECS.2009.5073822.
- [101] Z. Niu, W. Yao, Q. Ni, and Y. Song. DeReQ: a QoS routing algorithm for multimedia communications in vehicular Ad Hoc networks. In *2007 ACM International Conference on Wireless Communications and Mobile Computing (IWCMC '07)*, pages 393–398, Honolulu, HI, USA, 12-16 Aug. 2007. ACM. doi: 10.1145/1280940.1281025.

- [102] H. Oh. A Link Availability Predictor for Wireless Sensor Networks. <http://cs229.stanford.edu/proj2009/Haruki.pdf>. Last visited Sept. 2013.
- [103] A. Paier. *The vehicular radio channel in the 5 GHz band*. PhD thesis, Institut für Nachrichtentechnik und Hochfrequenztechnik (E389), Vienna University of Technology, Oct. 2010.
- [104] A. Paier, J. Karedal, N. Czink, C. Dumard, T. Zemen, F. Tufvesson, A. F. Molisch, and C. F. Mecklenbrauker. Characterization of Vehicle-to-Vehicle radio channels from measurements at 5.2 GHz. *Wireless Personal Communications*, 50(1):19–32, 2009. doi: 10.1007/s11277-008-9546-6.
- [105] A. Paier, L. Bernadó, J. Karedal, O. Klemp, and A. Kwoczek. Overview of Vehicle-to-Vehicle radio channel measurements for collision avoidance applications. In *IEEE 71st Vehicular Technology Conference: VTC 2010-Spring*, pages 1–5, Taipei, Taiwan, 16-19 May 2010. IEEE. doi: 10.1109/VETECS.2010.5493975.
- [106] A. D. Panagopoulos, P. D. M. Arapoglou, J. D. Kanellopoulos, and P. G. Cottis. Intercell radio interference studies in broadband wireless access networks. *IEEE Transactions on Vehicular Technology*, 56(1):3–12, Jan. 2007. doi: 10.1109/TVT.2006.883774.
- [107] J. Ploeg, A. F.A. Serrarens, and G. J. Heijenk. Connect & Drive: design and evaluation of cooperative adaptive cruise control for congestion reduction. *Journal of Modern Transportation*, 19(3):207–213, 2011. doi: 10.1007/BF03325760.
- [108] K. Ramachandran, M. Gruteser, R. Onishi, and T. Hikita. Experimental analysis of broadcast reliability in dense vehicular networks. *IEEE Vehicular Technology Magazine*, 2(4):26–32, Dec. 2007. doi: 10.1109/MVT.2008.917439.
- [109] N. Rogers, A. Seville, J. Richter, D. Ndzi, N. Savage, R. Caldeirinha, A. Shukla, M. Al-Nuaimi, K. Craig, E. Vilar, and J. Austin. A generic model of 1-60 GHz radio propagation through vegetation - Final Report. Technical report, UK Radiocommunications Agency, UK, May 2002.
- [110] V. Sakarellos, M. Chortatou, D. Skraparlis, A. D. Panagopoulos, and J. D. Kanellopoulos. Outage analysis of a millimeter wave triple-hop configuration with arbitrary position of the relay nodes. In *4th European Conference on Antennas and Propagation (EuCAP '10)*, pages 1–4, Barcelona, Spain, 12-16 Apr. 2010. IEEE.
- [111] V. Sakarellos, M. Chortatou, D. Skraparlis, A. D. Panagopoulos, and J. D. Kanellopoulos. Performance analysis of cooperative wireless backhaul networks operating at extremely high frequencies. *Journal of Infrared, Millimeter, and Terahertz Waves*, 32(4):496–505, Apr. 2011. doi: 10.1007/s10762-011-9775-8.

- [112] V. K. Sakarellos, D. Skraparlis, A. D. Panagopoulos, and J. D. Kanellopoulos. Optimum placement of radio relays in millimeter-wave wireless dual-hop networks [wireless corner]. *IEEE Antennas and Propagation Magazine*, 51(2): 190–199, Apr. 2009. doi: 10.1109/MAP.2009.5162063.
- [113] V. K. Sakarellos, D. Skraparlis, A. D. Panagopoulos, and J. D. Kanellopoulos. Cooperative diversity performance in millimeter wave wireless mesh networks: Outage analysis. In *3rd European Conference on Antennas and Propagation (EuCAP '09)*, pages 1410–1414, Berlin, Germany, 23–27 Mar. 2009. IEEE.
- [114] V. K. Sakarellos, D. Skraparlis, A. D. Panagopoulos, and J. D. Kanellopoulos. Outage performance analysis of a dual-hop radio relay system operating at frequencies above 10 GHz. *IEEE Transactions on Communications*, 58(11): 3104–3109, Nov. 2010. doi: 10.1109/TCOMM.2010.091310.0900692.
- [115] V. K. Sakarellos, D. Skraparlis, A. D. Panagopoulos, and J. D. Kanellopoulos. Outage performance of terrestrial radio communication networks operating above 50 GHz: Impact of rain attenuation. In *4th European Conference on Antennas and Propagation (EuCAP '10)*, pages 1–5, Barcelona, Spain, 12–16 Apr 2010. IEEE.
- [116] V. K. Sakarellos, D. Skraparlis, A. D. Panagopoulos, and J. D. Kanellopoulos. On the estimation of rain attenuation channels in millimeter wave radio networks. In *6th European Conference on Antennas and Propagation (EuCAP '12)*, pages 500–504, Prague, Czech Republic, 26–30 Mar. 2012. IEEE. doi: 10.1109/EuCAP.2012.6206128.
- [117] F. Salfner, M. Lenk, and M. Malek. A survey of online failure prediction methods. *ACM Comput. Surv.*, 42(3):10:1–10:42, Mar. 2010. doi: 10.1145/1670679.1670680.
- [118] S. R. Saunders and A. Aragón-Zavala. *Antennas and Propagation for Wireless Communication Systems*. John Wiley & Sons, Inc., New York, NY, USA, 2nd edition, Mar. 2007. ISBN 978-0-470-84879-1.
- [119] N. Savage, D. Ndzi, A. Seville, E. Vilar, and J. Austin. Radio wave propagation through vegetation: Factors influencing signal attenuation. *Radio Science*, 38(5), 2003. doi: 10.1029/2002RS002758.
- [120] M. Schack, J. Nuckelt, R. Geise, L. Thiele, and T. Kurner. Comparison of path loss measurements and predictions at urban crossroads for C2C communications. In *5th European Conference on Antennas and Propagation (EuCAP '11)*, pages 2896–2900, Rome, Italy, 11–15 Apr 2011. IEEE.
- [121] B. Schinzel. *Ausarbeitung zum Fachseminar Wintersemester 2008/09. Referent: Prof. Dr. Linn V2V Vehicle-to-Vehicle Communication*. Fachhochschule

- Wiesbaden. Fachbereich Design Informatik Medien. Studiengang Allgemeine Informatik, 2008.
- [122] R. Schmidt, T. Leinmuller, E. Schoch, F. Kargl, and G. Schafer. Exploration of adaptive beaconing for efficient intervehicle safety communication. *IEEE Network*, 24(1):14–19, Jan. 2010. doi: 10.1109/MNET.2010.5395778.
- [123] R. K. Schmidt, T. Leinmüller, and B. Böddeker. V2X Kommunikation. In *17. Aachener Kolloquium Fahrzeug- und Motorentechnik*, Echting, Deutschland, 2008.
- [124] R. K. Schmidt, B. Kloiber, F. Schüttler, and T. Strang. Degradation of communication range in VANETs caused by interference 2.0 - real-world experiment. In *3rd International Conference on Communication Technologies for Vehicles (Nets4Cars/Nets4Trains '11)*, pages 176–188, Oberpfaffenhofen, Germany, 23–24 Mar. 2011. Springer Berlin/Heidelberg.
- [125] H. Schumacher, H. Tchouankem, J. Nuckelt, T. Kurner, T. Zinchenko, A. Leschke, and L. Wolf. Vehicle-to-Vehicle IEEE 802.11p performance measurements at urban intersections. In *2012 IEEE International Conference on Communications (ICC '12)*, pages 7131–7135, Ottawa, ON, Canada, 10–15 June 2012. IEEE. doi: 10.1109/ICC.2012.6364714.
- [126] S. S. Seker and F. C. Kunter. Modeling of snow attenuation at mobile frequencies. In *20th Signal Processing and Communications Applications Conference (SIU '12)*, pages 1–4, Mugla, Turkey, 18–20 Apr. 2012. IEEE. doi: 10.1109/SIU.2012.6204445.
- [127] M. Sepulcre and J. Gozalvez. Dimensioning wave-based inter-vehicle communication systems for vehicular safety applications. In *IEEE 3rd International Symposium on Wireless Communication Systems (ISWCS '06)*, pages 312–316, Valencia, Italy, 6–8 Sept. 2006. IEEE. doi: 10.1109/ISWCS.2006.4362310.
- [128] M. Sepulcre and J. Gozalvez. On the importance of application requirements in cooperative vehicular communications. In *8th International Conference on Wireless On-Demand Network Systems and Services (WONS '11)*, pages 124–131, Bardonecchia, Italy, Jan. 2011. doi: 10.1109/WONS.2011.5720180.
- [129] M. Sepulcre, J. Gozalvez, J. Härri, and H. Hartenstein. Application-based congestion control policy for the communication channel in VANETs. *IEEE Communications Letters*, 14(10):951–953, Oct. 2010. doi: 10.1109/LCOMM.2010.091010.100345.
- [130] M. Sepulcre, J. Gozalvez, J. Härri, and H. Hartenstein. Contextual communications congestion control for cooperative vehicular networks. *IEEE Transactions on Wireless Communications*, 10(2):385–389, Feb. 2011. doi: 10.1109/TWC.2010.120610.100079.

- [131] M. Sepulcre, J. Mittag, P. Santi, H. Hartenstein, and J. Gozalvez. Congestion and awareness control in cooperative vehicular systems. *Proceedings of the IEEE*, 99(7):1260–1279, July 2011. doi: 10.1109/JPROC.2011.2116751.
- [132] M. Shulman. V2V Advancements in the last 12 months. <http://umtri.umich.edu/content/2014.GlobalSymposium.Shulman.pdf>, 22 Apr. 2014. Last visited Sept. 2014.
- [133] M. Shulman and R. Deering. Vehicle safety communications in the United States. *Conference on Experimental Safety Vehicles*, 2007. USA.
- [134] N. Sofra and K. K. Leung. Link classification and residual time estimation through adaptive modeling for VANETs. In *IEEE 69th Vehicular Technology Conference: VTC2009-Spring*, pages 1–5, Barcelona, Spain, 26–29 Apr 2009. IEEE. doi: 10.1109/VETECS.2009.5073646.
- [135] N. Sofra, A. Gkelias, and K. K. Leung. Link residual-time estimation for VANET cross-layer design. In *IEEE 2nd International Workshop on Cross Layer Design (IWCLD '09)*, pages 1–5, Palma de Mallorca, Spain, 11–12 June 2009. IEEE. doi: 10.1109/IWCLD.2009.5156521.
- [136] N. Sofra, A. Gkelias, and K. K. Leung. Route Construction for Long Lifetime in VANETs. *IEEE Transactions on Vehicular Technology*, 60(7):3450–3461, 2011. doi: 10.1109/TVT.2011.2161787.
- [137] L. Song, Q. Han, and J. Liu. Investigate key management and authentication models in VANETs. In *IEEE 2011 International Conference on Electronics, Communications and Control (ICECC '11)*, pages 1516–1519, Ningbo, China, 9–11 Sept. 2011. IEEE.
- [138] K. Srinivasan, P. Dutta, A. Tavakoli, and P. Levis. Understanding the causes of packet delivery success and failure in dense wireless sensor networks. In *4th ACM International Conference on Embedded Networked Sensor Systems (SenSys '06)*, pages 419–420, Boulder, CO, USA, Nov. 2006. ACM. doi: 10.1145/1182807.1182885.
- [139] Statista Website. Automobile - Wichtige Produkteigenschaften. Bedeutung verschiedener Produkteigenschaften von Automobilen für die Kaufentscheidung der Konsumenten in den nächsten fünf Jahren. <http://de.statista.com/statistik/daten/studie/151259/umfrage/wichtige-produkteigenschaftenbei-automobilen-bis-zum-jahr-2014/>. Last visited Oct. 2010.
- [140] I. Tan, W. Tang, K. Laberteaux, and A. Bahai. Measurement and analysis of wireless channel impairments in DSRC vehicular communications. In *IEEE International Conference on Communications (ICC '08)*, pages 4882–4888, Beijing, China, 19–23 May 2008. IEEE. doi: 10.1109/ICC.2008.915.

- [141] H. Tchouankem, T. Zinchenko, H. Schumacher, and L. Wolf. Effects of vegetation on Vehicle-to-Vehicle communication performance at intersections. In *IEEE 78th Vehicular Technology Conference: VTC2013-Fall*, Las Vegas, NV, USA, 2-5 Sept. 2013. IEEE.
- [142] The University of the State of New York. Reference Tables for Physical Setting/PHYSICS. New York: The State Education Department <http://www.p12.nysed.gov/assessment/reftable/physics-rt/physics06tbl.pdf>, Albany, NY, USA, 2002. Last visited Oct. 2012.
- [143] T. Tjelta and D. Bacon. Predicting combined rain and wet snow attenuation on terrestrial links. *IEEE Transactions on Antennas and Propagation*, 58(5): 1677–1682, May 2010. doi: 10.1109/TAP.2010.2044316.
- [144] M. Torrent-Moreno. *Inter-vehicle communications: achieving safety in a distributed wireless environment*. Ph.d. thesis, Universitätsverlag Karlsruhe, Karlsruhe, Germany, 2007.
- [145] M. Torrent-Moreno, D. Jiang, and H. Hartenstein. Broadcast reception rates and effects of priority access in 802.11-based vehicular Ad-Hoc networks. In *1st ACM International Workshop on Vehicular Ad Hoc Networks (VANET '04)*, pages 10–18, Philadelphia, PA, USA, 2004. ACM. doi: 10.1145/1023875.1023878.
- [146] M. Torrent-Moreno, M. Killat, and H. Hartenstein. The challenges of robust inter-vehicle communications. In *IEEE 62nd Vehicular Technology Conference: VTC2005-Fall*, volume 1, pages 319–323, Dallas, TX, USA, 28-25 Sept. 2005. IEEE. doi: 10.1109/VETEFCF.2005.1557524.
- [147] M. Torrent-Moreno, P. Santi, and H. Hartenstein. Distributed fair transmit power adjustment for vehicular Ad Hoc networks. In *3rd Annual IEEE Communications Society on Sensor and Ad Hoc Communications and Networks (SECON '06)*, volume 2, pages 479–488, 28-28 Sept. 2006. doi: 10.1109/SAHCN.2006.288504.
- [148] University of Twente. Connect & Drive (C&D) Project. <http://www.utwente.nl/ctw/aida/research/phd/ConnectenDrive.doc/>. Last visited Sept. 2013.
- [149] M. E. Van Valkenburg and W. M. Middleton. *Reference Data for Engineers: Radio, Electronics, Computer, and Communications*. Newnes, USA, 9th edition, Oct. 2001.
- [150] VSC. Final Report. US DOT, Vehicle Safety Communications Project, DOT HS 810 591, Apr. 2006.
- [151] VSC-A. Final Report. US DOT, Vehicle Safety Communications Applications (VSC-A) Project, DOT HS 810 073, Jan. 2009.

- [152] C. X. Wang, X. Cheng, and D. I. Laurenson. Vehicle-to-Vehicle channel modeling and measurements: recent advances and future challenges. *IEEE Communications Magazine*, 47(11):96–103, Nov. 2009. doi: 10.1109/MCOM.2009.5307472.
- [153] R. Wang, Z. Wang, Z. Chen, and L. Zhang. A 3G-802.11p based OLT-TDMA mechanism for cooperative safety in a dense traffic scenario. In *IEEE 73rd Conference Vehicular Technology: VTC2011-Spring*, pages 1–5, Yokohama, Japan, 15-18 May 2011. IEEE. doi: 10.1109/VETECS.2011.5956608.
- [154] F. Weinert and K. Bogenberger. Vorlesung: Das intelligente Fahrzeug; Block: Kooperative Systeme. Institut für Verkehrswesen und Raumplanung, Universität der Bundeswehr, München, May 2013.
- [155] M. A. Weissberger. An initial critical summary of models for predicting the attenuation of radio waves by trees. Electromagnetic Compatibility Analysis Center MD. Annapolis, MD, USA, July 1982.
- [156] W. Whyte, A. Weimerskirch, V. Kumar, and T. Hehn. A security credential management system for V2V communications. In *2013 IEEE Vehicular Networking Conference (VNC '13)*, pages 1–8, Boston, MA, USA, 16-18 Dec. 2013. doi: 10.1109/VNC.2013.6737583.
- [157] S. Yousefi, S. Bastani, and M. Fathy. On the performance of safety message discrimination in vehicular Ad Hoc networks. In *4th European Conference on Universal Multiservice Networks (ECUMN '07)*, pages 377–390, Toulouse, France, 14-16 Feb. 2007. IEEE. doi: 10.1109/ECUMN.2007.39.
- [158] S. Zeadally, R. Hunt, Y. S. Chen, A. Irwin, and A. Hassan. Vehicular Ad Hoc networks (VANETs): status, results, and challenges. *Telecommunication Systems*, 50(4):217–241, Aug. 2012. doi: 10.1007/s11235-010-9400-5.
- [159] W. Zhang, E. Salonen, and S. Karhu. Evaluation of attenuations for melting snow and the melting layer. In *20th European Microwave Conference*, volume 2, pages 1449–1454, Budapest, Hungary, 9-13 Sept. 1990. IEEE. doi: 10.1109/EUMA.1990.336271.
- [160] W. Zhang, A. Festag, R. Baldessari, and L. Le. Congestion control for safety messages in VANETs: Concepts and framework. In *IEEE 8th International Conference on ITS Telecommunications (ITST '08)*, pages 199–203, Phuket, Thailand, 24-24 Oct. 2008. doi: 10.1109/ITST.2008.4740256.
- [161] T. Zinchenko, H. Tchouankem, L. Wolf, and A. Leschke. Reliability analysis of Vehicle-to-Vehicle applications based on real world measurements. In *10th ACM International Workshop on Vehicular Inter-Networking, Systems, and Applications (VANET '13)*, pages 11–20, Taipei, Taiwan, 25-28 June 2013. ACM. doi: 10.1145/2482967.2482974.

-
- [162] T. Zinchenko, J. N. Meier, B Simsek, and L. Wolf. Real-time prediction of communication link quality for V2V applications. In *3rd International Conference on Connected Vehicles & Expo (ICCVE '14)*, Vienna, Austria, 3-7 Nov. 2014. IEEE.
- [163] T. Zinchenko, H. Tchouankem, and L. Wolf. Reliability of Vehicle-to-Vehicle communication at urban intersections. In *7th International Conference on Communication Technologies for Vehicles (Nets4Cars '14)*, St. Petersburg, Russia, 6-8 Oct. 2014. IEEE.
- [164] H. Zöller and W. Hugemann. Zur Problematik der Bremsreaktionszeit im Straßenverkehr. In *37. BDP-Kongreß für Verkehrspsychologie*, Braunschweig, Germany, 14-16 Sept. 1998.